CHEMICAL REVIEWS

Review

pubs.acs.org/CR

Quantum Chemical Calculations and Experimental Investigations of Molecular Actinide Oxides

Attila Kovács,*[,†,‡] Rudy J. M. Konings,*[,†] John K. Gibson,[§] Ivan Infante,[∥] and Laura Gagliardi[⊥]

[†]European Commission, Joint Research Centre, Institute for Transuranium Elements, P.O. Box 2340, Karlsruhe 76125, Germany

[‡]Department of Inorganic and Analytical Chemistry, Budapest University of Technology and Economics, Szt. Gellért tér 4, H-1111 Budapest, Hungary

[§]Chemical Sciences Division, Lawrence Berkeley National Laboratory, Berkeley, California 94720, United States

[∥]Kimika Fakultatea, Euskal Herriko Unibertsitatea (EHU/UPV) and Donostia International Physics Center (DIPC), P.K. 20080 Donostia, Euskadi, Spain

[⊥]Department of Chemistry, Supercomputing Institute, and Chemical Theory Center, University of Minnesota, 207 Pleasant Street SE, Minneapolis, Minnesota 55455, United States

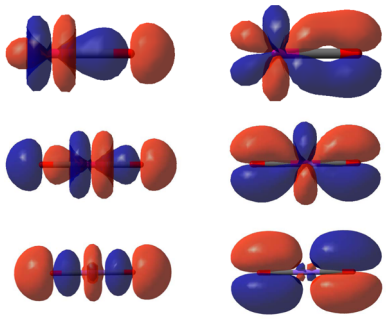

CONTENTS

1. Introduction 1725
2. Methods 1726
2.1. Theory 1726
2.1.1. Electron Correlation 1726
2.1.2. Relativistic Effects 1727
2.2. Experiment 1728
2.2.1. Rotational Spectroscopy 1728
2.2.2. Electronic Spectroscopy 1728
2.2.3. Infrared Spectroscopy 1729
2.2.4. Ion−Molecule Reactions 1729
3. Discussion 1729
3.1. Ground-State Electronic Structure of Actinide Monoxides 1729
3.2. Spectroscopic Constants of Actinide Monoxides 1731
3.3. Excited Electronic States and Electronic Spectra of Actinide Monoxides 1732
3.4. Ground-State Electronic Structure of Actinide Dioxides 1734
3.5. Spectroscopic Constants of Actinide Dioxides 1736
3.6. Excited Electronic States and Electronic Spectra of Actinide Dioxides 1739
3.7. Energetics (Ionization and Dissociation Energies) of Actinide Mono- and Dioxides 1742
3.8. Higher Actinide Oxides 1748
4. Conclusions 1748
Appendix 1749
Associated Content 1754
Special Issue Paper 1754
Author Information 1754
Corresponding Authors 1754
Notes 1754
Biographies 1754
Acknowledgments 1755
References 1755

1. INTRODUCTION

Actinides are the heaviest chemical elements with practical relevance. Among them, only thorium and uranium can be found in nature in substantial quantities, while natural plutonium has been detected in trace amounts. In uranium ores the radioactive decay of uranium produces transient amounts of actinium and protactinium, while in transmutation reactions isotopes of neptunium, americium, curium, berkelium, and californium can also be formed.[1] Actinides heavier than californium are purely synthetic elements, which are made from neutron bombardment of lighter elements.

Along with Th and U, the transuranium elements, Np, Pu, Am and Cm, have important applications and are synthesized in appreciable quantities in nuclear reactors. The other actinides are mostly used only for research, and the required quantities are produced either in nuclear reactors or in particle accelerators;[2] the most abundant isotope of protactinium, Pa-231, is produced by the decay of U-235. Although current applications are limited to the actinides Th, U, Pu and Am, Np and Cm are also significant in nuclear fuel cycles such that their chemical properties need to be understood.

Actinides most frequently occur as solid oxides, which are the best characterized among actinide compounds but with significant gaps in understanding of their properties. While solid actinide oxides, particularly those of Th, U, and Pu, are relatively well characterized, considerably less information is available on the gas-phase properties of actinide oxides. The main reasons for this knowledge gap are the large costs and special experimental setups required, such as for high evaporation temperature or laser ablation sources, and the extreme safety conditions necessary to handle radioactive materials, which is a

Received: August 5, 2014
Published: February 13, 2015

DOI: 10.1021/cr500426s
Chem. Rev. 2015, 115, 1725−1759

particularly problematic consideration for the actinides other than Th and U. In addition, experiments are often complicated by the complex vapor compositions and several accessible oxidation states of the actinides, as well as by a very high reactivity of atomic actinides with oxygen and moisture.

Computational modeling is particularly useful for systems that are not easy to study experimentally, as is the case for most of the actinides. Quantum chemistry can model molecular properties and transformations, and, in combination with experiment, it can lead to an improved understanding of species containing actinides. The recent development of theories able to treat systems with a high density of electronic states arising from degeneracy, or near degeneracy, of orbitals, and also with relativistic effects, has led to a rapid increase in the application and advancement of theoretical studies of actinides. As a result, a substantial amount of theoretical information is available for actinide oxides, the most ubiquitous and important category of actinide species.

The overarching goal here is to review the body of theoretical studies on actinide oxide molecules. As to date only the binary oxides have been investigated by systematic studies on the whole set of light actinides, An = Th−Cm, or in a few cases on the entire actinide series, these species alone can provide consistent information on changes in molecular properties across the series. In this Review, we present trends for several molecular properties utilizing data obtained at consistent theoretical levels. The accuracy of the computed data is assessed by comparison with available experimental results.

We note that three recent works reviewed gas-phase experimental data on actinide compounds: Heaven compiled the spectroscopic properties of ThO, UO, and UO_2;[3] Marçalo and Gibson analyzed the available literature data and suggested the most accurate gas-phase energetics of the early actinide oxides;[4] and finally Heaven et al. reviewed the molecular spectroscopy and gas-phase reactions of actinide compounds.[5] Computational methods for f-elements (including some example results for actinide oxides) have been assessed by Dolg et al.[6−8] General surveys of actinide compounds from a computational perspective including also some oxide data were provided by Pepper and Bursten,[9] Schreckenbach et al.,[10] Kaltsoyannis et al.,[11,12] and Wang et al.[13] The molecular data of neutral actinide oxides from experimental and some early theoretical studies were used for the update of their thermodynamic properties (heat capacity, entropy, enthalpy of formation) by Konings et al.[14]

2. METHODS

2.1. Theory

The characterization of the properties and spectroscopy of actinide oxide molecules is a formidable challenge for computational chemists because the manifold of accessible states is so dense that an accurate description of their electronic structure can be achieved only by evaluating with high precision both (a) the electron correlation energy and (b) the dominant relativistic effects.

2.1.1. Electron Correlation. Generally, the HF solution recovers more than 95% of the total energy, but the remainder (i.e., the electron correlation) is crucial to provide an accurate description of the properties of any system. Correlation energy is always classified into two types: (a) dynamic correlation energy, that is, the energy that comes from the instantaneous excitation of electrons that occurs when electrons "feel and avoid each other"; and (b) static correlation energy, that is, the energy that arises from rearrangement of electrons within a few quasi-degenerate low-lying electronic states.

Actinide-containing molecules are in the majority of cases inherently multiconfigurational systems, that is, systems whose electronic density matrices cannot be derived to a good approximation from a single Slater determinant or a single configuration-state-function (CSF). Such systems are usually described as "multireference" systems, which indicates that a converged treatment by most wave function theory methods requires a multiconfiguration reference state or a zero-order wave function. The special kinds of errors in the energy that arise from using a single-reference treatment of an inherently multiconfigurational system are referred to as "static", "non-dynamical", "near-degeneracy", or "left−right" correlation energy.

Below we provide a short description of the primary methodologies used to include electron correlation when studying actinide oxides.

2.1.1.1. CISD. In this method, a subset of determinants of the full configuration interaction (Full CI) expansion is selected to retrieve the entire correlation energy. Usually, only the singly and doubly excited configurations are retained; this truncated CI is called CISD.[15] The method depends on the single-reference wave function and can recover a large portion of the dynamic correlation energy. However, truncated CI methods in general are not size-extensive.[16,17] A method is said to be size extensive if it predicts the energy of a supersystem comprising two or more noninteracting subsystems to be equal to the sum of the energies of the subsystems computed separately. The wave function of the supersystem is equal to the product of the wave functions of the subsystems. Full CI is size extensive, while truncated CI methods, like CISD, are not. For this reason, CISD is not a good approximation when one wants to compare systems with increasing number of electrons.

2.1.1.2. MR-CISD. In multireference CI (MRCI) methods,[18,19] the reference wave function is a linear combination of Slater determinants or CSFs. Excitations up to the desired level of truncation of the CI expansion are added subsequently. This approach can provide the static correlation energy. However, the CI expansion usually includes only the single and double excitation terms, limiting the inherent accuracy of the method drastically. Moreover, the method is rather expensive because of the exponential scaling with the size of the system.

2.1.1.3. CASSCF/CASPT2. The Complete Active Space (CAS) method[20] is one possible way to generate a multiconfigurational wave function. In the CASSCF method, a set of molecular orbitals, called active orbitals, are defined, and all possible electronic configurations constructed from these orbitals with correct space and spin symmetry form a configuration space. In this configuration space, a full configuration interaction (FCI) wave function is generated, and the orbitals are optimized. CASSCF has become the most popular multiconfiguration method because the wave function is completely defined by the selected active orbitals. Because a FCI is performed within the CAS space, the major drawback of CASSCF is the exponential scaling of the number of configurations with the number of active orbitals. The largest number of CSFs is generated when the number of active electrons and active orbitals is about the same. CASSCF calculations with more than 18 electrons in 18 active orbitals are not currently feasible, limiting the types of chemical problems that can be treated. Moreover, due to the short-range electron−electron interaction, CASSCF does not include dynamic correlation energy being essential for a quantitative

DOI: 10.1021/cr500426s
Chem. Rev. 2015, 115, 1725−1759

treatment of chemical properties like bond energies and electronic excitation energies. Another drawback is the lack of core−valence correlation, which can also be important. Both of these effects can be added by a post-SCF method, using the MCSCF wave function as reference. Nowadays the most popular ones are multireference perturbation theory, such as complete-active-space second-order perturbation theory (CASPT2),[21−23] and multireference configuration interaction (MRCI).[19] These methods are limited in their applicability arising from a high computational cost being a function of the increasing size of the system. Modern extensions of these methods allow the use of larger active spaces with the formulation of restricted active space (RAS),[24] generalized active space (GAS), or SplitGAS wave functions,[25−27] as well as with the occupation-restricted-multiple-active-space (ORMAS) SCF method.[28] However, the applicability of these methods is still limited to small-to-middle-size systems.

2.1.1.4. Coupled Cluster (CC). One of the most successful nonvariational approaches to obtain the dynamic correlation energy is based on Coupled Cluster theory.[29] The so-called exponential ansatz, the exponential form of the correlated wave operator, is the key feature here. The exponentiated excitation operator generates a manifold of excited determinants by promoting electrons from occupied orbitals of the reference determinant to the virtual orbitals.

The CC method was introduced into quantum chemistry by Čížek et al.,[30−33] Bartlett and Purvis,[34,35] and Pople et al.[36] In this context, also the related many-electron theory (MET) of Sinanoğlu[37] and the method of Nesbet[38] merit mention. Bartlett and co-workers made important developments in introducing the full coupled-cluster singles and doubles (CCSD) method,[39] and adding full triple (CCSDT)[40,41] and quadruple (CCSDTQ)[42] clusters into the excitation operator. Various approximate versions, either iterative like CCSDT-n,[40,41] or noniterative like CCSD[T],[43] are also available. CCSD[T] is called nowadays the "gold standard" of quantum chemistry due to additions by Raghavachari et al.[44] and Watts et al.,[45] which give all fourth-order corrections to CCSD for any reference determinant.[43]

2.1.1.5. Fock-Space CC. The Fock-Space CC (FSCC) method[46] is a multireference CC approach that has proven to be very successful in computing highly accurate excitation energies of atoms and molecules.[47] In this method, a reference state is assumed, which is usually a closed-shell single-determinant and denoted as sector (0,0). In addition, the correlated space is defined together with a subspace of it, denoted as P. There are two possible paths: in sector (1,0) one electron is removed from the occupied region of the P space, or in sector (0,1) one electron is added to P. All of the excitations of this removed/added electron in the remaining correlated space are generated to account for the rest of the dynamic correlation energy. A full diagonalization of this dressed Hamiltonian in the P space provides the ionization potentials in sector (1,0) or electron affinities in sector (0,1). Basically, starting from a reference determinant in sector (0,0), we can obtain the electronic spectrum of the corresponding cation in sector (1,0) while that of the anion in sector (0,1). The main advantage of this method is that it takes into account also the multireference character of a state, whereas standard CC can only describe states dominated by one single determinant. The drawback is that by using single and double excitations in the P space, only singlet and triplet states can be retrieved.

Thus, the FSCC method is the natural method of choice for the computation of energy differences of spectroscopic interest. Its wide use in high-precision theoretical spectroscopic calculations or predictions is well documented in the literature. For a review on multireference CC methods and particularly the FS-MRCC approach, see refs 46,48,49; for a review on relativistic FS-MRCC applications, see refs 29,50−52. Attempts have been made to extend the FSCC method to various relativistic systems.[53−63]

2.1.1.6. Density Functional Theory. Density Functional Theory (DFT)[64−67] focuses on the electron density of the system, which depends on only three variables, instead of the many-body electronic wave function, which depends on $3N$ spatial variables. In Kohn−Sham Density Functional Theory, KS-DFT,[68] as extended to spin-polarized electronic systems,[69] the electronic energy is expressed as a functional of the electron spin densities and their gradients, as well as possibly as a functional of orbital-dependent quantities such as exchange energy density or kinetic energy density. The dependence on these quantities, as opposed to a dependence on the full two-particle density matrix,[70] makes the method computationally simpler and more affordable than wave function theory (WFT).[71] In KS-DFT,[68,69] the spin densities are given by a single Slater determinant, and the spin−orbitals of this determinant are used to evaluate the kinetic energy of the noninteracting electron system with the same density as the real system. The correction to the kinetic energy, the exchange energy, and the correlation energy are provided by a functional of the spin densities. However, this so-called exchange−correlation functional is so complicated that it will probably never be known exactly.[72] Approximations of the exchange-correlation functional can be demonstrated by a ladder, where each rung introduces an additional component to the energy density.[73−77] The rungs starting from the bottom are (1) the local spin density approximation, (2) the generalized gradient approximation (GGA), (3) the meta-GGA approximation, (4) the hybrid functional, and (5) the generalized random phase approximation. In this Review, we show a systematic benchmark of several GGA and hybrid functionals for actinide oxides.

2.1.2. Relativistic Effects.[78] Relativistic effects are included in all of the calculations compiled in this Review. They are generally divided into scalar effects consisting of the mass-velocity (relativistic dependence of electron mass on its velocity) and Darwin terms (smearing the effective potential felt by the electron), and the spin−orbit coupling (SOC, interaction of the magnetic moment of the electron due to its spin with the effective magnetic field the electrons perceive due to orbital motion around the nucleus). The scalar effects dominate for light atoms until the first-row transition metals. SOC becomes important for heavier atoms, particularly for actinides.

Relativity can be included in quantum chemical calculations in several ways.[79−81] The most accurate way is to solve explicitly the four-component Dirac equation[82] in an all-electron basis set.[83−88] However, four-component methods are computationally very expensive for molecules. More economical methods have been developed by separating the large and small components of the Dirac Hamiltonian and eliminating the small-component part. Different approximations for this mathematical operation resulted in a number of one- and two-component methods.[89−97] The most economical approach, however, is the use of relativistic effective core potentials[98,99] on top of a nonrelativistic ansatz. The error introduced by employing these approximations instead of a full relativistic

DOI: 10.1021/cr500426s
Chem. Rev. 2015, 115, 1725−1759

treatment is significantly smaller as compared to the error introduced by approximating the electron correlation treatment. Indicated below are the most frequently used approaches for inclusion of relativity in calculations of actinides.

2.1.2.1. SO-MRCI.[100] This was the first relativistic multireference ab initio method that provided reasonable results for heavy atoms. It involves configuration interaction in a basis of wave functions that include scalar relativistic effects. The approach has the disadvantage of slow convergence in cases where the shape of orbitals is affected strongly by SOC.

2.1.2.2. Douglas–Kroll–Hess (DKH) Method.[91,101] This is one of the presently most popular all-electron approaches. The two-component operator used here is obtained by a transformation of the four-component Dirac operator, while keeping the most important terms. It is divided into a scalar part and a SOC part. The scalar part (which includes some approximations due to the transformation) can be easily added to the nonrelativistic one-electron Hamiltonian.[102] SOC requires the addition of two-electron interaction, which can be obtained by the atomic mean field approach (AMFI).[102] An efficient technique for small and moderately large SOC is the state interaction (SI) method of Malmqvist et al.[103,104] It is based on the assumption that the strongest effects of SOC arise from the interaction of electronic states being close in energy. In the complete active space state interaction (CASSI) application, the electronic states are computed at the CASSCF/CASPT2 level. In the SOC calculations, the CSSCF wave functions serve as basis functions, while the CASPT2 energies serve as spin−orbit free energies in the SOC Hamiltonian. Disadvantages of this a posteriori method are that it does not fully account for orbital relaxation, and the accuracy depends on the accuracy of the CASPT2 energies.

2.1.2.3. Zeroth-Order Regular Approximation (ZORA).[105] The ZORA equation is the zeroth-order regular approximation to the Dirac equation. This popular formalism incorporates the relativistic components in the one-electron integrals. The method is mostly used in conjunction with the Kohn−Sham DFT equations.[106] The introduction of scaling of the orbital equations improved the performance on both the ZORA total energies and the computed molecular properties.[107] The two-component ZORA Hamiltonian includes SOC.

2.1.2.4. Exact Two-Component (X2C) Relativistic Hamiltonian.[108] This method derived from the four-component relativistic Dirac equation applies no approximations at the removal of the small components. In contrast to the above methods where the two-component approximation is introduced at the operator level followed by calculation of matrix elements over the final operator expressions, the X2C Hamiltonian is obtained by a one-step matrix algebra operation on the matrix representation of the Dirac operator.

2.1.2.5. Relativistic Effective Core Potentials (RECP).[98,99] The effective core potential (called often as pseudopotential, PP) model makes use of the generally inert nature of the core electrons during the chemical interactions of the elements and includes their indirect effect on the various properties (together with those of the nucleus) in the form of a parametrized core potential. The scalar relativistic effects belong also to this category and can be easily incorporated in the ECP. If SOC effects can be neglected, the RECP approaches can use the techniques of nonrelativistic quantum chemistry, providing results comparable to scalar-relativistic all-electron calculations. As RECP calculations are simple, relatively fast, and cheap, they have produced until now considerably more data on heavy atom systems than any other relativistic method. There are also some approaches to account for SOC effects,[109] but such studies remain very scarce.

The relativistic methods described above are incorporated in various quantum chemical codes. The ones most frequently used nowadays in actinide research are MOLCAS (CASPT2 with DKH and all-electron basis set),[110] ADF (DFT with ZORA and all-electron basis set),[111] Gaussian (DFT with RECP),[112] MOLPRO (CCSD(T) and DFT with RECP),[113] and DIRAC (FSCC with X2C and all-electron basis set).[114]

2.2. Experiment

Experimental determinations of key physical properties for elementary actinide molecules such as oxides are essential, and serve to validate computational results to establish confidence in computed values for unmeasured properties. Because of the difficulties in handling the actinide elements, all of which are radioactive, experimental determinations of physical properties of even simple molecules, such as monoxides and dioxides, are very limited. Most experimental studies have been carried out using the relatively long-lived Th-232 and U-238 isotopes, both of which are terrestrially natural. All other available actinides are synthetic, and their common isotopes exhibit levels of radioactivity that severely restrict experimental efforts. The investigation of physical properties of actinide oxide molecules besides those of Th and U has with few exceptions been limited to the gas-phase reactivity studies by Marçalo, Gibson, and co-workers on oxides of Pa, Np, Pu, Am, and Cm,[4,5,115,116] as described below. The actinides beyond Cm are too scarce and/or short-lived to allow systematic studies using current experimental facilities. Details of the experimental approaches can be found in the pertinent references; only a brief overview of some of the more important and contemporary techniques is provided here.

2.2.1. Rotational Spectroscopy. The best source of accurate gas-phase structural data of small molecules is their rotational spectra, which can be obtained directly by microwave spectroscopy or by high-resolution vibrational and electron spectroscopy achieving rotational fine structure of the bands. There have been only very limited studies of actinide molecules by microwave spectroscopy, notably of ThO, using a Balle−Flygare Fourier transform microwave spectrometer, as described by Cooke and co-workers.[117] These precise experiments are very challenging for even diatomic oxides such as ThO but provide crucial benchmarks with which to compare theory. In the future, it should be feasible to extend this line of inquiry to UO and to the more challenging triatomics ThO_2 and UO_2. It is unlikely that rotational spectra will soon be obtained for any other actinide oxides.

2.2.2. Electronic Spectroscopy. Among the most valuable electron spectroscopy techniques that have been employed to obtain rotational, vibrational, and electronic structural information for small actinide molecules are resonance-enhanced multiphoton ionization (REMPI), mass analyzed threshold ionization (MATI), and pulsed field ionization−zero kinetic-energy photoelectron spectroscopy (PFI-ZEKE), as described by Heaven, who has emphasized the significant complications introduced by open 5f and/or 6d shells for most small actinide molecules, which result in highly congested electronic spectra.[3] These obstacles have been partially circumvented by cooling the studied molecules. Two-color REMPI involves scanning the energy of the first photon to find the excited states of the neutral molecule, while a second photon is used to ionize the excited molecules enabling ion detection. In MATI and ZEKE, the

DOI: 10.1021/cr500426s
Chem. Rev. 2015, 115, 1725−1759

second photon excites the molecule to a long-lived Rydberg state, and ionization is achieved by a pulsed electric field; the primary difference between MATI and ZEKE is that in the former there is mass resolved ion detection. REMPI provides data on the excited state, whereas MATI and PFI-ZEKE provide both accurate IEs and detailed spectroscopic information to the resolution of rotational transitions. These spectroscopic details are obtained by tuning the first laser (photon) to excite and resolve individual rotational levels of the intermediate electronic excited state. In earlier work, classical emission spectra identified molecular electronic transitions to obtain information on the electronic structures of actinide molecules, specifically for ThO by Edvinsson and Lagerqvist[118] and for UO by Kaledin et al.[119]

2.2.3. Infrared Spectroscopy. IR spectra obtained for species isolated in cryogenic inert gas matrices, which generally approximate those of free species in the gas phase, at least for neon matrices, have provided vibrational frequencies and structures for a variety of actinide molecules, primarily using the techniques described by Andrews and co-workers.[120,121] In this work, uranium or thorium atoms are laser ablated and codeposited with reactant molecules such as O_2 in a cryogenic solid matrix, typically neon or argon. Earlier work with Th, U, and Pu employed discharge sputtering as the source of actinide atoms. Reactions between neutral or charged metal atoms and codeposited molecules are induced either by warming the matrix or by photolysis. The vibrational frequencies and structures of the synthesized molecules have been established by IR spectroscopy, often in conjunction with isotopic labeling.

2.2.4. Ion−Molecule Reactions. Marçalo, Gibson, and co-workers have studied reactions of actinide atomic and molecular ions with neutral molecules to acquire estimates for bond dissociation energies (BDEs) and ionization energies (IEs) by atom-transfer and electron-transfer bracketing approaches.[122] A generic example of the bracketing approach is provided by eq 1, where RO is an oxygen-atom donor such as CO_2, O_2, or N_2O.

$$M^+ + RO \rightarrow MO^+ + R \quad (1)$$

For eq 1 to proceed spontaneously under the low-energy conditions of the experiments, it must be thermoneutral or exothermic such that $\Delta H \leq 0$ and $BDE[M^+{-}O] \geq BDE[R{-}O]$. However, if eq 1 does not proceed, it cannot be assumed that $\Delta H \geq 0$ and $BDE[M^+{-}O] \leq BDE[R{-}O]$ because kinetic barriers may prevent an exothermic reaction. Judicious evaluation of oxygen-atom transfer reactions has provided ranges of BDEs for several $AnO^{+/2+}$ and $AnO_2^{+/2+}$ molecules; knowledge of the IEs enables derivation of BDE ranges for the corresponding neutrals via eq 2.

$$BDE[AnO] = BDE[AnO^+] + IE[AnO] - IE[An] \quad (2)$$

These bracketing methods are restricted in accuracy, and the resulting BDEs have typically been assigned uncertainties in the range of 10−60 kJ/mol. However, this approach has been applied to the widest range of actinides, from Th to Cm. The corresponding bracketing method for estimating IEs is given by eq 3, where $n = 1$ or 2.

$$MO^{n+} + X \rightarrow MO^{(n-1)+} + X^+ \quad (3)$$

For monopositive ions, that is, $n = 1$, electron transfer is essentially barrierless such that if eq 3 proceeds then $IE[MO] \geq IE[X]$, and if it does not proceed then $IE[MO] \leq IE[X]$. Using this approach, IE values for AnO (An = Pa, Np, Pu, Am, Cm) have been obtained to within an accuracy of ±0.2 eV, with the values being substantially more reliable than those obtained from electron impact measurements for high temperature vapors.[123] The uncertainties for $IE[AnO^+]$ derived from the bracketing approach, eq 3 for $n = 2$, are greater due to Coulombic barriers to charge-separation of the MOX^{2+} association complex into MO^+ and X^+.

It should be remarked that a more accurate approach for obtaining BDEs is the guided ion beam technique extensively employed by Armentrout[124] in which a molecular ion, such as MO^+, is accelerated to a high energy and dissociated by collision with an inert gas such as Xe. The energy threshold for dissociation provides a direct indication of $BDE[M^+{-}O]$. However, this approach has yet to be applied to actinide oxides.

3. DISCUSSION

3.1. Ground-State Electronic Structure of Actinide Monoxides

Knowledge of the ground-state electronic structure of a specific molecule is very important as it provides information on the geometrical structure, bonding, and several spectroscopic properties. This information can be gained from both experimental and theoretical investigations, with theory being more revealing in those cases where precise spectroscopic data are not accessible.

The first step in a quantum chemical computation is therefore to evaluate the ground-state electronic structure. This is not always straightforward in the case of actinide compounds where the energetic proximity of the actinide 7s, 6d, and 5f atomic orbitals and their diverse populations can result in excited electronic states energetically close to the ground state. In addition, these low-energy states could result in important changes in molecular spectroscopic parameters. In some cases, it could also occur, particularly using single-determinant approaches, that the optimization of the wave function converges to a low-lying excited state instead of the ground electronic state. We will show that this situation has emerged in early studies of PuO,[125] UO_2,[126] UO,[127] PuO^+,[128,129] PuO^{2+},[128] and NpO_2,[130] for which a comparison with more recent reliable results shows significant disparities (vide infra). In more recent theoretical works,[131−135] particular attention has been given to ensure that the calculations resulted in the lowest-energy electronic states. However, in cases of difficult systems, even with great care, the actual ground state of the molecule can appear as an excited state when less sophisticated theoretical models are employed.

Overall, provided a large enough active space and proper treatment of relativistic effects, multireference calculations can generally provide the ground electronic state with high enough accuracy and, in addition, can give reliable information on the low-lying electronic states. Prior to 2010, a plethora of multireference calculations appeared on some Th, U, and Pu oxide molecules. The problem was that in each of these efforts distinct computational settings (basis-set, active space size, and so on), and also different theories, were employed, which hindered an effective comparison between the different molecular species. The first systematic study on the mono and dioxides of early actinides (An = Th−Cm) applying comparable active space, basis sets, treatment of electron correlation, and relativistic effects was performed by Infante et al. This study covered both the neutral oxides and the (+) and (2+) cations at a reliable multireference level (SO-CASPT2). For this reason, this paper[132] can be recommended as a reference for the knowledge of the ground-state electronic structure of the early actinide oxides.

DOI: 10.1021/cr500426s
Chem. Rev. 2015, 115, 1725−1759

Table 1. Selected Computed and Experimental Results on the Ground-State Bond Distances of Neutral and Ionic Actinide Monoxides[a]

AnO	state	CASPT2[b]	SO-CASPT2[c]	M06[d]	PW91[e]	B3LYP[f]	experimental
ThO	$^1\Sigma_0^+$	1.863	1.863	1.812	1.835	1.833	1.84018613(24)[g]
PaO	$^2\Phi_{2.5}$	1.811	1.818	1.786	1.818	1.812	
UO	$^5I_4$	1.837	1.838	1.773	1.838	1.843	1.8383(6)[h]
NpO	$^6\Delta_{1.5}$	1.837	1.839	1.811	1.831	1.836	
PuO	$^7\Pi_0$	1.818	1.820	1.804	1.828	1.830	
AmO	$^8\Sigma_{0.5}^+$	1.800	1.801	1.820	1.845	1.836	
CmO	$^9\Sigma_4$	1.835	1.836	1.827	1.840	1.842	
BkO	$^8\Phi$					1.835	
CfO	$^7\Pi$					1.822	
EsO	$^6\Delta$					1.822	
FmO	^3H					1.850	
MdO	$^2\Pi$					1.898	
NoO	$^1\Sigma$					1.923	
LrO	$^2\Sigma^+$					1.871	
ThO^+	$^2\Sigma_{0.5}^+$	1.827	1.827	1.776	1.803	1.801	1.807[i]
PaO^+	$^3H_4$	1.805	1.804	1.754	1.792		
UO^+	$^4I_{4.5}$	1.799	1.796	1.784	1.796	1.798	1.801(5)[j]
NpO^+	$^5\Gamma_2$	1.797	1.798	1.770	1.791		
PuO^+	$^6\Pi_{0.5}$	1.777	1.789	1.767	1.788		
AmO^+	$^7\Sigma_0^+$	1.776	1.782	1.765	1.787		
CmO^+	$^8\Sigma_{0.5}$	1.795	1.792	1.783	1.802		
ThO^{2+}	$^1\Sigma_0^+$	1.792	1.790	1.744	1.768		
PaO^{2+}	$^2\Phi_{2.5}$	1.752	1.733	1.727	1.755		
UO^{2+}	$^3H_4$	1.728	1.720	1.703	1.736		
NpO^{2+}	$^4I_{4.5}$	1.722	1.723	1.694	1.730		
PuO^{2+}	$^5\Gamma_2$	1.720	1.731	1.698	1.743		
AmO^{2+}	$^6\Pi_{0.5}$	1.774	1.808	1.742	1.778		
CmO^{2+}	$^7\Sigma_0^+$	1.788	1.791	1.854	1.780		

[a]Equilibrium bond distances given in angstroms. Additional computed data are given in the Appendix. [b]CASPT2 calculations, without the inclusion of spin−orbit coupling, using all electron basis set.[150] [c]Spin−orbit CASPT2 calculations using all electron basis set.[132] [d]DFT calculations using the M06 exchange-correlation functional in conjunction with the small-core pseudopotential of the Stuttgart−Cologne group for the actinides[143] and 6-311+G(2df) basis set for oxygen.[131] [e]DFT calculations using the PW91PW91 exchange-correlation functional in conjunction with the small-core pseudopotential of the Stuttgart-Cologne group for the actinides[143] and 6-311+G(2df) basis set for oxygen.[131] [f]DFT calculations using the B3LYP exchange-correlation functional in conjunction with the small-core pseudopotential of the Stuttgart−Cologne group for the actinides[143] and aug-cc-pVTZ basis set for oxygen.[135] [g]From microwave spectroscopy.[117] [h]Confirmed by high-resolution electronic spectroscopy.[119] [i]From PFI-ZEKE spectroscopy (no experimental error was given).[148] [j]From high-resolution photoelectron spectroscopy.[159]

The electronic ground states of the neutral and ionic monoxides are presented in Table 1. Only ThO and UO neutral and cation have been characterized experimentally.

The ground state of ThO was found to be a $^1\Sigma^+$ according to the measurements by Edvinsson et al.[118,136−140] based on conventional absorption and emission electron spectroscopic studies. Quantum chemical calculations performed since the late 1980s until recently have confirmed this as the nature of the ground state.[132,141−150]

The ground state of ThO^+ was determined to be a $^2\Sigma^+$ by PFI-ZEKE[148] in agreement with quantum chemical calculations.[132,148,150] In this same work, Goncharov and Heaven measured also the ro-vibrational spectra of the ground and some low-lying excited states of ThO and ThO^+ to determine their molecular constants.

The ground state of UO was detected for the first time by Heaven et al. from REMPI spectroscopic experiments.[151] The $^5I_4$ ground state was supported by the studies of Kaledin et al. using classical absorption and emission electron spectroscopy[152,153] and high-resolution electronic spectroscopy.[119] In the latter study, 33 electronic transitions of the molecule were also measured, and the ro-vibrational spectra enabled the determination of the UO molecular constants with good accuracy. The electronic spectroscopy studies of Kaledin et al. were accompanied by ligand field model[154,155] calculations characterizing the ground electronic state.[119,152,153] For this molecule, early quantum chemical works were inconsistent with the assessment of its ground state. While MCSCF calculations of Krauss and Stevens[156] resulted in the correct determination of the ^5I ground state, without the inclusion of spin−orbit coupling, single-determinant MP2[127] and B3LYP[157] studies reported erroneously $^3\Sigma$ and $^5\Gamma$ states, respectively. Paulovič et al.[158] and Infante et al.[132] predicted the correct $^5I_4$ ground state using the SO-CASPT2 method, in agreement with the experimental data.[119]

The ground electronic state of UO^+ was elucidated by high-resolution photoelectron spectroscopy,[159] which provided also the first nine electronically excited states of the ion. The rotationally resolved spectra facilitated also the experimental determination of the molecular constants. All of the quantum chemical calculations performed on UO^+, the early SO-MCSCF calculations of Krauss and Stevens[156] and the more sophisticated

DOI: 10.1021/cr500426s
Chem. Rev. 2015, 115, 1725−1759

SO-CASPT2 calculations by Paulovič et al.[158] and Infante et al.,[132] supported the $^4I_{4.5}$ ground-state assignment of UO^+.

The electronic structures of the other actinide monoxides were investigated only computationally. Two studies based on single-reference approaches, QCISD calculations on PuO[125] and B3LYP calculations on PuO^+,[128,129] reported erroneous ground states. The most reliable computational data for these and other monoxides (An = Th−Cm) including the mono and dications were determined by Infante et al. at the SO-CASPT2 level of theory.[132] Calculations at seven different DFT levels were performed on all seven monoxides by Averkiev et al.[131]

It is noteworthy that a very recent SO-CASPT2 study on the excited states of PaO^+ suggested a ground electronic state ($^3\Delta_1$)[133] different from that ($^3H_4$) reported previously.[132] The new study showed that the ^3H ground state and the first excited state ($^3\Delta$) (without the inclusion of spin−orbit coupling) lie very close in energy, and the spin−orbit coupling interactions involving additional close-lying states shift the $^3\Delta_1$ state below $^3H_4$ in energy.[133]

The neutral monoxides of late actinides (An = Bk−Lr) have recently been calculated using DFT.[135] Various electronic configurations were probed to find the lowest energy state. Previous results were available only on the simple electronic structure of LrO investigated earlier at DFT[160,161] and CCSD(T)[161] levels. All of the calculations agree on the $^2\Sigma^+$ ground state of this molecule.[135,160,161] However, we consider that the late actinides need to be studied using a multireference approach to assess their electronic structure with more precision.

3.2. Spectroscopic Constants of Actinide Monoxides

Accurate experimental bond distances are available for ThO from electronic[148] and microwave spectra,[117] for UO[119] from the analysis of the rotational fine structure in high-resolution photoelectron spectra, while for ThO^+[148] and UO^+[159] from PFI-ZEKE spectroscopy. Fairly accurate quantum chemical predictions on the bond distance and vibrational frequency of ThO in the ground electronic state are available from 1994 (cf., the Appendix). From these earlier studies, very good agreement with the experimental data was achieved by Cao et al.,[22] Buchachenco,[149] and Andrews et al.[121] using CCSD(T), while by Goncharov et al.[148] using the B3PW91 exchange-correlation functional in conjunction with the Stuttgart−Cologne small-core pseudopotential (SCPP) and large valence basis sets. ThO^+ has been calculated in two of the latter studies[121,148] with similarly good accuracy. In addition, the excellent reproduction of the experimental bond distance of ThO^+ by Mazzone et al.[162] using the B3LYP method in conjunction with the above pseudopotential and appropriate valence basis set should be mentioned. For the ThO^- anion, Andrews et al. reported sophisticated CCSD(T) calculations as part of a comparative study with ThO and ThO^+.[121] The results correspond to a considerable lengthening of the ThO bond upon electron attachment (ThO^-) and shortening upon electron removal (ThO^+). Parallel B3LYP calculations gave good agreement for the spectroscopic properties.

The other frequently investigated actinide monoxide was the open-shell UO (cf., the Appendix). From the earlier calculations both for the neutral molecule and for the UO^+ ion, the multireference SO-CASPT2 ones of Paulovič et al.[158] and the SO-CISD ones of Tyagi[163] delivered results in very good agreement with experiment. The close B3LYP bond distance of UO^+ by Michelini et al.[164] belongs to an excited electronic state.

Four recent computational studies, one on the entire actinide row[135] and the others on the early actinides (An = Th−Cm),[131,132,150] compare these species in a consistent way and provide information on the variation of the bond distances along the actinide row (vide infra). In addition, they reflect the performance of several applied theoretical models, ranging from CASPT2 to several exchange-correlation functionals within the framework of DFT (vide infra).

In Table 1, we report selected ground-state bond distances of neutral and ionic actinide monoxides, computed with different levels of theory and experimentally measured. The geometries of neutral and ionic actinide oxides (for An = Th−Cm) were obtained by Infante et al.[132] at the SO-CASPT2 level. Later, Kovács and Konings[150] evaluated the bond distances of neutral and ionic AnO (An = Th−Cm) monoxides from CASPT2 potential energy curves, without the inclusion of spin−orbit coupling. There is in general good agreement between the CASPT2 values in which SO is included[132] and those in which SO is not included.

DFT calculations utilizing the Stuttgart−Cologne small-core relativistic pseudopotentials on actinide oxides were also reported in other studies.[131,135,150] Kovács and Konings computed the neutral and cationic AnO_2 species (An = Th−Cm) using eight different exchange-correlation functionals (BLYP, B3LYP, BP86, B3P86, mPW1PW91, PBE1PBE, TPSSTPSS, HCTH).[150] Calculations on neutral and ionic An = Th−Cm monoxides and dioxides were performed by Averkiev et al. using additional density functionals (PW91, M05, M06, M06-L, MOHLYP, MPW3LYP). B3LYP calculations on neutral monoxides and dioxides of late actinides (An = Bk−Lr) were reported by Kovács et al.[135] In this same article, the authors show the trend for the whole actinide series. The bond distances of the neutral monoxides from selected theoretical levels are presented in Figure 1.

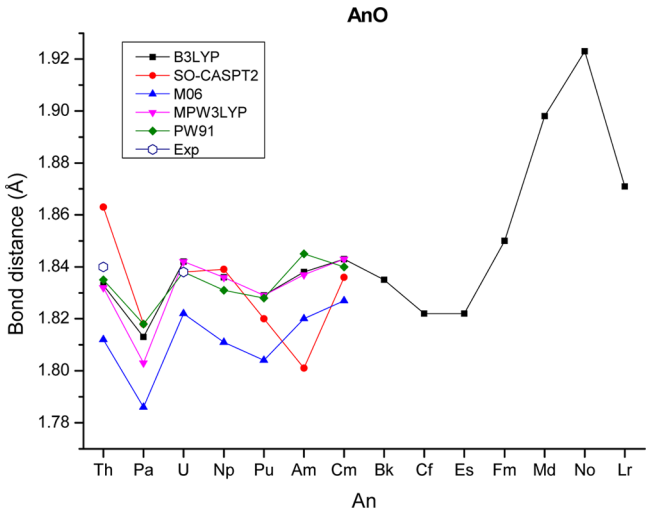

Figure 1. Bond distances of neutral actinide monoxides.

All methodologies predict the same trend in the AnO bond distance (An = Th−Cm) along the series. The DFT and SO-CASPT2 results are similar to the exception of the AmO molecule for which SO-CASPT2 predicts a shorter bond length. We note also the good agreement of the B3LYP, MPW3LYP, and PW91 data with the experimental bond distances of ThO[117] and UO,[119] indicating that these functionals in conjunction with the

DOI: 10.1021/cr500426s
Chem. Rev. 2015, 115, 1725−1759

SCPPs and triple-ζ valence basis sets provide a good AnO bond distance.

The trend in the bond distance along the series does not reflect the "actinide contraction" found for the actinide ionic radii,[165] indicating that the orbital interactions play an important role. Accordingly, the bond distances were interpreted on the basis of the population of molecular orbitals obtained at the B3LYP level of theory (cf., Figure 2):[135]

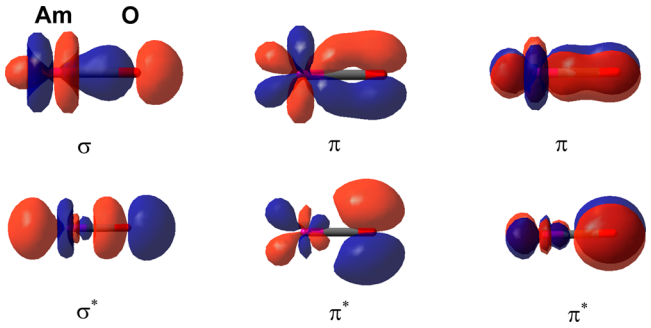

Figure 2. Characteristic bonding (σ, π) and antibonding (σ^*, π^*) Kohn–Sham orbitals of AmO.

(i) The shorter bond length of PaO with respect to ThO can be explained in terms of the contribution of the Pa 5f orbitals to the bonding, in agreement with the SO-CISD calculations by Pitzer and co-workers.[166]

(ii) The shorter bond length of PaO with respect to UO may be attributed to the closed $7s^2$ subshell of PaO in contrast to the $7s^1$ configuration in UO (closed subshells are accompanied generally by smaller radii than open ones[167]).

(iii) The bond length increase from EsO to NoO is in agreement with the gradual filling of (first π^* then σ^*) antibonding molecular orbitals.

(iv) The short bond of LrO presumably results from the stabilization effects of the closed 5f subshell.

The gas-phase vibrational frequencies and other vibrational constants of ThO[136,168] and UO[119] have been obtained from high-resolution electronic spectra, while those of ThO^+[148] and UO^+[159] are from PFI-ZEKE photoelectron spectra. Solid matrix isolation in noble gases provides higher concentrations of the species than in the vapor. IR spectroscopic measurements on species trapped in noble gas matrices have been performed for ThO,[144,169−171] UO,[157,172−174] and PuO.[175] For the other actinide monoxides, there is no direct experimental information on the vibrational frequencies, but only estimates based on the known data of the other actinide oxides or related lanthanide compounds.[123,176−179]

High-resolution electronic and photoelectron spectroscopic studies of gas-phase species usually report harmonic vibrational frequencies and first anharmonicities. Matrix-isolation IR techniques provide anharmonic frequencies of the optically active stretching fundamentals, which are usually affected by matrix shifts leading generally to lower wavenumbers than the gas-phase values. In case of the UO molecule, a strong vibronic perturbation has been observed in both the gas phase[119] and a Ne matrix.[157] A perturbation-free IR spectrum of UO could be recorded in an Ar matrix,[157] where the stronger interaction of the argon matrix with UO shifted the electronic and vibrational energy levels to positions unfavorable for vibronic interactions.

The experimental and selected computed data are presented in Table 2, while additional data are given in the Appendix. Computational studies have been performed on the following molecules: ThO,[121,141−149,180] ThO^+,[121,148] ThO^-,[121] UO,[127,156−158,181] UO^+,[156,158] PuO,[125,182,183] PuO^+,[128,129,182] PuO^{2+},[128,182] AmO,[134] AmO^+,[134] and CmO.[134] The results strongly depend on the methodologies employed and in most cases differ considerably from the available experimental results. We highlight here the sophisticated CCSD(T) calculations by Andrews et al. achieving excellent agreement with the experimental harmonic vibrational frequencies of ThO and ThO^+ as part of their systematic study on the neutral and ionic (ThO, ThO^+, ThO^-) species.[121]

A consistent benchmark for vibrational data on a large set of actinide mono- and dioxides species has been provided by two recent works.[135,150] In the first one by Kovács and Konings,[150] the vibrational stretching frequencies of the neutral and ionic AnO (An = Th–Cm) monoxides were determined by solving numerically the ro-vibrational Schrödinger equation for the potential energy curves of the ground electronic states obtained at the relativistic CASPT2 level of theory, without the inclusion of spin–orbit coupling. This procedure provided also anharmonic terms. In the second study,[135] the neutral monoxides of all of the actinides (An = Th–Lr) were computed using the B3LYP exchange-correlation functional in conjunction with SCPP and aug-cc-pVTZ valence basis sets. Inspection of Table 2 shows that there is generally good agreement with experiment, with similar trends along the actinide row.

3.3. Excited Electronic States and Electronic Spectra of Actinide Monoxides

Several theoretical studies were performed on the optical properties of actinide monoxides. The most investigated molecule both experimentally[118,136−140,184,185] and theoretically[141−143,146,147,163,180,186] is ThO. From the computational standpoint, the most sophisticated works are those by Paulovič et al.,[147] Kühle et al.,[143] and Tyagi[163] that apply relativistic multiconfigurational calculations including both dynamic electron correlations and spin–orbit effects. The experimental spectrum of the ThO molecule has been assigned from the computed electronic terms up to 19 000 cm^{-1} by Paulovič[147] and Kühle,[143] and up to 25 000 cm^{-1} by Tyagi.[163] The assignments performed by the different authors are in reasonable agreement with the experiment, while the best overall match was achieved by Paulovič et al. at the two-component SO-CASPT2/AE level of theory (cf., Table 3). Tyagi calculated also the ThO^+ low-lying excited states[163] that were later used for the assignment of the measured electronic transitions by Goncharov and Heaven.[148]

Pitzer and co-workers performed the first computational study on PaO^+, which predicted the electronic states up to 15 000 cm^{-1} based on SO-CISD calculations.[166] More recently, the absorption electronic spectra of PaO, PaO^+, and PaO^{2+} were predicted using SO-CASPT2 up to ca. 25 000 cm^{-1}.[133] This study included a detailed description of the most significant spin–orbit and spin–orbit free states for all three species, and most importantly it did not confirm the less sophisticated SO-CISD results. In particular, a different ground state for PaO^+ was suggested (vide supra in section 3.1).

The measured electronic spectrum of UO was reported in several papers.[119,151−153,187] The most complete experimental information (in the ranges of 0–5100 and 14 000–21 100 cm^{-1}) is presented in ref 119, which includes also the assignment of each peak on the basis of ligand field theory calculations.

DOI: 10.1021/cr500426s
Chem. Rev. 2015, 115, 1725–1759

Table 2. Selected Computed and Experimental Results on the Ground-State Vibrational Frequencies of Neutral and Ionic Actinide Monoxides[a]

	CASPT2[b]		B3LYP[c]	experimental	
AnO	ω_e	$\omega_e x_e$	ω_e	frequency	$\omega_e x_e$
ThO	878.9	2.3	910	ω_e = 895.77[d]	2.39[d]
				887.1 (Ne),[e] 878.8 (Ar),[f] 876.4 (Ar)[g]	1.9(9)[f]
PaO	926.7	2.1	932		
UO	857.9	1.2	844	ω_e = 846.5(6)[h]	
				889.5 (Ne),[i] 820 (Ar),[j] 819.8 (Ar),[k] 815.45 (Kr)[j]	2.5(8)[j]
NpO	899.8	3.0	836		
PuO	858.2	2.8	821	822.28 (Ar),[l] 817.27 (Kr)[l]	3.0(5)[l]
					1.7(5)[l]
AmO	872.2	3.4	781		
CmO	834.9	2.9	825		
BkO			833		
CfO			833		
EsO			825		
FmO			735		
MdO			673		
NoO			650		
LrO			756		
ThO^+	930.8	2.6	961	ω_e = 954.97(6)[m]	2.45(3)[m]
PaO^+	932.3	2.6			
UO^+	910.9	2.4	913	ω_e = 911.9(2)[n]	2.39(4)[n]
NpO^+	966.8	2.7			
PuO^+	918.5	2.2			
AmO^+	964.9	3.6			
CmO^+	951.3	2.2			
ThO^{2+}	987.6	2.7			
PaO^{2+}	1040.0	2.6			
UO^{2+}	1047.2	2.8			
NpO^{2+}	1082.0	3.4			
PuO^{2+}	1012.5	−1.0			
AmO^{2+}	810.6	6.0			
CmO^{2+}	819.5	12.3			

[a]Harmonic vibrational frequencies except for the experimental matrix-IR data and anharmonicities ($\omega_e x_e$) given in cm^{-1}. Additional computed data are given in the Appendix. [b]CASPT2 calculations, without the inclusion of spin−orbit coupling, using all electron basis set.[150] [c]DFT calculations using the B3LYP exchange-correlation functional in conjunction with the small-core pseudopotential of the Stuttgart−Cologne group for the actinides[143] and aug-cc-pVTZ basis set for oxygen.[135] [d]From high-resolution electronic spectroscopy.[136,168] [e]From matrix-isolation IR measurements.[121,144,170] [f]From matrix-isolation IR measurements.[169,171] The anharmonicity has been derived using isotope substitution experiments. [g]From matrix-isolation IR measurements.[121] [h]From high-resolution electronic spectroscopy.[119] Because of the strong perturbation effects on UO, the band in the spectrum appears at 882.4 cm^{-1}, while the ω_e value is the derived unperturbed result. [i]From matrix-isolation IR measurements.[157] The anharmonicity has been derived from isotope substitution experiments in the Ar matrix. [j]From matrix-isolation IR measurements.[172] [k]From matrix-isolation IR measurements.[157,173] [l]From matrix-isolation IR measurements.[175] The anharmonicity values have been derived for the bands measured in the Ar and Kr matrix, respectively. [m]From PFI-ZEKE spectroscopy.[148] [n]From PFI-ZEKE spectroscopy.[159]

Quantum chemical calculations on UO at the multireference SO-CISD level were performed by Tyagi,[163] who reported vertical transition energies and intensities up to 6540 cm^{-1} and adiabatic values up to 4641 cm^{-1}. These latter values confirm the assignment of the experimental data by Kaledin et al.[119] The potential energy curves of some excited states of UO were presented in two papers. The first paper describes some quintet and triplet states computed using a MCSCF approach;[181] the second study treats the lowest quintet and septet states computed at the CASPT2 level.[158] An additional experimental study dealt with two known electronic transitions of UO around 18 400 cm^{-1} in the presence of tunable static electric (Stark effect) or magnetic (Zeeman effect) fields, and determined the molecular permanent electric dipole moments and magnetic g factors.[188] The ground-state dipole moment of UO from this study (3.363 ± 0.026 D) is in reasonable agreement with a previous theoretical value of 3.86 D obtained by MCSCF calculations[181] and supports a considerable ionic character of the bonding.

Electronic transitions involving the ground and the first nine excited states of UO^+ between 0 and 5220 cm^{-1} were detected by PFI-ZEKE spectroscopy[159] (cf., Table 4). These experimental data were compared to previous theoretical predictions of the low-energy spectrum of UO^+ based on MCSCF calculations[156] and ligand field theory.[119] These predictions had considerable deviations from the experiment. The best agreement with the measured excitation energies was achieved by Tyagi at the SO-CISD level of theory (cf., Table 4), but these results lacked three states that are detected experimentally in the range of 0−5220 cm^{-1}.[163]

No experimental information is available on the excited states of the heavier actinide monoxides. A theoretical study at SO-CASPT2 level, without the inclusion of spin−orbit coupling, on

DOI: 10.1021/cr500426s
Chem. Rev. 2015, 115, 1725−1759

Table 3. Calculated Vertical Electronic Transitions[a] of ThO and Comparison to Experimental Data

state	experimental[b]	MRCI[c]	SO-CASPT2[d]	SO-CISD[e]
0^+	0	0	0	0
1	5317	5768	5549	5732
2	6128	6628	6693	6726
3	8600	8213	8408	8587
0^-		11 051	10 370	10 530
0^+	10 601	11 328	10 388	10 839
1	11 129	12 252	11 181	11 866
2		12 190	12 891	12 422
1	14 490	17 156	14 112	17 333
2		14 504	14 640	14 446
1	15 946	19 040	19 813	20 221
0^+	16 320	19 084	17 912	20 213
2	18 010	19 401	17 339	19 275
0^-		18 884	20 188	21 682
0^+				21 758
1	21 734			21 962
2				22 903
1	22 635			22 579
3				22 585
0^+	23 155			23 668
1	24 856			24 491

[a]Energies in cm^{-1}. [b]From ref 118. [c]MRCI calculations, without the inclusion of spin−orbit coupling, by Küchle et al. using the small-core pseudopotential of the Stuttgart−Cologne group for Th.[143] [d]Two-component spin−orbit CASPT2 calculations using all electron basis set.[147] [e]Spin−orbit CISD calculations by Tyagi[163] using a medium-core (68 electron) pseudopotential for Th.[295]

Table 4. Calculated Electronic Transitions[a] of UO^+ and Comparison to Experimental Data

state	experimental[b]	SO-MCSCF[c]	SO-CISD[d]
4.5	0	0	0
3.5	764.93(20)	1319	582
2.5	1132.42(20)	1895	856
1.5	1284.5(3)	2094	1076
0.5	1324.9(3)	3296	
5.5	4177.83(20)	2563	3744
4.5	4758.46(20)	3599	4180
3.5	4982.44(20)		4287
3.5	5161.96(20)	4045	
1.5		4223	
2.5	5219.37(20)	4797	4549
5.5		6488	4941
4.5		6837	5522
6.5		5459	7021
5.5		10 460	7453
4.5		10 492	8801

[a]Energies in cm^{-1}. [b]From PFI-ZEKE spectroscopic measurements by Goncharov et al.[159] [c]Spin−orbit MCSCF calculations by Krauss and Stevens using a large-core (78-electron) pseudopotential for U.[156] [d]Spin−orbit CISD calculations by Tyagi[163] using a medium-core (68-electron) pseudopotential for U.[295]

PuO, PuO^+, and PuO^{2+} reports the vertical excitation energies to low-lying excited states up to 3900 cm^{-1}.[182]

3.4. Ground-State Electronic Structure of Actinide Dioxides

Theoretical data on the ground electronic states are compiled in Table 5 for neutral and ionic AnO_2 species.

Most theoretical studies on the ground-state ThO_2 focused on the problem of its bent geometry, which differs from the linear structure characteristic of other actinide dioxides.[189−193] The bent structure of ThO_2 is stabilized by a strong 6d−5f hybridization stemming from a similar radial extent, although with distinct energies, of the 5f and 6d orbitals.[191] Accordingly, the ground state of ThO_2 is dominated by a significant 6d population,[192] unlike other isoelectronic actinide oxide ions in which the 5f is dominant.

An extensively studied molecule from both experimental and theoretical standpoints is UO_2, the electronic ground state of which has been object of debate for a long time. Early quantum chemical calculations predicted a $^3\Sigma_g^-$ ground state,[194,195] which was later replaced by a ^3H_g state.[196] Recently, theoretical investigations pointed to a $^3\Phi_{2u}$ ground state.[57,157,163,197−200] This last state has been confirmed by modern photoionization spectroscopic (REMPI) measurements on gaseous UO_2.[201,202] A characteristic feature of the electronic structure of UO_2 that has been deduced from recent calculations[57,163,197−200] and the REMPI spectra[201] is the small-energy spin−orbit splitting of the spin−orbit free ground state: the $^3\Phi_{3u}$ state indeed lies only 368 cm^{-1} above the $^3\Phi_{2u}$ ground state. The effect of this low-lying state on the electronic spectrum is discussed in section 3.6.

Once the ground state of UO_2 in the gas phase was unambiguously identified, the debate moved to the assessment of the ground state of UO_2 in noble gas matrices. Solid matrix isolation is often used to obtain spectroscopic data of molecules that are difficult to study in the gas phase. In principle, the matrix would act as an inert cage; however in the presence of a heavy element, such as uranium, it is crucial to understand whether the actinide can significantly interact with the noble gas atoms.

IR measurements on UO_2 isolated in Ar and Kr matrices[157,172−174] suggested $^3H_{4g}$ as the ground electronic state on the basis of the unexpectedly low asymmetric stretching frequency (776 cm^{-1}) as compared to the gas-phase and Ne matrix values (about 850 cm^{-1}).[157,203] The change of the ground state in the Ar and Kr matrices was attributed to stronger interactions of the lowest-energy states with the more polarizable and heavier noble gases.[174,203] These noble gas elements coordinate in the equatorial plane and stabilize the $^3\Phi_{2u}$ ground state less than some other states ($^3\Sigma^-_{0g}$, $^3H_{4g}$, $^3H_{4u}$). Energy decomposition analysis shows that the $^3\Phi_{2u}$ state is considerably destabilized due to the repulsion between the valence 3p Ar orbitals and the very diffuse 7s orbital of U, which is occupied by one electron in the $^3\Phi_{2u}$ state. The repulsion is weaker for the $^3\Sigma$ and ^3H states, in which the 7s U orbital is unoccupied and the two unpaired electrons occupy the more contracted 5f and 6d orbitals.[174,203] According to SO-CASPT2 calculations, the $^3\Sigma^-_{0g}$, $^3H_{4g}$, $^3H_{4u}$ states, which lie above the $^3\Phi_{2u}$ state by 3500−5500 cm^{-1} in the isolated UO_2 molecule, fall in energy below the $^3\Phi_{2u}$ state by 3000−6000 cm^{-1} in the $UO_2(Ar)_4$ complex.[174] DFT and CCSD(T) calculations on the $^3\Phi_{2u}$ and $^3H_{4g}$ states in $UO_2(Ar)_5$ without including spin−orbit effects gave results[203] qualitatively similar to those with SO-CASPT2 by Infante et al.[174] Unlike the results in Ar, in a Ne matrix the high-wavenumber vibrational absorption of the $^3\Phi_u$ ground state was observed experimentally.[157] The negligible interactions of UO_2 with the more inert Ne noble gas atoms suggest a behavior similar to that of the gas-phase experiment. This renders a $^3\Phi_{2u}$ ground state, as was indeed confirmed by CASPT2 calculations without including spin−orbit coupling on the $UO_2(Ne)_4$ complex.[174]

In contrast to the REMPI experiments and theoretical calculations, dispersed fluorescence spectra provide a ground

DOI: 10.1021/cr500426s
Chem. Rev. 2015, 115, 1725−1759

Table 5. Selected Computed Results on the Ground-State Bond Distances of Neutral and Ionic Actinide Dioxides[a]

AnO_2	state	SO-CASPT2[b]	M06[c]	PW91[d]	B3LYP[e]	CCSD(T)[f]	estimated[g]
ThO_2	$^1A_1$	1.923 (111.9°)	1.872 (120.8°)	1.898 (118.5°)	1.898 (119.0°)	1.905 (116.5°)	1.896
PaO_2	$^2\Sigma_{0.5g}$	1.816	1.786	1.813	1.806		
UO_2	$^3\Phi_{2u}$	1.766[h]	1.816	1.808	1.789		1.790
NpO_2	$^4H_{3.5g}$	1.761	1.795	1.803	1.767		
PuO_2	$^5\Phi_{1u}$	1.744	1.786	1.802	1.748		
AmO_2	$^6\Pi_{2.5u}$	1.807	1.800	1.827 (175.1°)	1.826		
CmO_2	$^7\Sigma_{0g}$	1.832	1.815	1.840	1.839		
BkO_2	^6X				1.820		
CfO_2	^5X				1.817		
EsO_2	^4X				1.795		
FmO_2	^3X				1.791		
MdO_2	^2X				1.812		
NoO_2	$^1\Sigma$				1.843		
LrO_2	$^2\Pi$				1.940 (101.5°)		
ThO_2^+	$^2\Sigma_{0.5u}$	1.832	1.827	1.870	1.868		
PaO_2^+	$^1\Sigma_{0g}$	1.767	1.745	1.777	1.768		
UO_2^+	$^2\Phi_{2.5u}$	1.745	1.730	1.764	1.753		1.758
NpO_2^+	$^3H_{4g}$	1.723	1.708	1.745	1.733		
PuO_2^+	$^4\Phi_{1.5u}$	1.704	1.692	1.728	1.714		
AmO_2^+	$^5\Sigma_{0g}$	1.721	1.690	1.733	1.716		
CmO_2^+	$^6\Pi_{0.5g}$	1.746	1.716	1.759	1.748		
ThO_2^{2+}	$^1\Sigma_{0g}$	1.903	1.867	1.856	1.851		
PaO_2^{2+}	$^2\Sigma_{0.5g}$	1.726	1.738	1.785	1.772		
UO_2^{2+}	$^1\Sigma_{0g}^+$	1.710	1.672	1.710	1.693	1.690	
NpO_2^{2+}	$^2\Phi_{2.5u}$	1.700	1.665	1.708	1.688		
PuO_2^{2+}	$^3H_{4g}$	1.675	1.650	1.696	1.673		
AmO_2^{2+}	$^4\Phi_{1.5u}$	1.679	1.642	1.688	1.666		
CmO_2^{2+}	$^5\Sigma_{0g}$	1.674	1.653	1.707	1.688		

[a]Equilibrium bond distances given in angstroms, bond angles different from 180.0° in parentheses. Additional computed data are given in the Appendix. [b]Spin−orbit CASPT2 calculations using all electron basis set.[132] [c]DFT calculations using the M06 exchange-correlation functional in conjunction with the small-core pseudopotential of the Stuttgart-Cologne group for the actinides[143] and 6-311+G(2df) basis set for oxygen.[131] [d]DFT calculations using the PW91PW91 exchange-correlation functional in conjunction with the small-core pseudopotential of the Stuttgart−Cologne group for the actinides[143] and 6-311+G(2df) basis set for oxygen.[131] [e]DFT calculations using the B3LYP exchange-correlation functional in conjunction with the small-core pseudopotential of the Stuttgart−Cologne group for the actinides[143] and aug-cc-pVTZ basis set for oxygen.[135] For ThO_2 and UO_2^{2+}, very close results were obtained earlier by Jackson et al. (cf., the Appendix) using a slightly different basis set.[224] [f]CCSD(T) calculations using the small-core pseudopotential of the Stuttgart−Cologne group for the actinides[143] and augmented VTZ and VQZ basis sets for ThO_2 and UO_2^{2+}, respectively.[224] [g]Estimated from available experimental vibrational frequencies.[150] [h]Spin−orbit CASPT2 calculations using all electron basis set.[197]

state of UO_2 trapped in solid Ar[204] that contradicts the reported $^3H_{4g}$ ground state.[157,174,203] The different result can be explained in terms of group theory. According to simple selection rules, electrons excited from the $^3\Phi_{2u}$ ground state can access states of g symmetry (as observed in the REMPI spectra). On the contrary, electrons excited from a $^3H_{4g}$ ground state would access states of u symmetry resulting in a considerably different pattern of optically active transitions. However, Lue et al. found a good correlation between the experimental spectra for UO_2 gas and UO_2 in solid Ar, which would not be possible if the ground state changes from u to g symmetry. In addition, the transition energies to the lowest-energy manifold in the fluorescence experiments (in the range of 0−2000 cm^{-1}) were in good agreement with the computed[198,199] and partly observed[202] energies of the low-lying $^3\Phi_{2u}$, $^3\Phi_{3u}$, $^3\Delta_{2u}$, and $^3\Delta_{1u}$ states. Thus, the dispersed fluorescence results would support the preservation of the 5f7s configuration in the Ar matrix.[204]

Although the study of Infante et al.[174] did not address the dispersed fluorescence measurements, the reported computed results provide some insights into the apparent disparities. The authors indicated that not only the $^3H_{4g}$ but also other 5f6d configurations (among them $^3H_{4u}$) can be stabilized sufficiently by Ar ligands to become the ground state in an argon matrix. This would be in agreement with the preservation of the u symmetry in the matrix. However, no information is available on the vibrational frequencies of the $^3H_{4u}$ state, specifically whether it would fit the observed 776 cm^{-1} value in Ar,[157,172,173] nor on the possible lowest energy states, and their energy positions, in the presence of matrix effects. The computations of Infante et al. addressed a few selected states only, and the calculations were performed on the geometry-constrained $UO_2(Ar)_4$ model.[174] Further high-level calculations are necessary to clarify the nature of UO_2 in an Ar matrix in which a relaxed arrangement of many more Ar atoms around UO_2 would more accurately model the matrix conditions.

The ground electronic state of UO_2^+ was examined in the gas phase using PFI-ZEKE spectroscopy.[205] The vibrational resolution of the experimental spectra facilitated the determination of the symmetric stretching and bending vibrational frequencies. From the excited electronic states, only the first one

DOI: 10.1021/cr500426s
Chem. Rev. 2015, 115, 1725−1759

was detected at 2678 cm^{-1}. Numerous theoretical studies at the scalar relativistic level indicate a $^2\Phi_u$ ground state.[131,150,157,206−209] Calculations including spin−orbit effects (SO-CASPT2[209] and IHFSCC[132]) pinpoint the experimentally determined $^2\Phi_{2.5u}$ as the ground state.

The $^1\Sigma_{0g}^+$ ground electronic state of the UO_2^{2+} ion, commonly called uranyl, originates from its stable closed-shell electronic structure.[210−212] Numerous studies reported quantum chemical calculations on its bonding and ground-state spectroscopic properties.[130−132,150,157,191,206,207,213−216]

The correct ground electronic state of NpO_2 ($^4H_{3.5g}$), along with those of its cations, was reported in the SO-CASPT2 study by Infante et al.[132] Modeling the electronic structure of neutral NpO_2 is not an easy task, as some DFT studies resulted also in $^4\Sigma_g$[130] and $^4\Phi_u$[131] ground states. The ground state of NpO_2^{2+} in solid compounds has been established from EPR experiments as $^2\Phi_{2.5}$,[217] while that of NpO_2^+ was reported from the analysis of the absorption spectra in water solution as $^3H_4$,[218] in agreement with recent SO-CASPT2 results.[132]

Among the plutonium dioxides, experimental data are available only for the PuO_2^{2+} ion. On the other hand, numerous calculations were performed on the ground-state properties of PuO_2 and PuO_2^{2+}, while only a few have been reported for PuO_2^+. The ground electronic state of PuO_2 was debated: most single-determinant studies gave a ground state ($^5\Sigma_g^+$)[21,130,131,182,219] different from more sophisticated SO-CASPT2 calculations ($^5\Phi_{1u}$).[132,182] The theoretical determinations of the $^4\Phi_{1.5u}$ and $^3H_{4g}$ ground states of PuO_2^+[131,132,182] and PuO_2^{2+},[58,130,131,182,215,220,221] respectively, were more consistent among different methodologies. In addition, calculations confirmed the $^3H_4$ ground state of PuO_2^{2+} that was obtained by electron spin resonance[217] and spectroscopic measurements[222] in matrix environments.

The computed ground-state electronic structures of americium and curium dioxides have been reported only recently. Kovács et al. determined the ground states of AmO_2 and CmO_2 using CASPT2 calculations, without the inclusion of spin−orbit coupling.[134] More recently, these values were further extended with the inclusion of the spin−orbit coupling term and the assessment of the mono- and dicationic forms.[132] Ground electronic states for AmO_2^{n+} (n = 1,2,3) ions have been reported also by Notter et al.[223] using various multireference (CASSCF, CASPT2, CISD) and DFT (BLYP, B3LYP, PW91) calculations. The electronic structures of AmO_2^+ and AmO_2^{2+} agree with those from other studies.[131,132,134] On the other hand, this is the only study that reports the $^3H_{4g}$ ground state of AmO_2^{3+}.

The neutral dioxides of late actinides (An = Bk−Lr) have recently been calculated using the B3LYP exchange-correlation functional.[135] Various electron configurations were probed to find the lowest energy state.

3.5. Spectroscopic Constants of Actinide Dioxides

Calculations predict a linear molecular structure for all dioxides except for neutral ThO_2 and LrO_2. These two molecules are bent with computed bond angles of around 120° and 100°, respectively (cf., Table 5).

Bond distances of the neutral molecules from selected theoretical results are presented in Figure 3. Most curves for the early actinides (An = Th−Cm) are in close correspondence. The divergence between the DFT and SO-CASPT2 curves for UO_2, NpO_2, and PuO_2 is presumably due to the incorrect ground electronic states predicted at the M06 DFT level.[131,132] Very likely also the NpO_2 and PuO_2 structures computed at the

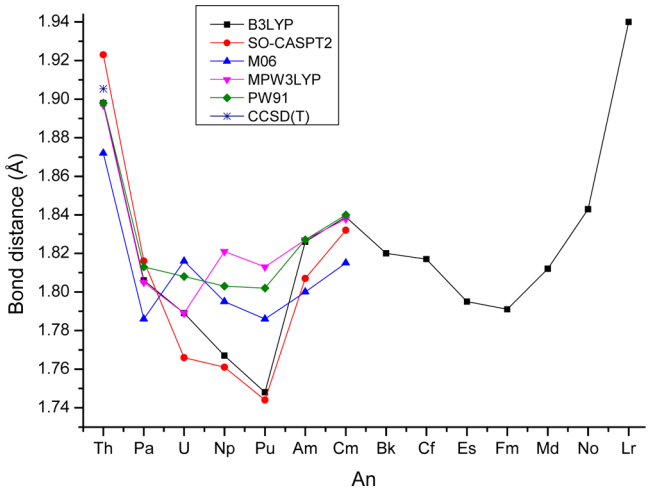

Figure 3. Bond distances of neutral actinide dioxides.

MPW3LYP and PW91 levels present discrepancies, although this could not be established in ref 131 due to symmetry breaking effects. The best agreement with the SO-CASPT2 bond distances can be observed at the B3LYP level, with differences being around (or smaller than) 0.01 Å for PaO_2, NpO_2, PuO_2, and CmO_2. In case of ThO_2, UO_2, and AmO_2, the B3LYP bond distances differ by ca. 0.02 Å from the SO-CASPT2 values. We note that for UO_2 two considerably different bond distances have been reported. We recommend here the value of 1.766 Å from an SO-CASPT2 calculation performed with a larger basis set and active space[197] with respect to the value of 1.827 Å from refs 132 and 197. The former value is also supported by four-component DC-IHFSCCSD calculations, which predict a bond distance of 1.770 Å.[57]

CCSD(T) calculations have been performed for the closed-shell ThO_2,[192,224] PaO_2^+,[192] and UO_2^{2+}[192,214,224] molecules. The two earlier studies[192,214] suffered from the relatively small basis set (limited by the technical facilities of that time) resulting in too long equilibrium bond distances. The computations on ThO_2 and UO_2^{2+} by Jackson et al.[224] applying augmented valence triple- (aVTZ) and quadruple-ζ (aVQZ) basis sets represent the highest-level calculations hitherto on actinide dioxides. Hence, these are presently the most reliable theoretical geometries for the two molecules (given in Table 5 and the bond distance of ThO_2 in Figure 3). From the other five theoretical levels given in Figure 3, the B3LYP, MPW3LYP, and PW91 bond distances of ThO_2 are in good agreement with the CCSD(T) value, while the SO-CASPT2 bond distance is overestimated by 0.02 Å. The similar overestimation for UO_2^{2+} (cf., Table 5) may imply such an error of SO-CASPT2 for closed-shell actinide systems.

Recently, Andrews et al. detected new Th oxide species, ThO_2^-, Th_2O_2, and Th_2O_4, which originate from the reaction of laser ablated Th and molecular oxygen in Ne and Ar matrices;[121] this novel identification was made possible by CCSD(T) and B3LYP calculations. In this same study, several additional oxides (ThO, ThO^+, ThO^-, ThO_2, ThO_2^+, Th_2O, Th_2O_3) were also computed.

In the absence of experimental data, it is difficult to assess the reliability of the computed geometries. However, some insights can be gained from the IR spectra of matrix isolated Th, U, Pu dioxides. From ^{18}O isotope substitution experiments and normal coordinate analysis, a bent structure was deduced for ThO_2 with a bond angle of 122.5° ± 2°.[169] This value is slightly larger than the bond angle obtained by recent quantum chemical

DOI: 10.1021/cr500426s
Chem. Rev. 2015, 115, 1725−1759

calculations.[121,131,150,224] (We note that a previous experimental value from a lower resolution IR spectrum was 106°.[225]) For the other dioxides, UO_2, UO_2^+, and PuO_2, linear structures were deduced in agreement with the calculations.[172,175]

For estimation of the experimental equilibrium bond distances of some AnO_2 species, it is possible to follow the empirical method developed by Kovács and Konings, who have observed a linear correlation between the computed bond distances and measured vibrational frequencies.[150] The approach was validated on the known accurate gas-phase geometries and frequencies for ThO, ThO^+, UO, and UO^+ (vide infra). It could be shown that this method can provide reliable data (geometry or frequency) when the counterpart information (frequency or geometry) is accurately known.

The reported vibrational frequencies of ThO_2 and UO_2 isolated in various noble gas matrices[144,157,169−173] were used for estimation of the bond distances in these molecules.[150] First, the matrix-IR data were extrapolated using the observed matrix shifts to estimate the gas-phase values of the stretching vibrational frequencies. Using the correlation between the bond distances and gas-phase vibrational frequencies, the equilibrium bond distances of 1.896 and 1.790 Å were predicted for ThO_2 and UO_2, respectively. These predicted values are in very good agreement with the bond distances 1.898 and 1.789 Å, respectively, obtained by the B3LYP exchange-correlation functional in conjunction with the Stuttgart−Cologne small-core pseudopotentials and polarized triple-ζ valence basis sets,[150] while the agreement is slightly worse with the CCSD(T)/aVTZ result on ThO_2 (1.905 Å), which, however, would probably somewhat decrease with larger basis set as the benchmark study on UO_2^{2+} showed.[224] Similar good performance of the model was found in the case of UO_2^+ (not given in Figure 3), for which the bond distance estimated from the correlation with the vibrational frequencies was 1.758 Å, while the B3LYP computed value was 1.753 Å (cf., Table 5).

A consistent set of data for the whole actinide row is available only from B3LYP calculations. In agreement with other computed data for An = Th−Cm, in Figure 3 it is possible to discern a double-well trend for the An−O bond lengths along the whole An series. The most characteristic features of these curves are interpreted on the basis of the population of valence Kohn−Sham orbitals from B3LYP calculations (cf., Figure 4):[135]

(i) The gradual decrease from PaO_2 to PuO_2 is in agreement with the contraction of the ionic radii from Pa to Pu. Thus, the "actinide contraction" seems to appear in these dioxides showing very similar bonding interactions. The only notable difference in the population of the valence orbitals is the gradual occupation of the nonbonding 5f orbitals from PaO_2 to PuO_2, which do not significantly influence the bonding or the bond distances.

(ii) The increased bond distances from AmO_2 to NoO_2 with respect to those from PaO_2 to PuO_2 can be explained by the depopulation of the $7s^1$ electron (present in PaO_2−PuO_2) in favor of the π_u^* antibonding orbital in AmO_2−NoO_2.

(iii) The increase from FmO_2 to NoO_2 is in agreement with the gradual filling of the π_u^* antibonding orbitals.

(iv) The considerably longer bond distances of the bent ThO_2 and LrO_2 molecules are consistent with their double-bond character and the steric repulsion between the oxygen atoms.

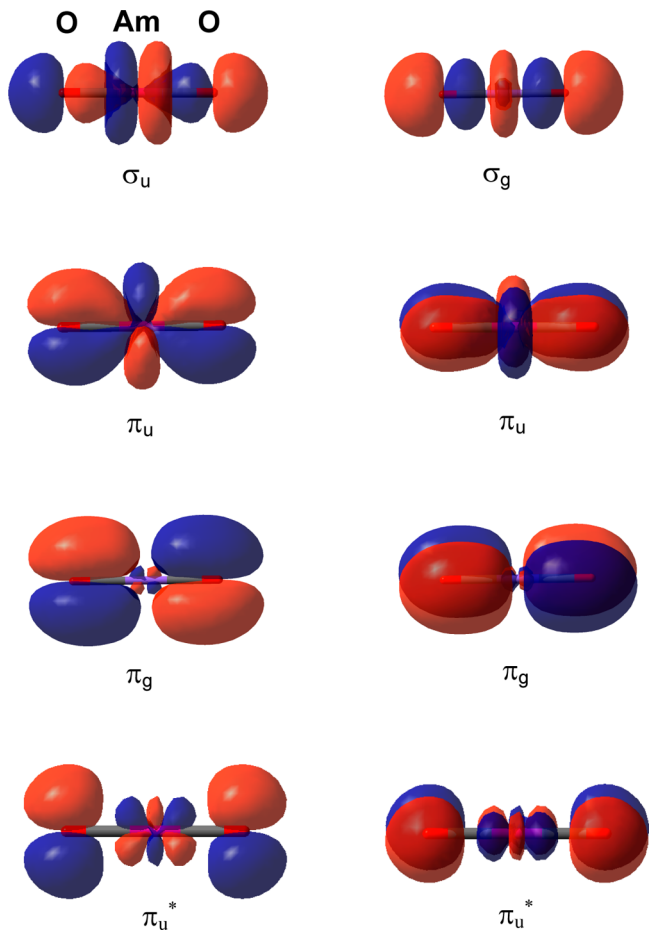

Figure 4. Characteristic bonding (σ, π) and antibonding (σ^*, π^*) Kohn−Sham orbitals of AmO_2.

For some actinide dioxide species, information is available on the geometries of excited states computed in the few studies dealing with adiabatic electronic transitions. Such data were reported for UO_2^{2+} from SO-MRCI,[226] SO-CASPT2,[227] SO-TDDFT[228] and TDDFT, LR-CCSD, SO-LR-CCSD[216] studies, while for NpO_2^{2+} from SO-MRCI,[226] and for PuO_2^{2+} from CASSCF, AQCC,[215] and CISD+Q calculations.[220]

Information on vibrational frequencies of gaseous actinide dioxides has been reported from high-resolution photoelectron spectroscopic studies of UO_2[201] and UO_2^+,[205] and by IR spectroscopy of ThO_2,[144,169,170,171] UO_2,[157,172,173,174] UO_2^+,[157,173,208] and PuO_2[175] in solid matrices. Recently, fundamental bands of some new Th oxide species (ThO_2^-, Th_2O_2, and Th_2O_4) isolated in Ne and Ar matrices have been reported by Andrews et al.[121] The assignment was based on CCSD(T) and B3LYP calculations. In this same study, the harmonic fundamental frequencies of several additional oxides (ThO, ThO^+, ThO^-, ThO_2, ThO_2^+, Th_2O, Th_2O_3) have also been computed.

A few paragraphs above we described how the matrix-IR data of ThO_2, UO_2, and UO_2^+ were used to estimate the bond distances of these molecules. Some matrix-IR data are available also for PuO_2, but this case is less straightforward as the experimental information is much more limited.[175] Moreover, the experimental frequency (794 cm^{-1}) is considerably lower than the frequency calculated for the $^5\Phi_{1u}$ ground electronic state (933 cm^{-1}), suggesting an important interaction between the trapped molecule and the solid matrix.[150] SO-CASPT2

DOI: 10.1021/cr500426s
Chem. Rev. 2015, 115, 1725−1759

Table 6. Selected Computed and Experimental Results on the Ground-State Vibrational Frequencies of Neutral and Ionic Actinide Dioxides[a]

AnO_2	computed[b] ω_{as}, ω_s, ω_β	empirical[c] ν_{as}, ν_s, ν_β	experimental frequency
ThO_2	756.0, 807.7, 165.3	762, 813, 151	ν_{as} = 756.9, ν_s = 808.7 (Ne),[d] ν_{as} = 735.0, ν_s = 787.3 (Ar)[e]
	766, 820, 155		
PaO_2	871, 828, 59	852, 899, 82	
UO_2	926, 874, 141	920, 865, 136	ν_β = 121,[f] ν_{as} = 914.8 (Ne),[g] 776 (Ar),[h] 776.10 (Ar), 767.95 (Kr)[i]
NpO_2	933, 874, 194	939, 880, 185	
PuO_2	933, 863, 183	934, 862, 184	ν_{as} = 794.2 (Ar), 786.8 (Kr)[j]
AmO_2	795, 740, 90	815, 757, 105	
CmO_2	779, 720, 96	778, 721, 90	
BkO_2	791, 725, 152		
CfO_2	795, 716, 183		
EsO_2	816, 738, 213		
FmO_2	816, 730, 221		
MdO_2	789, 703, 182		
NoO_2	753, 668, 170		
LrO_2	686, 271, 114		
ThO_2^+	752, 631, 38	623, 780, 51	
PaO_2^+	995, 938, 108	989, 931, 108	
UO_2^+	1005, 937, 151	985, 916, 144	ω_s = 921(4), ω_β = 145.5, $\omega_s x$ = 2.0(22), $\omega_\beta x$ = 0.3[k] ν_{as} = 980.1 (Ne),[g,l] 952.3 (Ar),[h,l] 940.6 (Kr),[h,l] 929.0 (Xe)[l]
NpO_2^+	1015, 937, 210	1023, 947, 215	
PuO_2^+	1019, 927, 255	1027, 938, 261	
AmO_2^+	997, 876, 267	970, 851, 262	
CmO_2^+	884, 755, 193	870, 752, 192	
ThO_2^{2+}	772, 755, 126	727, 695, 107	
PaO_2^{2+}	891, 626, 94	594, 961, 144	
UO_2^{2+}	1113.0, 1031.6, 174.5	1124, 1045, 162	
	1135, 1044, 166		
NpO_2^{2+}	1126, 1019, 184	1085, 977, 154	
PuO_2^{2+}	1117, 997, 251	1102, 984, 237	
AmO_2^{2+}	1089, 948, 306	1045, 906, 291	
CmO_2^{2+}	957, 768, 304	964, 783, 309	

[a]The vibrational frequencies (ω and ν meaning harmonic and anharmonic, respectively) are given in cm^{-1}. The notations as, s, and β mean asymmetric stretch, symmetric stretch, and bend, respectively, while ωx is the anharmonicity. Additional computed data are given in the Appendix. [b]For ThO_2 and UO_2^{2+}, the first sets of computed frequencies represent very high-level CCSD(T) anharmonic frequencies corrected also for spin−orbit coupling (basis sets augmented VTZ and augmented VQZ for ThO_2 and UO_2^{2+}, respectively).[224] The other listed data represent a consistent set of harmonic vibrational frequencies obtained using the B3LYP exchange-correlation functional in conjunction with the small-core pseudopotential of the Stuttgart−Cologne group for the actinides[143] and aug-cc-pVTZ basis set for oxygen.[135,150] For ThO_2 and UO_2^{2+}, very close results were obtained earlier by Jackson et al. (cf., the Appendix) using a slightly different basis set.[224] [c]The empirical anharmonic frequencies refer to gaseous phase and have been evaluated using available experimental and/or DFT computed frequencies.[150] For UO_2^{2+}, the empirical frequencies re-evaluated in this Review based on a recent more reliable CCSD(T)/aVQZ bond distance[224] are given in the table; the ones from ref 150 are 1082, 987, 127 cm^{-1}, respectively. [d]From matrix-isolation IR measurements.[121,144,170] [e]From refs 121,169,171. [f]Gas-phase value of the bending vibration from resonance enhanced multiphoton ionization (REMPI) measurements.[201] [g]From matrix-isolation IR measurements.[157] [h]From ref 173. [i]From ref 172. [j]From matrix-isolation IR measurements.[175] [k]Gas-phase values from PFI-ZEKE measurements.[205] [l]From matrix-isolation IR measurements.[208]

computations indicated that some excited states with dominant $^5\Sigma_g^+$ contribution, without the inclusion of spin−orbit coupling, are very close in energy to the $^5\Phi_{1u}$ ground state.[182] Like the UO_2 case, it may be possible that upon interaction with the Ar and Kr noble gas atoms the $^5\Sigma_g^+$ states are more stabilized, and therefore one of those can become the ground state.[21,150] The CCSD(T)/LCPP calculations of Archibong and Ray (using the harmonic approximation) indicated that the asymmetric stretching frequency of the $^5\Sigma_g^+$ state is slightly lower than that of the $^5\Phi_u$ state.[21] Further studies, particularly measurements in a Ne matrix or gas phase, are necessary to clarify this issue.

Several quantum chemical calculations performed at various levels of theory reported vibrational frequencies for ThO_2,[144,170,191,224] PaO_2^+,[191] UO_2,[126,130,157,197,203,207] UO_2^+,[157,206−208] UO_2^{2+},[130,157,191,206,207,214,215,224] NpO_2,[130] NpO_2^{2+},[130] PuO_2,[21,130,182,183,219] PuO_2^+,[182] and PuO_2^{2+}.[130,182,215,220,221] These results are given in the Appendix. The frequency values depend strongly on the computational level (and on the electronic state) and in most cases differ considerably from the available experimental results. We note here the sophisticated results of Jackson et al.[224] on ThO_2 and UO_2^{2+}. Their anharmonic stretching frequencies of ThO_2 obtained by CCSD(T) in conjunction with small-core RECP (including SOC) and augmented valence triple-ζ basis set approached the experimental (Ne matrix) data within a few cm^{-1}.

The first systematic study on the vibrational frequencies of the dioxides (An = Th−Cm) was performed by Kovács and Konings[150] using eight different exchange-correlation functionals. To obtain the most reliable frequency values, a composite method was applied. Very good correlation was observed between the vibrational frequencies and bond distances calculated at the various DFT levels. This correlation facilitated the estimation of either the frequency or the bond distance when the other is known.[150]

DOI: 10.1021/cr500426s
Chem. Rev. 2015, 115, 1725−1759

Table 7. Proposed Assignments of the REMPI Spectrum[a] of UO_2 on the Basis of Various Computations

experimental			SO-CI[b]		SO-CASPT2[c]		SO-CISD[d]		DC-IHFSCC[e]	
term energy	transition energy	lower state	energy	assignment	energy	assignment	energy	assignment	energy	assignment
0			0	2u	0	2u		2u	0	2u
360			431	3u	378	3u	439	3u		3u
1094	1094	2u			2567	1u	1037	1u		1u
1401	1401	2u			2908	2u	1587	2u		2u
17 859	17 499	3u	20 261	3u → 4g	15 452	3u → 2g	16 542	2u → 1g	17 516	3u → 4g
18 159	18 159	2u	20 262	2u → 1g	16 725	2u → 1g	17 328	3u → 4g	16 625	3u → 3g
18 587	18 227	3u			17 274	3u → 4g	19 613	2u → 1g	17 340	3u → 2g
18 423	18 423	2u	20 938	2u → 1g	17 645	2u → 1g	18 935	2u → 3g		2u → 1g
					23 277	3u → 4g				
					24 859	2u → 3g				
					24 964	3u → 2g				
27 259	27 259	2u	25 471	2u → 2g	26 349	2u → 1g	27 661	2u → 3g	21 247	3u → 1g
~29 060	~28 700	3u			26 617	3u → 2g	28 885	3u → 2g		3u → 2g
					28 121	3u → 4g				
30 014	29 654	3u					29 623	3u → 4g		
29 700	29 700	2u	26 222	2u → 2g	28 124	2u → 1g	29 670	2u → 1g	32 071	3u → 2g
31 838	31 478	3u			36 770	3u → 3g	34 245	3u → 3g	31 125	3u → 2g
31 838	31 838	2u	33 092	2u → 2g	36 783	2u → 2g	34 625	2u → 2g	31 203	2u → 3g

[a]Energies in cm^{-1}. The transition energies are the observed ones, term energies (when different) were deduced on the basis of the starting state (2u or 3u) of the transition.[202] The computed energy values refer to term energies. [b]Spin−orbit CI calculations by Chang et al.[198] [c]Spin−orbit CASPT2 calculations by Gagliardi et al.[199] using all electron basis set. [d]Spin−orbit CISD calculations by Tyagi[163] using a medium-core (68-electron) pseudopotential for U.[295] [e]Four-component (including SOC) calculations by Infante et al.[57] using all electron basis set.

Empirical frequency values for the SO-CASPT2 bond distances[132] (except for ThO_2) were derived from linear regression equations fitted to the DFT data (frequency vs bond distance). The approach was tested on ThO, ThO^+, UO, and UO^+ and provided excellent agreement with accurate gas-phase data: the frequencies estimated on the basis of the experimental bond distances were within 2 cm^{-1} of the actual experimental gas-phase values for ThO and UO, while for ThO^+ and UO^+ (with less accurate experimental bond distances) the differences were still very small, 14 and 8 cm^{-1}, respectively.[150] The reliability of the estimated frequencies for the other actinide dioxides, however, depends on the reliability of their SO-CASPT2 bond distances, for most of which unfortunately no information is available.

The CCSD(T)/aVQZ calculations on UO_2^{2+} by Jackson et al.[224] have provided a more accurate geometry for this closed-shell molecule. This bond distance differs by 0.02 Å from the SO-CASPT2 one. To get the most reliable prediction for the fundamentals of UO_2^{2+}, we re-evaluated in this Review its empirical frequencies using the CCSD(T) bond distance as reference. These new data are given in Table 6, showing good agreement with the CCSD(T) frequencies.[224]

We also checked whether the estimated frequencies would confirm two tentative vibrational assignments for the matrix-IR spectra of plutonium oxides measured by Green and Reedy.[175] Using isotopic ^{18}O substitution, they have suggested that the pattern found in the experiment was in agreement with the presence of AmO_2 (as impurity) and PuO_2^+ as the most suitable candidates. This assignment is, however, most likely incorrect. The two bands of the $An^{16}O_2$ species appear in the spectrum at 954.18 and 857.75 cm^{-1} (in Ar matrix). On the other hand, the estimated anharmonic frequencies of the asymmetric stretch of AmO_2 and PuO_2^+ are 815 and 1027 cm^{-1}, respectively (cf., Table 6).[150] If we take into account a typical ca. 30 cm^{-1} matrix shift for Ar, these bands would shift at most to 785 and 1000 cm^{-1}, respectively. It is clear that these values deviate considerably from the observed wavenumbers, such that the assignment of the experimental bands to AmO_2 and PuO_2^+ is rather unlikely. However, as also observed for uranium dioxides, it is possible that these species are still present in the matrix but with different ground-state electronic structures than in the gas phase.

The vibrational frequencies of some excited states of three dioxide species were computed in studies on adiabatic electronic transitions. These data have been obtained for UO_2^{2+} by SO-MRCI,[226] SO-CASPT2,[227] SO-TDDFT,[228] and SO-LR-CCSD,[216] for PuO_2 by CCSD, CCSD(T), and CASSCF,[21] and for PuO_2^{2+} by CASSCF calculations.[215]

3.6. Excited Electronic States and Electronic Spectra of Actinide Dioxides

Neither gas-phase experimental nor theoretical studies have been reported on the electronic spectra of neutral and ionic ThO_2 species. However, it can be assumed that the stable closed-shell ground electronic structures of ThO_2 and ThO_2^{2+} will not allow excitations below 20 000 cm^{-1}.[229]

The excited states and absorption electronic spectra of PaO_2 and its mono- and dications were calculated recently using the SO-CASPT2 method up to ca. 40 000 cm^{-1}.[133] Lacking experimental data, this is the only information on the electronic transitions of these species.

The excited states and the electronic spectra of neutral and ionic UO_2 have been investigated extensively. An interesting feature of the electronic spectrum of UO_2 is that the first excited state ($^3\Phi_{3u}$) lies only 360 cm^{-1} above its spin−orbit coupled partner $^3\Phi_{2u}$ (ground state).[57,163,197−201] The two types of experimental spectroscopic studies on UO_2 provided only partial electronic spectra: the gas-phase REMPI experiment provided a narrow range of energies above the ground state in the 17 000−19 000 and 27 000−32 000 cm^{-1} ranges.[202] Photoionization efficiency (PIE) curves were also recorded to distinguish between the close-lying 2u ($^3\Phi_{2u}$) and 3u ($^3\Phi_{3u}$) states.

DOI: 10.1021/cr500426s
Chem. Rev. 2015, 115, 1725−1759

Information in the 0−2000 and the 15 000−27 000 cm^{-1} intervals was provided in solid Ar[204] by dispersed fluorescence spectra, which, however, might suffer from matrix effects discussed above in section 3.4.

Beyond the problem of the identification of the correct ground electronic state for UO_2 (vide supra), several theoretical studies dealt with the determination of its electronic spectrum. Two early studies were restricted only to low-lying transitions: the three lowest states were calculated at the relativistic Hartree−Fock−Slater level,[196] while several more low-energy states (up to 4200 cm^{-1}) were characterized by SO-CASPT2 calculations using a small active space.[197] Subsequently, more detailed theoretical studies were performed using different theoretical methodologies: SO-CI,[198] SO-CASPT2,[199] SO-CISD,[163] and DC-IHFSCC.[57] The first assignment of the REMPI spectrum (between 17 400−32 000 cm^{-1}) was provided by Han et al.,[202] based on early computational data by Chang.[198] However, subsequent more sophisticated calculations[57,163,199] provided several revisions to these assignments. The most accurate assignments based on different approaches are compared in Table 7.

The data in Table 7 indicate a good agreement between the SO-CASPT2 results of Gagliardi et al.[199] and the experimental data. Although there are some discrepancies between computed and experimental energies, the SO-CASPT2 results reproduce extremely well the lowest 2u and 3u states, as determined by the photoionization efficiency curves.[202] The less sophisticated SO-CI study by Chang[198] shows considerable deviations from the experimental energies as well as for the characters of excited states, but a few low-lying transitions that could be correlated with experiment have the correct order. The best numerical agreement with the experimental energies, most likely due to compensation of errors, was obtained by Tyagi at the SO-CISD level;[163] however, this method resulted in some incorrect lower states and also differed from the SO-CASPT2 results for several excited states.

Altogether, the SO-CASPT2 study of Gagliardi et al.[199] was demonstrated as the most successful in describing the UO_2 electronic spectra. Unfortunately, this computed spectrum is not complete as the uranium 6d orbitals had to be omitted from the active space. Nevertheless, it covered the symmetry-allowed u → g excitations corresponding to the 5f7s → 5f7p promotions from the ground 2u (and its spin−orbit pair 3u) state. The authors proposed also three additional intense transitions around 24 000 cm^{-1}, a range not covered by the experiments.[202]

The DC-IHFSCC study of Infante et al.[57] provided more excited states than the studies discussed above, because it considered also the 6d orbitals in the computations. Some of the DC-IHFSCC excitation energies are in excellent agreement with experiment, but there are also a few considerable deviations (cf., Table 7). In addition, the lower states of the transitions to the 16 625, 21 247, and 32 071 cm^{-1} computed states contradict the experimental information from ref 202, most likely because only vertical transitions were considered in the calculations.

The excited states of UO_2^+ were investigated theoretically at the SO-CASPT2[209] and DC-IHFSCC[57] levels up to 33 000 and 20 000 cm^{-1}, respectively. The gas-phase PFI-ZEKE experiment[205] located only the first excited state at 2678 cm^{-1}. The DC-IHFSCC calculations by Infante et al.[57] reproduced the energy of this first excited state within 58 cm^{-1}, while the SO-CASPT2 calculations underestimated it by 400 cm^{-1}.[209] The vertical excitation energies from the two computational studies, however, agree reasonably well with each other in the 0−10 000 cm^{-1} range. A similar reasonable agreement was obtained by comparison with the data of UO_2^+ in aqueous solution.[230,231]

Several experimental and theoretical studies were performed on AnO_2^{2+} actinyl ions (An = U, Np, Pu, Am); this is the most common form in which uranium is found in aqueous solutions, and is also an important species for neptunium, plutonium, and americium. The large number of studies on these species is largely motivated by the need for information on the properties of soluble hexavalent actinide compounds, which are very important for nuclear waste disposal and environmental transport. The electronic spectra of various AnO_2^{2+} derivatives were measured in acidic solutions, but also inside crystals where the AnO_2^{2+} ions are coordinated by anionic ligands in equatorial positions. The interactions with these ligands are generally dominated by relatively weak electrostatic interactions that were not expected to considerably change the electronic structure of the AnO_2^{2+} moiety. Accordingly, these experimental data can provide useful information on the electronic structure of AnO_2^{2+} ions, while computations of the isolated ions can be used to assist the assignment of the experimental spectra.

Among the actinyls, the most important is the uranyl ion. Many published works have reported and interpreted its electronic spectra (see, e.g., refs 210, 211, and 232−239) as well as calculated its electronic structure (see, e.g., refs 130, 132, 157, 191, 206, 207, 213−216, and 240). Early experimental and theoretical studies are reviewed in refs 212, 222, 241, and 242, while recent ones are in ref 243.

The excited states of uranyl and its complexes were investigated in detail in several quantum chemical studies. The ground and excited electronic states of the free uranyl ion UO_2^{2+} were computed for the first time by Zhang and Pitzer, who used a relativistic core and spin−orbit potentials and a multireference graphical unitary group configuration interaction approach.[244] Two extensive benchmark calculations reported the performance of various quantum chemical methods for excited states of the UO_2^{2+} ion. Réal et al. tested several wave function (LR-CCSD, CASSCF/CASPT2, MRCI, AQCC) and TDDFT methods with B3LYP, BHLYP, CAM-B3LYP exchange-correlation functionals.[216] They pointed out the main differences of the various methods on the vertical and adiabatic excitation energies, but in the absence of gas-phase reference experimental data they did not make any conclusions about the accuracy of the computed data. Tecmer et al. compared the performance of TDDFT in conjunction with several exchange-correlation functionals (LDA, PBE, BLYP, B3LYP, PBE0, M06, M06-L, M06-2X, CAM-B3LYP) using reference data from IHFSCC calculations.[240] From these studies, the M06, PBE0, and especially CAM-B3LYP functionals were recommended for quantitative studies of actinide spectroscopy. In addition, an assessment of CASPT2 was also performed, and semiquantitative agreement with IHFSCC was found.

The adiabatic electronic transitions in UO_2^{2+} and $UO_2Cl_4^{2-}$ have been calculated in three studies. Matsika and Pitzer[226] used a layer-cluster method to model the electronic spectrum of $Cs_2UO_2Cl_4$, which was previously recorded by Flint and Tanner[237] and analyzed by Denning et al.[210,212] The cluster contained 1873 atoms, but only the middle actinyl ion, the closest chloride, and cesium ions were treated explicitly at the SO-MRCI level, while the remaining ions were substituted by point charges. These studies seemed to confirm the suggestion,

DOI: 10.1021/cr500426s
Chem. Rev. 2015, 115, 1725−1759

Table 8. Calculated Electronic Transitions and Symmetric U−O Stretching Frequencies[a] of UO_2^{2+} and $UO_2Cl_4^{2-}$ and Comparison to Available Experimental Data

		exp.[b]		SO-CASPT2[c]		SO-TDDFT[d]		SO-MRCI[e]		CAM-B3LYP[f]	IHFSCC[g]
	state	T_e	ω_e	T_e	ω_e	T_e	ω_e	T_e	ω_e	T_e	T_e
UO_2^{2+}	0^+_g			0	974	0	984	0	1103	0	0
	2_g			17 227	815	17 909	847	21 421	845	11 805	11 105
	3_g			18 239	811	18 933	847	22 628	847	11 805[h]	11 105[h]
	1_g			18 888	847	22 022	854	20 719	867	13 215	12 296
	2_g			20 911	844	23 569	854	23 902	900	17 084	14 426
	3_g			24 026	843			26 118	898	15 135	12 303
	4_g			24 190	808	24 637	822	27 893	880	17 084[h]	14 426[h]
	1_g			26 259	797					20 461	17 593
	3_g			26 446	767			31 710		18 896[h]	17 659[h]
	4_g			26 500	786						
	2_g			27 923	627					18 896	17 659
$UO_2Cl_4^{2-}$	A_g	0	832	0	819	0	803	0	968		
	B_{2g}	20 095.7	714.8	20 028	712	20 059	733	20 364	885	18 119	18 128
	B_{3g}	20 097.3	714.6					20 363	885	18 120	18 124
	B_{1g}	20 406.5	710.3	20 330	703	19 908	732	21 013	879	17 913	18 816
	A_g	21 316	696	21 139	698	20 308	739	21 838	878	18 236	19 492
	B_{2g}	22 026.1	712	21 809	711	21 088	739	22 808	874	19 494	20 760
	B_{3g}	22 076	710					22 830	874	19 475	20 768
	A_g	22 406	717	22 984	721	21 605	741	21 618	902	20 494	21 848
	B_{1g}	22 750	711	23 228	714	21 693	740	24 780	900	20 808	21 905
	B_{2g}	26 197.3	724.7	26 534	722			26 763	903	24 711	25 185
	B_{3g}	26 247.6	724.3					26 871	904	24 698	25 201
	B_{1g}	27 719.6	708	28 527	703			29 169	896	26 014	27 634
	A_g	27 757	705.4	28 530	703			29 145	890	26 017	27 637

[a]Transition energies and vibrational frequencies are given in cm^{-1}. For computed fundamental frequencies of ground-state UO_2^{2+}, see the Appendix. [b]From ref 212. The spectroscopic terms correspond to D_{2h} symmetry. [c]Adiabatic transitions from spin−orbit CASPT2 calculations by Pierloot and van Besien[227] using all electron basis set. For $UO_2Cl_4^{2-}$, D_{4h} symmetry has been applied. [d]Adiabatic transitions from spin−orbit time-dependent DFT calculations by Pierloot and van Besien[228] using all electron basis set. For $UO_2Cl_4^{2-}$, D_{4h} symmetry has been applied. [e]Adiabatic transitions from spin−orbit MRCI calculations by Matsika and Pitzer[226] using a large-core (78-electron) pseudopotential for U.[296] [f]Vertical transition energies from CAM-B3LYP calculations on pure UO_2^{2+} (model a) and FDE embedded $UO_2Cl_4^{2-}$ with relaxation of nearest Cs atoms (model f).[247] [g]Vertical transition energies from IHFSCC calculations on pure UO_2^{2+} (model a) and FDE embedded $UO_2Cl_4^{2-}$ with relaxation of nearest Cs atoms (model f).[247] [h]Tentative assignment.

based on the experimental spectra, that the energies of the low-lying excited states are relatively independent of the presence and nature of the equatorial ligands.[233] The comparative SO-MRCI calculations on UO_2^{2+} and $UO_2Cl_4^{2-}$ showed fairly small (at most 2000 cm^{-1}) shifts of the excitation energies and no change in the character of the excited states.[226,244]

Pierloot and Besien[227] calculated the isolated UO_2^{2+} and $UO_2Cl_4^{2-}$ ions using the SO-CASPT2 method. The accuracy of this method was proven by the very close correspondence between the calculated excitation energies and the available experimental data on $UO_2Cl_4^{2-}$. The calculated adiabatic excitation energies agreed much better (within 1000 cm^{-1}) with the experimental data than those obtained previously by the SO-MRCI calculations (vide supra).[226] While the results were satisfactory, the authors warned that the effect of the ligands on the electronic transitions of bare UO_2^{2+} cannot be neglected. This study indicated a nontrivial blue-shift (by 1500−4300 cm^{-1}) of the excitation energies upon coordination by the chloride ligands. In addition, a change in the character of the luminescent state was found:[227] the Δ_g (predominantly $\sigma_u \rightarrow \phi_u$ excitation) in UO_2^{2+} changed to Π_g (predominantly $\sigma_u \rightarrow \delta_u$ excitation) in $UO_2Cl_4^{2-}$.

To probe the performance of time-dependent Density Functional Theory with the inclusion of either scalar or extended by spin−orbit relativistic effects, further calculations were performed on UO_2^{2+} and $UO_2Cl_4^{2-}$.[228] In this comparative study using the SO-TDDFT method,[245] the SAOP exchange-correlation functional[246] was found to give the best excitation energies, with the deviations from experiment similar to those of SO-CASPT2, and thus with a better performance than SO-MRCI. Very recently, Gomes et al. assessed systematically improvable models for the electronic spectrum of uranyl in $Cs_2UO_2Cl_4$.[247] IHFSCC and TDDFT/CAM-B3LYP calculations were performed for bare uranyl, uranyl with point-charge embedding, $UO_2Cl_4^{2-}$, and uranyl with frozen density embedding (FDE).

The performance of the five above-mentioned theoretical levels is compared for UO_2^{2+} and $UO_2Cl_4^{2-}$ in the range of 17 000−32 000 cm^{-1} in Table 8. Except for the second Δ_g state of UO_2^{2+} and the second B_{2g} state of $UO_2Cl_4^{2-}$, the SO-CASPT2[227] and SO-TDDFT[228] adiabatic transition energies are in very good agreement with experiment, while the SO-MRCI results[226] have several deficiencies. The SO-CASPT2 calculations reproduced the experimental transition energies of $UO_2Cl_4^{2-}$ to within 807 cm^{-1}, and the harmonic vibrational frequencies to within 13 cm^{-1}. The performance of SO-TDDFT is slightly inferior, while that of SO-MRCI level is considerably worse. The IHFSCC and TDDFT/CAM-B3LYP results of Gomes et al.[247] are considerably (by ca. 9000 cm^{-1}) red-shifted for bare UO_2^{2+} as compared to the other listed computed

DOI: 10.1021/cr500426s
Chem. Rev. 2015, 115, 1725−1759

excitation energies (cf., Table 8). On the other hand, the modeling of solid $Cs_2UO_2Cl_4$ with FDE-embedding of UO_2^{2+} proved to be more successful, with the appearance of only a small red shift (by 1000−2000 cm^{-1}) for the calculated energies with respect to the experimental data.

Among the neptunium oxides, experimental information on the electronic states is available only for neptunyl (NpO_2^{2+}) and its Np(V) derivative NpO_2^{+}. The electronic spectra of these ions coordinated with chloride and nitrate ligands have been reported in aqueous solution[248−250] and in crystalline phases.[251−254]

Quantum chemical calculations have been reported for NpO_2^{2+} and NpO_2^{+} with the main goal being to interpret and assign the experimental absorption spectra. Vertical transitions of the two free ions were calculated by Matsika and Pitzer at the SO-MRCI level.[255] In a subsequent study, the same authors computed the adiabatic transitions of NpO_2^{2+} (but correlating in the active space only seven electrons with respect to the 15 in the previous study).[226] Most of the vertical values were in very good agreement with the experimental data[253,254] on crystalline $Cs_2NpO_2Cl_4$; however, the adiabatic energies showed significant discrepancies, suggesting a considerable error cancellation for the vertical energies. The worse performance of the adiabatic calculations was attributed as most likely due to an unsatisfactory description of the electron correlation. The NpO_2^{2+} and NpO_2^{+} free ions were also investigated by Infante et al.[58] using the DC-IHFSCC method (accounting for electron correlation at a more sophisticated level than MRCI). The better agreement with the facets of the experimental spectrum allowed a different assignment of some prominent bands of these ions.

The electronic spectra of hydrated NpO_2^{2+} and NpO_2^{+} with five explicit coordinating water molecules were modeled at the SO-MRCI level.[256] In this same study, the authors also replaced water with five chloride ions. The results on the two coordination models were in fair agreement with each other and with the experimental spectra of the two ions in aqueous solutions.[256]

Among the Pu dioxide species, the plutonyl (PuO_2^{2+}) ion has received most of the attention from both experimentalists and theoreticians.[58,182,215,217,218,220−222,257−260] On the other hand, PuO_2 has been investigated only theoretically by Archibong and Ray at various post-Hartree−Fock levels including CCSD(T)/LCPP,[21] and more recently by La Macchia et al. using SO-CASPT2 calculations.[182]

Experimental information on the low-lying electronic states of PuO_2^{2+} is available from early UV−vis and near-IR measurements of acidic solutions[257−259] and have been interpreted using ligand field theory.[218] The low-lying electronic states were calculated in subsequent studies using multireference approaches: three excited states and adiabatic excitation energies were reported from CASSCF calculations by Ismail et al.,[215] while up to 23 excited states and vertical and adiabatic transitions were calculated by Maron et al. at the SO-CISD+Q level of theory.[220] In addition, vertical excitation energies for 11 low-lying states were calculated by Hay et al. using the SO-CI method;[260] 12 states were investigated by several multireference methods including SO-CASPT2 using a small CAS(2,4) and SO-DDCI;[221] vertical excitation energies to 21 low-lying excited states were determined using DC-IHFSCC by Infante et al.[58]

In the most recent study, La Macchia et al. performed a SO-CASPT2 study on PuO_2, PuO_2^{+}, and PuO_2^{2+}.[182] Their low-lying excited states (corresponding to vertical excitation energies) up to 12 500 cm^{-1} were determined from calculations both with and without spin−orbit coupling. This work and that by Infante et al.[58,182] are in good agreement with each other and also with the experimental (HCl solution) data,[218] and perform better than other less sophisticated calculations (cf., Table 9).

Table 9. Calculated Vertical Electronic Transitions[a] of PuO_2^{2+} and Comparison to Experimental Data

state	experimental[b]	DC-IHFSCC[c]	SO-CASPT2[d]	SO-CASPT2[e]	SO-CISD+Q[f]
4_g	0	0	0	0	0
0_g		2530	2268	4190	4295
1_g		4870	5065	6065	7044
5_g		6700	6955	8034	6593
0_g	10 185	10 334	10 436	12 874	7393
1_g	10 500	10 983	10 450	12 906	12 874
0_g	10 700	11 225	11 262	14 606	9415
6_g		11 651	12 257	14 326	7848
0_g	12 037	12 326		14 910[g]	14 169[g]
0_g	15 420	16 713			16 984[g]
1_g	16 075	17 737			27 005
4_g	17 800	18 565			23 091
0_g	19 100	20 029			33 314
1_g	19 810	22 703			33 164[g]
6_g	22 200	22 889			30 254
5_g	21 840	23 022			
3_g		29 710			33 366
2_g		32 198			33 388
0_g		32 759			35 210
1_g		34 080			34 520
4_g		34 702			33 318
2_g		34 982			35 670

[a]Energies in cm^{-1}. Assignment according to ref 58. [b]Solution data from ref 218. [c]Four-component (including SOC) Dirac−Coulomb intermediate Hamiltonian Fock-space coupled-cluster calculations by Infante et al.[58] using all electron basis set. [d]Spin−orbit CASPT2 calculations by La Macchia et al. using all electron basis set and a large active space.[182] [e]Spin−orbit CASPT2 calculations by Clavaguéra-Sarrio et al. using all electron basis set and a small active space.[221] [f]Spin−orbit multireference CISD calculations by Maron et al.[220] using the small-core Stuttgart−Cologne pseudopotential for Pu.[143] [g]Assignment different from those in refs 58,182.

Only one theoretical study has been reported on the excited states of americium dioxides, with the targets being AmO_2^{+}, AmO_2^{2+}, and AmO_2^{3+}.[223] Notter et al. computed the vertical excitation energies of these ions up to ca. 30 000 cm^{-1} using three different methodologies, which also include spin−orbit interactions. These approaches are the four-component CISD (4c-CISD), SO-CASSCF, and SO-CASPT2. The lack of experimental data led the authors to perform a comparison among the three theoretical levels by considering the SO-CASPT2 approach as the most accurate for the better description of the dynamic electron correlation. The 4c-CISD and SO-CASSCF methods, which are supposed to account similarly for dynamical correlation provided they have the same active space, agreed well in describing the states differing from the ground states only in occupation of the nonbonding (5f) orbitals. In the 4c-CISD results, due to the deficiency that the spinors were not optimized for excitations, large discrepancies were obtained for states formed by excitation from bonding to nonbonding orbitals, as well as from nonbonding to antibonding orbitals.

3.7. Energetics (Ionization and Dissociation Energies) of Actinide Mono- and Dioxides

In contrast to molecular geometries, vibrational frequencies, and electronic transitions, there is very detailed and almost complete

DOI: 10.1021/cr500426s
Chem. Rev. 2015, 115, 1725−1759

Table 10. Selected Computed and Experimental[a] Ionization Energies (eV) of AnO and AnO_2 Oxides

	IE1				IE2			
oxide	SO-CASPT2[b]	M06[c]	B3LYP[c]	experimental	SO-CASPT2[b]	M06[c]	B3LYP[c]	experimental
ThO[d]	6.56	6.84	6.52	6.6035 ± 0.0008	11.94	11.84	12.21	11.8 ± 0.7
PaO	6.28	6.67	6.30	5.9 ± 0.2	12.10	12.42	12.63	11.8 ± 0.7
UO[e]	6.05	6.09	6.18	6.0313 ± 0.0006	13.07	12.95	13.08	12.4 ± 0.6
NpO	5.97	5.79	6.26	6.1 ± 0.2	13.43	13.60	13.75	14.0 ± 0.6
PuO[f]	6.17	5.88	6.38	6.1 ± 0.2	14.36	14.38	14.42	14.0 ± 0.6
AmO[g]	6.21	6.08	6.50	6.2 ± 0.2	15.05	15.37	15.33	14.0 ± 0.6
CmO	6.68	6.27	6.67	6.4 ± 0.2	15.92	15.40	15.44	15.8 ± 0.4
ThO_2	8.50	8.52	8.56	8.9 ± 0.4	15.10	16.43	16.30	16.6 ± 1 (15.1 ± 1.0)[h]
PaO_2	5.70	6.13	6.34	5.9 ± 0.2	16.99	17.03	16.93	16.6 ± 0.4
UO_2[i]	6.21	6.07	6.25	6.128 ± 0.003	14.36	15.14	15.08	14.6 ± 0.4
NpO_2	6.27	6.21	6.36	6.33 ± 0.18	15.58	16.27	16.21	15.1 ± 0.4
PuO_2[j]	6.20	6.60	6.61	7.03 ± 0.12	15.37	16.40	16.32	15.1 ± 0.4
AmO_2	6.76	6.96	7.17	7.23 ± 0.15	16.28	16.59	16.44	15.7 ± 0.6
CmO_2	8.27	8.22	8.27	8.5 ± 1.0	16.15	16.48	16.52	17.9 ± 1 (16.1 ± 1.0)[h]

[a]Most of the listed experimental values are obtained through indirect measurements using the FTICR/MS method by Marçalo and Gibson. The data for NpO_2, PuO_2, and AmO_2 were obtained by electron-transfer bracketing.[4] The REMPI method[3] providing the most accurate data has been applied for UO_2,[201,202] ThO,[148] and UO.[3,159,201] [b]Spin−orbit CASPT2 calculations by Infante et al. using all electron basis set.[131,132] [c]DFT calculations by Averkiev et al.[131] using the small-core Stuttgart−Cologne pseudopotential for actinides.[143] [d]Computed IE1 and IE2 (eV) from other studies: 6.44 (B3PW91/SCPP);[148] 6.45 (MRCI/SCPP);[148,163] 6.4 and 12.2 (ZORA-PW91/AE);[162] 6.3 and 11.8 (B3LYP/SCPP);[162] 6.54 (CCSD(T)/SCPP).[121] [e]Computed IE1 and IE2 (eV) from other studies: 6.17 (relativistic DFT);[186] 5.71 (relativistic Hückel);[271] 6.05 (SO-CASPT2/AE).[158] [f]Computed IE1 and IE2 (eV) from another study: 6.16 and 14.56 (CASPT2/AE);[182] 6.17 and 14.36 (SO-CASPT2/AE);[182] 6.31 and 14.52 (DKH-B3LYP/AE).[182] [g]Computed IE1 (eV) from another study: 6.2 (SO-CASPT2/AE).[134] [h]The values in parentheses are suggested revisions to the rough "experimental" estimates, on the basis of the SO-CASPT2 data. For details, see text. [i]Computed IE1 and IE2 (eV) from other studies: 6.27 and 15.31 (B3LYP/SCPP);[157] 5.40 (CASSCF/AE);[197] 6.17 (CASPT2/AE);[197] 6.19 (B3LYP/PP);[197] 5.92 (DC-IHFSCC/AE);[57] 6.22 and 14.86 (ZORA-PW91/AE);[164] 6.29 and 15.32 (B3LYP/SCPP).[164] [j]Computed IE1 and IE2 (eV) from other studies: 9.92 (CCSD(T)/LCPP);[21] 6.73 and 15.48 (CASPT2/AE);[182] 6.20 and 15.37 (SO-CASPT2/AE);[182] 6.70 and 16.3 (DKH-B3LYP/AE).[182]

experimental information on the ionization and dissociation energies of actinide mono- and dioxides, AnO_n^{y+} (n = 1,2; y = 0,1,2) for An = Th−Cm, although the associated uncertainties are substantial in several cases. In this section, we assess the theoretical results as compared to experimental values and evaluate whether theory can be employed to refine the experimental values.

Early thermochemical data for all studied actinide oxides are compiled in refs 261−263, and those of Th oxides are in ref 264. Recent reviews of ionization and dissociation energies of actinide oxides appeared also in refs 4,115,116. For the present assessment, we use the most up-to-date compilation and critical evaluation of ionization and dissociation energies based on experimental results and semiempirical correlations provided by Marçalo and Gibson.[4] Key values in this set are the very accurate first ionization energies obtained relatively recently by Heaven and co-workers for ThO,[148] UO,[3,159,201] and UO_2[201,202] using high-resolution photoionization spectroscopic methods. These results demonstrated that earlier electron impact ionization threshold values for high-temperature oxide molecules exhibit substantial errors. Other ionization energies are estimated from bracketing experiments, which establish approximate electron transfer thresholds from neutral molecules to bare or oxo-ligated actinide ions. Bond dissociation energies and formation enthalpies were derived from earlier studies, as well as from recent work by Marçalo and co-workers in which oxygen-atom transfer reactions were employed to obtain a range of dissociation energies.[122,178,265−267]

The only direct determinations of actinide oxide bond dissociation energies were by Armentrout and Beauchamp for UO^+ and UO_2^+ using collision induced dissociation;[268] their values are very close to those given in ref 4. Formation enthalpies for the neutral monoxides and dioxides of Th, U, Np, and Pu, as well as for CmO, had been previously reported, as summarized by Konings et al.[263] The corresponding values suggested by Marçalo and Gibson[4] are generally in good agreement, although with larger assigned uncertainties. The notable exception is the two values for CmO, which differ from one another by 99 kJ/mol. For consistency, all of the values employed here are from the evaluation by Marçalo and Gibson. It should be noted that Kleinschmidt and Ward obtained remarkably accurate bond dissociation energies and formation enthalpies for PaO and PaO_2 in 1986 from high-temperature vapor equilibrium measurements.[269] A high future priority from the experimental perspective should be to accurately measure bond dissociation energies for Th and U oxide cations using the guided ion beam technique as has been extensively developed and refined by Armentrout;[270] a few key accurate bond dissociation energies would serve as an important basis to better evaluate theoretical methodologies. An important goal is to obtain accurate bond dissociation energies for transuranic oxides; regretably, these measurements, like spectroscopic studies, are unlikely to be realized in the near future due to the substantial complications introduced in handling the more radioactive synthetic actinides.

To derive the most accurate currently available values, Marçalo and Gibson analyzed collectively the bond dissociation energies (BDEs) and ionization energies (IEs) of neutral and positively charged oxides, as they are related according to Hess's law (eq 2, vide supra in section 2.2).[4] By this comprehensive analysis, the most accurate available BDE and IE values confirmed and/or enabled a re-evaluation of the less accurate values and their experimental errors.

The experimental ionization energies for the actinide mono- and dioxides from ref 4 are given in Table 10. We use these data

DOI: 10.1021/cr500426s
Chem. Rev. 2015, 115, 1725−1759

as reference values for the assessment of the computations. We note that, lacking reliable experimental information, the ionization energies of CmO_2, IE(CmO_2) and IE(CmO_2^+), and the second ionization energy of ThO_2, IE(ThO^+), are rough estimates considered to be accurate to within only ±1 eV.

Before the very recent systematic studies on the ionization energies of actinide oxides by Infante et al.[132] and Averkiev et al.,[131] a few studies were carried out at various theoretical levels. The IE1 of ThO was calculated using B3PW91,[148] MRCI,[148,163] and CCSD(T)[121] methods. Both IE1 and IE2 of ThO were obtained by B3LYP and all-electron ZORA-PW91 calculations,[162] with the latter results in better agreement with experiment. Early calculations on the ionization energies of UO have included a simple relativistic density functional[186] and the relativistic extended Hückel[271] approach. These results deviate considerably from experiment. The recent SO-CASPT2 study of Paulovič et al., however, provided a good-quality value (6.05 eV) for IE1.[158]

The largest number of calculations on the IEs has been carried out mostly for UO_2 at various levels of theory. The first computed IE1 and IE2 data were obtained by Zhou et al. using B3LYP calculations.[157] Gagliardi et al. probed several relativistic multireference levels including small and large basis sets and active spaces in conjunction with CASPT2, with and without the inclusion of spin−orbit coupling, as well as the B3LYP method for IE1.[197] IE1 was also computed using the DC-IHFSCC method by Infante et al.,[57] while IE1 and IE2 were obtained at the ZORA-PW91 and B3LYP levels by Michelini et al.[164] We note that the latter study included also UO, but not its ground electronic state was used.

Among the transuranium oxides, PuO_2 and AmO were investigated earlier using quantum chemical calculations. The first study on the IE1 of PuO_2 was performed by means of CCSD(T) and some lower level calculations.[21] As the electronic structure of this molecule is close to being monodeterminantal, the large deviation with respect to the experimental value (9.92 eV calculated vs 7.03 eV experimental) was speculated to be attributed to the false computed ground state of PuO_2^+ and/or to the large-core pseudopotential applied. Subsequent computations at the SO-CASPT2 level[182] resulted in an IE1 value (6.20 eV) that was in much better, but still not quite satisfactory, agreement with experiment. In contrast, the IE1 of AmO calculated using the SO-CASPT2 method was in very good agreement with experiment.[134] Data from the above listed studies are given in the footnote of Table 10.

The systematic study of Infante et al. on the ionization energies of AnO and AnO_2 oxides (An = Th−Cm) utilized state-of-the-art methods like CASPT2, SO-CASPT2, X2C-DC-CCSD, and X2C-DC-CCSDT(T).[132] Among these, the X2C-DC-CCSD and X2C-DC-CCSD(T) are mostly single-reference methods; their inclusion in the study was based on the CASPT2 results indicating that the ground electronic states of the target oxides (except for PuO and NpO and their ions) have a nearly single-reference character. The best agreement with experiment was achieved with the CASPT2 and SO-CASPT2 methods (inclusion of the spin−orbit interaction resulted only in marginal changes, except for PuO_2). The computed data were within the experimental error bar for most oxides (cf., Table 10, Figure 5), but it should be kept in mind that for about one-half of the available experimental data the assigned errors are quite large. The intriguing disagreement between experiment and theory for PuO_2 was investigated in more detail using a larger active space by means of the RASSCF/RASPT2 technique.[132] However, the

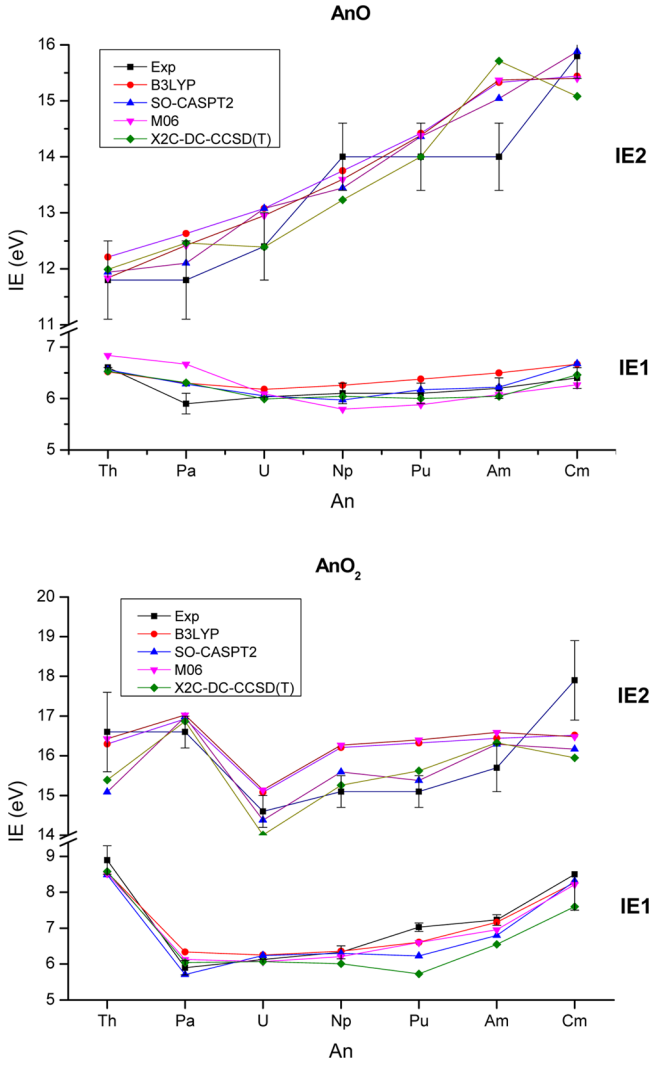

Figure 5. Experimental (with error bars) and selected computed ionization energies of neutral actinide oxides.

result (6.32 eV, without SO) did not show improvement as compared to what is considered the most reliable experimental value (7.03 ± 0.12 eV).[123] For this reason, the ionization energy of PuO_2 remains still an object of controversy due to unexpectedly large differences between recent measurements and computations. It is indeed unfortunate that it is not yet practical to accurately determine ionization energies of transuranium oxides using high-resolution photoelectron spectroscopy such as that employed by Heaven for thorium and uranium oxides.

In a recent work by Averkiev et al.,[131] several quantum chemical methods were compared to assess their performance for the first and second ionization energies of AnO and AnO_2 (An = Th−Cm). The listed CASPT2, X2C-DC-CCSD, and X2C-DC-CCSD(T) data were derived from the data of Infante et al.,[132] extending them with spin−orbit corrections from SO-CASPT2 and zero-point vibrational energy (ZPVE) corrections from M06 calculations. In addition, seven exchange-correlation functionals (M05, M06, M06-L, B3LYP, MOHLYP, MPW3LYP, PW91PW91) were also benchmarked and included ZPVE (from the same level) and spin−orbit (from SO-CASPT2) corrections. The performance of these selected methods is shown in Figure 5. The best agreement is achieved for the SO-CASPT2, M06, and

DOI: 10.1021/cr500426s
Chem. Rev. 2015, 115, 1725−1759

Table 11. Performance (Mean Unsigned Error) of the Tested Methods[a] for 28 Ionization Energies,[b] MUE(IE28), for 21 Bond Dissociation Energies,[c] MUE(BDE21), and Together for Both the Ionization and the Dissociation Energies MUE(E49) in electronvolts

	Wave Function Theory				Density Functional Theory						
	X2C-DC-CCSD	X2C-DC-CCSD(T)	CASPT2-SO	CASPT2	M05	M06	M06-L	B3LYP	MOHLYP	MPW3LYP	PW91
MUE(IE28)	0.50	0.50	0.41	0.42	0.49	0.47	0.62	0.47	0.63	0.48	0.55
MUE(BDE21)	0.53	0.56	0.65	0.69	0.52	0.47	0.63	0.43	0.71	0.43	1.10
MUE(E49)	0.51	0.52	0.51	0.54	0.50	0.47	0.63	0.45	0.66	0.46	0.79

[a]Data were taken from ref 131. All of the data include zero-point vibrational energy (ZPVE) corrections from the DFT calculations (scaled according to refs 297,298). The wave function theory data were corrected by the ZPVE from M06 calculations. Except for CASPT2, all of the data include correction for spin−orbit coupling taken from the SO-CASPT2 calculations. The WFT calculations used all electron basis sets, while the DFT ones used the small-core Stuttgart−Cologne pseudopotential for the actinides.[143] [b]The first and second ionization energies of AnO and AnO_2 (An = Th−Cm). [c]The dissociation energies $AnO_2^{n+} \rightarrow AnO^{n+} + O$ (An = Th−Cm, n = 0−2).

Table 12. Selected Computed and Experimental Dissociation Energies (kJ/mol)[a] of AnO and AnO_2 Oxides

	SO-CASPT2[b]	MPW3LYP[b]	M06[b]	B3LYP[b]	B3LYP[c]		experimental[d]
oxide	D_0	D_0	D_0	D_0	D_0	D_{298}	D_{298}
ThO[e]					914	920	872 ± 25[f]
PaO					861	867	801 ± 59
UO[g]					811	817	758 ± 13[f]
NpO					768	774	744 ± 21
PuO[h]					598	604	658 ± 10[f]
AmO[i]					492	498	582 ± 34
CmO[j]					684	690	709 ± 43
ThO_2	615	661	649	657	658	664	684 ± 14[f]
PaO_2	795	758	707	749	787	792	780 ± 48 (812 ± 30)[f]
UO_2[k]	611	720	712	716	723	728	750 ± 14[f]
NpO_2	707	649	699	645	626	631	632 ± 43 (651 ± 30)[f]
PuO_2[l]	561	594	640	590	575	580	599 ± 22[f]
AmO_2[m]	498	456	481	452	475	478	509 ± 65 (498 ± 30)[n]
CmO_2[o]	452	427	444	423	421	424	405 ± 70 (444 ± 30)[n]

[a]Energies for the dissociation reactions $AnO_2 \rightarrow AnO + O$ and $AnO \rightarrow An + O$ at the indicated temperatures (0 K, 298.15 K). [b]The SO-CASPT2 calculations used all electron basis sets, while the DFT ones used the small-core Stuttgart−Cologne pseudopotentials for the actinides[143] and 6-311+G(2df) basis set for oxygen.[131] [c]B3LYP calculations in conjunction with the small-core pseudopotential of the Stuttgart−Cologne group for the actinides[143] and aug-cc-pVTZ basis set for oxygen.[135] [d]From ref 4, except where noted. [e]Computed values (kJ/mol) from other studies for ThO, D_e = 861 (CASSCF/SCPP), D_0 = 815 (MRCI+SCC/SCPP), D_0^{BSSE} = 865 (CCSD(T)/SCPP);[22] for ThO^+, D_e = 997 (ZORA-PW91/AE), D_e = 846 (B3LYP/SCPP);[162] for ThO^{2+}, D_e = 993 (ZORA-PW91/AE), D_e = 833 (B3LYP/SCPP).[162] [f]From ref 263. [g]Computed values (kJ/mol) from other studies for UO: D_0 = 741 (CASPT2/AE), D_0^{BSSE} = 712 (SO-CASPT2/AE);[158] for UO^+, D_0 = 751 (CASPT2/AE), D_0^{BSSE} = 729 (SO-CASPT2/AE).[158] [h]Computed values (kJ/mol) from other studies for PuO: D_{298} = 656 (PBE0/SCPP), D_{298} = 639 (B3LYP/SCPP).[273] [i]Computed values (kJ/mol) from other studies for AmO: D_0 = 446 (CASPT2/AE),[134] D_{298} = 551 (PBE0/SCPP), D_{298} = 539 (B3LYP/SCPP).[273] [j]Computed value (kJ/mol) from another study for CmO: D_0 = 682 (CASPT2/AE).[134] [k]Computed values (kJ/mol) from other studies for UO_2^+, D_0 = 869 (ZORA-PW91/AE), D_0 = 743 (B3LYP/SCPP);[164] for UO_2^{2+}, D_0 = 670 (ZORA-PW91/AE), D_0 = 478 (B3LYP/SCPP).[164] [l]Computed values (kJ/mol) from another study for PuO_2: D_{298} = 596 (PBE0/SCPP), D_{298} = 594 (B3LYP/SCPP).[273] [m]Computed values (kJ/mol) from another study for AmO_2: D_e = 582 (CASPT2/AE),[134] D_{298} = 503 (PBE0/SCPP), D_{298} = 490 (B3LYP/SCPP).[273] [n]The values in parentheses were suggested in the present study on the basis of the B3LYP data from ref 135. [o]Computed value (kJ/mol) from another study for CmO_2: D_e = 446 (CASPT2/AE).[134]

B3LYP levels; these values are compiled with the experimental values in Table 10. The average deviations from experiment are given in Table 11 for each method. Notably, a comparison between CASPT2 and SO-CASPT2 shows that the SO correction provides a slight improvement on both the ionization and the dissociation energies.

It is evident from Table 11 that there is a good agreement between the SO-CASPT2, M06, and B3LYP values for IE1 of AnO and AnO_2 as well as for IE2 of AnO. As mentioned above, there are no reliable experimental data for IE2 of ThO_2 and CmO_2;[4] hence, this explains the large errors assigned to the "experimental" estimates. Unfortunately, the three sets of computed results in Table 11 are not consistent for IE2 of AnO_2 molecules as noted for the other ionization energies. We assume the superiority of SO-CASPT2 over M06 and B3LYP based on the better agreement with the experimental IE2 values of UO_2, NpO_2, PuO_2, and AmO_2 (cf., Table 12). On the basis of the SO-CASPT2 data, we suggest that the IE2 values of ThO_2 and CmO_2 are considerably lower than the previous estimates,[4] actually being around 15.1 and 16.1 eV, respectively, with uncertainties of ±1.0 eV.

The best available experimental dissociation energies[4] are given in Table 12. Computational studies dealing with dissociation energies are scarce. Besides some calculations on selected species (vide infra), two recent systematic studies dealt with the dioxides of early actinides (An = Th−Cm)[131] and with the mono- and dioxides of the whole actinide row.[135]

DOI: 10.1021/cr500426s
Chem. Rev. 2015, 115, 1725−1759

The dissociation of ThO was first calculated by Cao et al.[22] using HF, CASSCF, MRCI+SCC, and CCSDT(T) benchmark calculations; the value at the CCSD(T)/SCPP level provided very good agreement with the experimental value. The bond dissociation energies of ThO^+ and ThO^{2+} were calculated by Mazzone et al.[162] using the B3LYP and ZORA-PW91 exchange-correlation functionals, the latter results showing worse agreement with experiment.

The bond dissociation energies of mono- and dicationic uranium oxides were calculated by Michelini et al. using B3LYP/SCPP and ZORA-PW91/AE methods.[164] Unfortunately, their calculated $^4\Delta$ and $^3\Sigma_g$ electronic states do not correspond to the ground states of UO^+ and UO^{2+}, respectively (cf., Table 1). For the correct ground states of UO_2^+ and UO_2^{2+}, the best agreement with experiment was achieved for the B3LYP level. In addition, the dissociation energy of UO^+ was obtained at the SO-CASPT2 level by Paulovič et al.[158] Dissociation energies for AmO, AmO_2, CmO, and CmO_2 were reported from CASPT2 calculations by Kovács et al.[134] Very recently, Zaitsevskii et al. calculated bond dissociation enthalpies of PuO, PuO_2,[272,273] AmO, and AmO_2[273] using two-component relativistic DFT calculations (for the values see footnote of Table 12). We note the remarkable agreement of these data with experiment. Unfortunately, detailed information on the calculated electronic states of the molecules is not available (only that they were the lowest energy ones obtained); therefore, whether the data refer indeed to the ground states is not unambiguously confirmed. From the oxides of late actinides, only the bond dissociation energy of LrO was computed using the B3LYP, CCSD(T),[161] and ZORA-BP methods.[160]

In the first of the two most relevant studies, Averkiev et al.[131] tested four wave function theories and seven DFT methods taking into account both zero-point vibrational energy and spin−orbit corrections for the $AnO_2^{n+} \rightarrow AnO^{n+} + O$ (An = Th−Cm, n = 0, 1, 2) bond dissociation energies. The best agreement was achieved for the B3LYP, MPW3LYP (with average deviations of ca. 40 kJ/mol), and M06 levels (45 kJ/mol);[131] these values are listed together with the experimental values for n = 0 in Table 12. The average deviation for each method from experiment is given in Table 11. The average deviation of SO-CASPT2 for all of the oxides is 60 kJ/mol, implying that this method is inferior to DFT for obtaining these bond dissociation energies.

The bond dissociation enthalpies of the neutral monoxides and dioxides of the whole actinide row (An = Th−Lr) were covered by the DFT computations of Kovács et al.[135] using the B3LYP exchange-correlation functional. For actinides the same SCPP[22,143,161] was used as by Averkiev et al.;[131] however, the valence basis set for oxygen was larger (of aug-cc-pvTZ quality). In this study, spin−orbit effects were neglected, while the thermal effects at 298 K (3−6 kJ/mol with respect to 0 K) were considered. These data are shown in Table 12 and Figure 6. The average deviations as compared to the available experimental data of the early actinide (An = Th−Cm) oxides were 20 and 50 kJ/mol for the neutral dioxides and monoxides, respectively. By comparing the two B3LYP columns in Table 12, it can be seen that the computed results of Kovács et al.[135] are generally in better agreement with experiment than those of Averkiev et al.[131]

The differences between computations and experiment are less straightforward in the case of the experimental data with the large uncertainties. More exact information about the performance of the computational methods may be obtained considering only the oxides with the smallest experimental uncertainties: ThO, UO, NpO, PuO, ThO_2, UO_2, PuO_2. If a (roughly) systematic error in the computations could be identified, we could suggest more accurate values (with smaller uncertainty ranges) for the less reliable experimental dissociation energies of the other oxides. For this analysis, we selected the superior B3LYP results by Kovács et al.[135] For the monoxides (ThO, UO, NpO, PuO), we obtained an average deviation of 48 kJ/mol. Unfortunately, the sign of the deviations is not systematic: for ThO, UO, NpO the dissociation energies were overestimated, while for PuO it was underestimated. The large deviations and the variable scattering direction make these computations unable to provide an improvement over the other experimental data that suffer from large uncertainties.

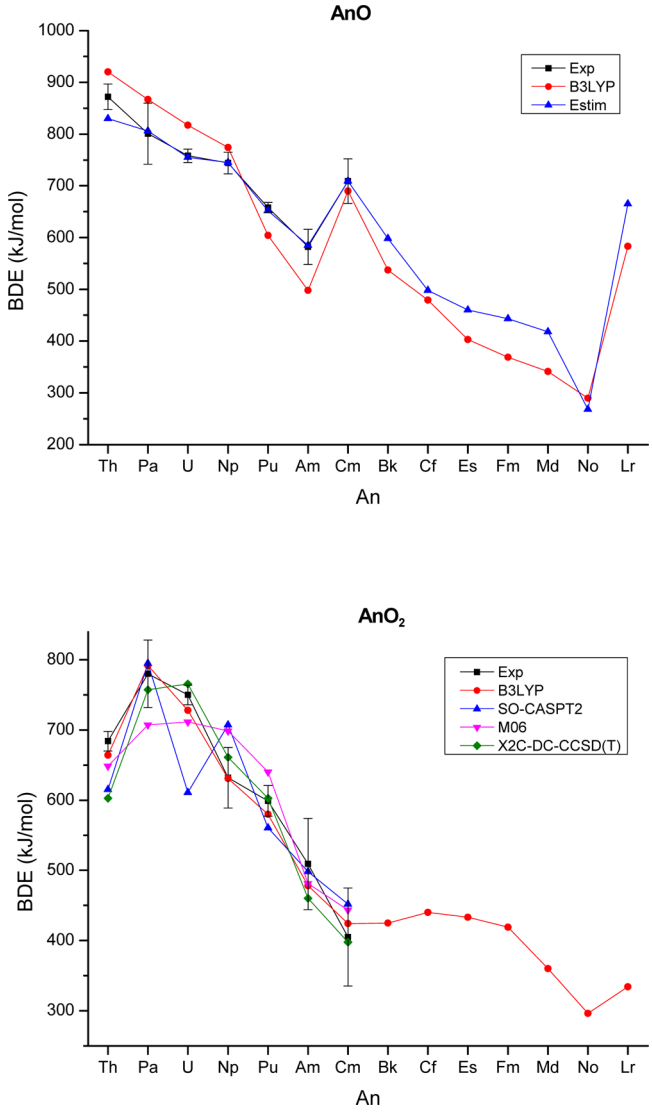

Figure 6. Experimental (with error bars) and selected computed bond dissociation energies of neutral actinide oxides.

In contrast to the monoxides, the B3LYP results on the BDE of ThO_2, UO_2, and PuO_2 show a systematic underestimation by ca. 20 kJ/mol.[135] On the basis of the B3LYP data and correcting for the underestimation, the other dioxides, PaO_2, NpO_2, AmO_2, and CmO_2, would have BDE values around 812, 651, 498, and 444 kJ/mol, respectively, with an estimated uncertainty of 30 kJ/mol.

The performance of SO-CASPT2 for the dissociation energies on the basis of the experimental data of ThO_2, UO_2, and PuO_2

DOI: 10.1021/cr500426s
Chem. Rev. 2015, 115, 1725−1759

Table 13. Available Ground-State Data[a] of AnO_3 and AnO_4 Molecules

oxide	state	sym.	An−O_1	An−O_2	O_1−An−O_1	method[b]	vibrational frequencies	BDE	ref
UO_3						MI-IR (Kr)	740.7, 848.1		172
			1.76[c]	1.79[c]	T-shape[c]	MI-IR (Ar)	745.6, 852.5		157,172,173,278,279
						MI-IR (Ar)	151.5, 186.2, 211.6		283
	$^1A_1$	C_{2v}	1.75	1.83	161	HF/LCPP	214, 242, 262, 838, 964, 991		213
	$^1A_1$	C_{2v}	1.810	1.853	158.8	B3LYP/SCPP	782 (209), 885 (479), 887 (34)		157
						MI-IR (Ne)	760.3, 865.3		157
	$^1A_1$	C_{2v}	1.745	1.828	165.2	HF/SCPP	215, 264, 272, 836, 998, 1009		281
	[d]	C_{2v}	1.771	1.786	161	PBE0/SCPP	155, 188, 200, 816, 923, 924		282,286
	[d]	C_{2v}	1.808	1.849	157	B3LYP/SCPP	141, 163, 186, 787, 884, 889		282,286
UO_3^-	[d]	C_{2v}	1.879	1.914	155	PBE0/SCPP			282
	[d]	C_{2v}	1.902	1.931	150	B3LYP/SCPP			282
PuO_3	$^1A_{1g}$[e]	C_{2v}	1.752	1.811		B3LYP/SCPP	880, 912		192
	$^7B_1$	C_{2v}	2.206	1.914	102.2	B3LYP/LCPP			285
	^3X	C_{2v}	1.749	1.858	169	B3LYP/SCPP	193, 240, 253, 813, 917, 969	387	272,286
	^3X	C_{2v}	1.749	1.853	170	PBE0/SCPP	239, 257, 278, 803, 911, 957	379	272,286
PuO_4	[d]	D_{4h}	1.766			B3LYP/SCPP	735, 873, 920		192
	[d]	D_{4h}	1.754			MP2/SCPP	1026, 1050, 1140		192
	[d]	D_{4h}	1.777			CCSD(T)/SCPP			192
	[d]	D_{4h}	1.774			B3LYP/SCPP		262	273
	[d]	D_{4h}	1.753			PBE0/SCPP		262	273
AmO_3	[d]	C_{2v}	1.75	2.07	179	PBE0/SCPP		306	273
AmO_4	[d]	D_{4h}	1.74			PBE0/SCPP		204	273
CmO_3	[d]	C_{2v}	1.768	2.069	176	PBE0/SCPP	196, 228, 238, 507, 770, 884	229	286

[a]Bond distances are given in angstroms, bond angles in degrees, vibrational frequencies in cm^{-1}, bond dissociation ($AnO_n \rightarrow AnO_{n-1} + O$) energies in kJ/mol. For the vibrational data, the calculated infrared intensities are in parentheses. [b]MI-IR indicates matrix-isolation IR spectroscopy. The abbreviations LCPP and SCPP correspond to the large-core (78-electron) and small-core (60-electron) Stuttgart−Cologne pseudopotentials.[143] [c]Calculated from the observed fundamental frequencies using normal coordinate analysis.[279] [d]Character of the electronic state not given. [e]Standard enthalpy of formation ($Pu + 2O_2 \rightarrow PuO_4$) is 776 kJ/mol.[192]

deserves also a note: the average deviation is 77 kJ/mol, considerably larger than that for B3LYP (vide supra).

For the late actinide (An = Bk−Lr) oxides, estimated data are available for the monoxides. Haire proposed a promotion model[274] to interpret the experimentally observed trend in the An−O dissociation energies and to predict missing values.[275] The model assumes that the actinides are divalent in the monoxides and have one 7s and one 6d electron that participate in the bonding. Hence, to form the chemical bond, one of the $7s^2$ electrons of the neutral actinide atoms has to be promoted to a 6d orbital. Exceptions are Th and Pa forming double bonds with $6d^27s^2$ configuration. The "intrinsic" energies of dissociation to neutral actinide with $6d^17s^1$ ($6d^27s^2$ for Th and Pa) orbital occupation, being in fact an excited state of the actinide, should fall on a slightly decreasing line along the actinide row from Th to No. Because the actinide atoms relax to their ground state upon dissociation, the experimental dissociation energies differ from the intrinsic ones by the promotion energies. Later studies considering $7s^16d^2$ configurations (for actinides other than Th and Pa) appeared to be more consistent with the experimental data[179,263] and with the triple bond character of the monoxides from recent quantum chemical calculations.[132,134,135,276] The estimated data from the promotion model are given in Figure 6.[179,274] Despite the raw empirical character of the model in contrast to the very complex electronic structure of these molecules, the trend is in agreement with the B3LYP computations,[135] with the deviations between the dissociation energy values varying between 20−80 kJ/mol (cf., Figure 6).

For the ionic oxides of late actinides, only the estimated dissociation energy of BkO^+ was reported. Utilizing the promotion energy model in combination with the dissociation

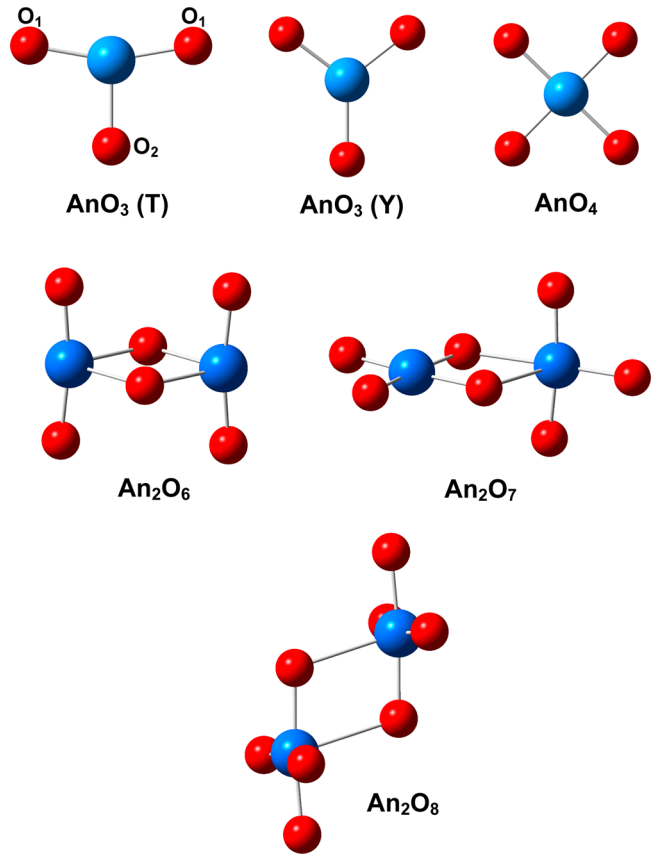

Figure 7. Structures of AnO_3, AnO_4, An_2O_6, An_2O_7, An_2O_8 molecules.

DOI: 10.1021/cr500426s
Chem. Rev. 2015, 115, 1725−1759

energy of TbO^+, its dissociation energy was estimated to be 610 kJ/mol.[277] This value (and the estimation of the dissociation energy of PuO^+ to be 655 kJ/mol) is consistent with the oxide ion yields observed by mass spectrometry.[277]

3.8. Higher Actinide Oxides

The actinide trioxide molecules UO_3 and PuO_3 have been observed experimentally and modeled theoretically (data given in Table 13 while the structures are in Figure 7) The UO_3 molecule has been detected and investigated by IR spectroscopy.[172,173,278−280] Using ^{18}O isotope substitution, it was shown that the molecule has a T-shaped C_{2v} geometry possessing a near-linear OUO moiety with an equatorial coordination of the third oxygen. This type of structure has been found also by Hartree−Fock[213,281] and DFT calculations[157,282] (data given in Table 13). Zaitsevskii computed also the UO_3^- ion to obtain the adiabatic electron affinity of UO_3 using PBE0 and B3LYP methods.[282]

The IR spectrum of UO_3 has been measured in solid Ar,[157,172,173,278−280] Kr,[172] and Ne.[157] Altogether five absorption bands were measured in Ar matrix (cf., Table 13) for $U^{16}O_3$. Mixed oxygen isotopic (^{18}O) spectra were also recorded, which facilitated the vibrational assignments.[279,283] The assignments of the bands were later supported by quantum chemical calculations,[157,213,281] although two of these studies based on HF theory[213,281] gave only poor agreement with the experiment. In contrast, the computed stretching frequencies[157] at the B3LYP level (taking into account the matrix shift and anharmonicity) are in very good agreement with experimental values, implying that the optimized geometry obtained at this level[157] (cf., Table 13) is also reliable. It is worthy to note that the sixth fundamental of $U^{16}O_3$ (843.5 cm^{-1}) was deduced only by calculations and was not observed in the experiment.[279]

The only experimental information on the PuO_3 molecule is its detection by mass spectrometry at very low concentrations upon sublimation of plutonium dioxide[284] (this trioxide has yet to be confirmed). The first theoretical study on PuO_3 was performed at the B3LYP level by Straka et al.; however, only the bond distances and two stretching frequencies were given for the $^1A_{1g}$ state, without any discussion.[192] The electronic and molecular structure as well as the vibrational spectra have been calculated by HF and two DFT exchange-correlation functionals (using the less reliable LCPP for Pu) by Gao et al.[285] From the studied lowest quintet, septet, and nonet states, the septet $^7B_1$ Y-shaped C_{2v} structure has been reported as the ground electronic state and the $^5B_2$ Y-shaped C_{2v} structure as an excited state at 25 kJ/mol higher in energy. The contradiction with the results of Straka et al. (state character and geometry, cf., Table 13), as well as the expected lower-than-quintet spin multiplicity for the ground state, imply that the $^7B_1$ state of Gao et al. is an excited state. The structure obtained very recently by Zaitsevskii et al.[272,273] by two-component relativistic DFT calculations has a T-shape and bond distances similar to those of UO_3, and is in good agreement with the geometry reported by Straka et al. (cf., Table 13). There is, however, disagreement in the spin multiplicity from the two studies: in contrast to the singlet state reported by Straka et al.,[192] the calculations of Zaitsevskii et al. resulted in a (chemically more reasonable) triplet.[286]

Early theoretical works on PuO_3^+ reported this ion as unstable,[128,287] but later calculations found a stable electronic state ($^6B_2$) with a C_{2v} symmetry and Y-shaped structure.[285] As these data were obtained with the same theoretical level that led to the erroneous PuO_3 structure, we warn about their reliability.

Molecular PuO_4, for which experimental evidence has been presented,[288] has been calculated by Straka et al.[192] using various ab initio (HF, MP2, CCSD(T)) and DFT and by Zaitsevskii et al.[272,273] using two-component relativistic DFT methods. A planar D_{4h} structure has been found as the most stable one with bond distances close to those of PuO_2 and PuO_3 (cf., Tables 5 and 13). In addition, three Pu−O stretching frequencies and the standard enthalpy of formation[192] as well as the bond dissociation energy have been reported (Table 13).

Very recently, Huang et al. performed DFT, MP2, CCSD(T), and SO-CASPT2 calculations on various isomers of PuO_4.[289] They found a quintet $PuO_2(O_2)$ (plutonyl(V)-superoxide) form lower in energy by ca. 70 kJ/mol than the singlet D_{4h} structure. This study provided the first information on the electronic structure of the two isomers. In addition, the geometrical parameters, vibrational frequencies, IR intensities, electronic, and ionization spectra have been reported.

The AmO_3 and AmO_4 molecules have been calculated by Zaitsevskii et al.[273] using two-component relativistic DFT. The structures resemble those of corresponding UO_3, PuO_3, and PuO_4 (cf., Table 13) except for the equatorial Am−O bond, which is considerably longer than those in UO_3 and PuO_3. In addition, the bond dissociation energies have been reported (Table 13), while no information was given on the electronic structure.

In the same study, Zaitsevskii et al. computed the dimers Pu_2O_6, Am_2O_6, Pu_2O_7, Am_2O_7, Pu_2O_8 and the mixed oxides $PuAmO_6$, $PuAmO_7$, and $PuAmO_8$.[273] The optimized structures agree with those of metal oxide dimers, with the actinide atoms being connected by two bridging oxygens (cf., Figure 7). The thermochemistry of the formation of the dimers from the monomer oxides as well as from each other was also evaluated.

The CmO_3 molecule has been reported on the basis of thermochromatographic experiments.[290] Very recently, DFT calculations on CmO_3 have been presented by Zaitsevskii et al.[291] The obtained T-shaped C_{2v} structure has a quasilinear O−Cm−O moiety (in contrast to the more bent one in the trioxides of U, Pu, and Am, cf., Table 13) and a considerably longer equatorial Cm−O bond length.

Theoretical studies were carried out on the hypothetical UO_6, in the octahedral isomer of which uranium would occur in its largest formal oxidation state (XII).[292,293] Recent detailed relativistic DFT studies of Xiao et al. accompanied by single-point CCSD(T) energy calculations confirmed the local minimum character of this octahedral isomer lying by ca. 540 kJ/mol higher in energy than the triplet peroxide form, $UO_2(O_2)_2$.[293] Similar peroxide moieties appear in several uranium minerals.[294]

4. CONCLUSIONS

In this Review, we have compiled the available experimental and theoretical information on gaseous actinide oxides covering both the neutral and the ionic species. Very little experimental information is available on the structure-related molecular data (electronic structure, molecular geometry, vibrational frequencies). The missing data (required, e.g., for the evaluation of thermodynamic properties) are supplied by recent multireference and DFT calculations for the oxides of An = Th−Cm and by DFT calculations for An = Bk−Lr. A crucial question is how reliable are the computed data?

The ground-state electronic structures of the oxides of An = Th−Cm have been obtained by the well-tested SO-CASPT2 method, and therefore they are very likely reliable.

DOI: 10.1021/cr500426s
Chem. Rev. 2015, 115, 1725−1759

This assumption is supported by the agreement with experimentally determined ground states for ThO, ThO^+, UO, UO^+, UO_2, UO_2^+, UO_2^{2+}, and PuO_2^{2+}. The ground electronic states of the oxides of An = Bk−Lr were reported only from B3LYP calculations. The reliability of B3LYP for this molecular property has been demonstrated by the agreement with the SO-CASPT2 results for almost all of the neutral and ionic oxides for An = Th−Cm. However, we cannot exclude some deviations in the character of the ground state in cases of strongly multiconfigurational electronic structures, as well as in cases of a potential inversion of the ground state with low-lying excited states within a few kJ/mol in energy.

Similarly to the electronic structures, few experimental data are available for molecular geometries and vibrational frequencies. From the high-level CCSD(T) calculations performed for thorium oxides and UO_2^{2+}, the calculated spectroscopic constants of ThO, ThO^+, ThO_2 (for which molecules reliable experimental data are available) are in excellent agreement with experiment. Some additional data with proper quality could be obtained in the following way: on the basis of empirical relationships evaluated from the computed geometries and vibrational frequencies, reliable knowledge of either parameter can enable confident prediction of the other. Presently, experimental vibrational frequencies are generally more available than geometrical parameters, and are easier to obtain by matrix-isolation infrared spectroscopy. However, in the application of these data, the matrix shift has to be taken into account, and caution is required because of a possible change in the relative energies of the electronic states upon interaction with the solid matrix. Both effects can be explored by careful quantum chemical computations. Thus, in further research, the computations have a crucial role for the evaluation of accurate molecular parameters.

On the basis of the theoretical data compiled in this Review, we assessed the performance of the most frequently applied computational methods. For the bond distances we utilized the existing experimental data on ThO, ThO^+, UO, and UO^+ and those of ThO_2, UO_2, and UO_2^+ derived from the vibrational frequencies (expected to be quite reliable). The best agreement was obtained for the B3LYP, MPW3LYP, and PW91PW91 exchange-correlation functionals in conjunction with SCPP and extended triple-ζ valence basis set resulting in average deviations of 0.004, 0.004, and 0.006 Å, respectively. The average deviation of SO-CASPT2 proved to be 0.017 Å. The performance of the above DFT levels seems to be by far the best; however, further supporting experimental data (particularly for actinides beyond U) would be desirable to further validate these conclusions. Nevertheless, at our present state of knowledge, these (and other related DFT) methods may provide geometrical parameters for the experimentally nonmeasured species to an accuracy within the usual experimental error ranges.

In contrast to geometry and vibrational properties, considerable experimental information is available for the bond dissociation and ionization energies of actinide oxides with An = Th−Cm. Many of these values, however, have large experimental uncertainties where the role of computations could be to narrow the uncertainty range. The high quality of the computed energies using state-of-the-art computational methods facilitated the derivation of somewhat more accurate dissociation energies for PaO_2, NpO_2, AmO_2, and CmO_2 with an estimated uncertainty of ±30 kJ/mol. Unfortunately, the performance of today's methods for the monoxides seems to be worse; thus for them such computational assistance is not yet possible. We note that in a comparative analysis some DFT methods (B3LYP, MPW3LYP, M06, M05 with average deviations of 0.43, 0.43, 0.47, 0.52 eV, respectively) proved to be superior to SO-CASPT2 (average deviation 0.65 eV) for the dissociation energies of actinide oxides. On the other hand, for the ionization energies SO-CASPT2 was superior (average deviation 0.41 eV), while the best DFT methods (B3LYP, M06) performed somewhat worse (average deviation 0.47 eV).

The above performance comparisons call for a warning against considering results from state-of-the-art multireference calculations (e.g., SO-CASPT2, being presently the best multireference method that can be applied for large-scale calculations) as superior for predicting all properties of actinide compounds. They are definitely superior for the ground and excited-state electronic structures, and are unavoidable for modeling electronic spectra. For the prediction of other molecular data, however, some DFT exchange-correlation functionals, in conjunction with good-quality small-core pseudopotentials and valence basis sets, seem to be more suitable.

Despite the demonstration of good performance of some exchange-correlation density functionals, the deficiencies of DFT for such difficult systems should be recognized. A description of strongly multiconfigurational systems is limited using DFT, a single-determinant method. Another problem is that in the case of close-lying electronic states, DFT can predict a different energetic sequence for the electronic states than more reliable multireference methods. This is critical in cases where the ground and first excited states are close in energy, with a potential consequence that the DFT ground state corresponds to a low-lying excited state at the more reliable multireference levels. Therefore, the ground electronic states obtained in DFT calculations should be checked carefully by comparison with experimental and advanced multireference electronic structure data, if available. Comparison of molecular parameters (geometry and vibrational frequency) may not be sufficient, because a fortuitous good agreement for computed properties can occur even with an erroneous DFT electronic ground state. Furthermore, if the erroneous and real ground states are very close in energy, the computed dissociation and ionization energies will exhibit only small errors. Similarly, if the relevant valence orbitals are similar in the two states, the bond distances and vibrational frequencies can be similar.

Nevertheless, the present compilations justify the important role of advanced quantum chemical calculations in actinide research. They are very helpful in both interpreting complex experimental results and for predicting molecular data not available from experiment. The progress in computational science will hopefully soon be able to provide more accurate data and the study of larger molecules at adequate theoretical levels, whereas new experimental studies planned at JRC-ITU and also at Lawrence Berkeley National Laboratory on the less common and highly radioactive early actinides (Pa, Np, Pu, Am, Cm) will provide a broader basis for benchmarking computations.

APPENDIX

Tables A1 and A2 list relevant theoretical studies on the ground-state molecular properties of actinide mono- and dioxides.

DOI: 10.1021/cr500426s
Chem. Rev. 2015, 115, 1725−1759

Table A1. Compilation of Relevant Quantum Chemical Studies on the Ground-State Properties of Neutral and Ionic Actinide Monoxides[a]

	ThO			ThO^+			ThO^{2+}			
computational method	state	r_e	ω_e ($\omega_e x_e$)	state	r_e	ω_e ($\omega_e x_e$)	state	r_e	ω_e ($\omega_e x_e$)	ref
CCI/LCPP	$^1\Sigma^+$	1.923	852							141
Dirac−Fock−Roothaan/AE	$^1\Sigma^+$	1.873	923							142
MRCI/SCPP[b]	$^1\Sigma^+$	1.862	867							143
CASSCF/LCPP		1.886	865							180
ZORA-PW91/AE	$^1\Sigma^+$	1.853	882							144
4c-MRCI/AE	$^1\Sigma^+$	1.874	937							145
2c-CASSCF/AE[b]	$^1\Sigma^+$	1.877	866							146
SO-CASPT2/AE[b]	$^1\Sigma_0^+$	1.866	856							147
MRCI+SCC/SCPP[b]	$^1\Sigma^+$	1.845	902							22
CCSD(T)[d]/SCPP[b]	$^1\Sigma^+$	1.845	891							22
B3PW91/SCPP	$^1\Sigma^+$	1.846	898	$^2\Sigma^+$	1.814	960				148
B3LYP/SCPP[b]				$^2\Sigma^+$	1.808		$^1\Sigma^+$	1.771		162
CCSD(T)/SCPP	$^1\Sigma^+$	1.845	898.7 (3.19)							149
SO-CASPT2/AE	$^1\Sigma_0^+$	1.863		$^2\Sigma_{0.5}^+$	1.827		$^1\Sigma_0^+$	1.790		132
CCSD(T)/SCPP[b]	$^1\Sigma^+$	1.845	895.5	$^2\Sigma^+$	1.809	954.4				121
CASPT2/AE	$^1\Sigma^+$	1.863	878.9 (2.3)	$^2\Sigma^+$	1.827	930.8 (2.6)	$^1\Sigma^+$	1.792	987.6 (2.7)	150
M06/SCPP	$^1\Sigma^+$	1.812		$^2\Sigma^+$	1.776		$^1\Sigma^+$	1.744		131
PW91/SCPP	$^1\Sigma^+$	1.835		$^2\Sigma^+$	1.803		$^1\Sigma^+$	1.768		131
B3LYP/SCPP	$^1\Sigma^+$	1.833	910	$^2\Sigma^+$	1.801	961				135
	PaO			PaO^+			PaO^{2+}			
computational method	state	r_e	ω_e ($\omega_e x_e$)	state	r_e	ω_e ($\omega_e x_e$)	state	r_e	ω_e ($\omega_e x_e$)	ref
SO-CISD/MCPP				$^3H_4$	1.852					166
SO-CASPT2/AE	$^2\Phi_{2.5}$	1.818		$^3H_4$	1.804		$^2\Phi_{2.5}$	1.733		132
CASPT2/AE	$^2\Phi$	1.811	926.7 (2.1)	^3H	1.805	932.3 (2.6)	$^2\Phi$	1.752	1040.0 (2.6)	150
M06/SCPP	$^2\Phi$	1.786		^3H	1.754		$^2\Phi$	1.727		131
PW91/SCPP	$^2\Phi$	1.818		^3H	1.792		$^2\Phi$	1.755		131
B3LYP/SCPP	$^2\Phi$	1.812	932							135
SO-CASPT2/AE	$^2\Phi_{2.5}$			$^3\Delta_1$	1.789					133
	UO			UO^+			UO^{2+}			
computational method	state	r_e	ω_e ($\omega_e x_e$)	state	r_e	ω_e ($\omega_e x_e$)	state	r_e	ω_e ($\omega_e x_e$)	ref
B3LYP/SCPP	$^5\Gamma$	1.850	846							157
MP2/LCPP	$^3\Sigma^-$	1.833	1035.9							127
MCSCF/LCPP	^{5}I	1.889	845							156, 181
SO-MCSCF/LCPP				$^4I_{4.5}$	1.842	935				156, 181
CASPT2/AE	^{5}I	1.850	920	^{4}I	1.796	1074				158
SO-CASPT2/AE	$^5I_4$	1.842	855	$^4I_{4.5}$	1.802	912				158
MCSCF/MCPP	$^5I_4$	1.842								163
CISD/MCPP	$^5I_4$	1.854		$^4I_{4.5}$	1.821					163
SO-CISD/MCPP	$^5I_4$	1.849		$^4I_{4.5}$	1.812					163
B3LYP/SCPP[b]				$^4\Delta$	1.794		$^3\Sigma_g$	1.753		164
SO-CASPT2/AE	$^5I_4$	1.838		$^4I_{4.5}$	1.796		$^3H_4$	1.720		132
CASPT2/AE	^{5}I	1.837	857.9 (1.2)	^{4}I	1.799	910.9 (2.4)	^{3}H	1.728	1047.2 (2.8)	150
M06/SCPP	^{3}X	1.773		^{4}I	1.784		^{3}H	1.703		131
PW91/SCPP	^{5}I	1.838		^{4}I	1.796		^{3}H	1.736		131
B3LYP/SCPP	^{5}I	1.843	844	^{4}I	1.798	913				135
	NpO			NpO^+			NpO^{2+}			
computational method	state	r_e	ω_e ($\omega_e x_e$)	state	r_e	ω_e ($\omega_e x_e$)	state	r_e	ω_e ($\omega_e x_e$)	ref
SO-CASPT2/AE	$^6\Delta_{1.5}$	1.839		$^5\Gamma_2$	1.798		$^4I_{4.5}$	1.723		132
CASPT2/AE	$^6\Delta$	1.837	899.8 (3.0)	$^5\Gamma$	1.797	966.8 (2.7)	^{4}I	1.722	1082.0 (3.4)	150
M06/SCPP	$^6\Delta$	1.811		$^5\Gamma$	1.770		^{4}I	1.694		131
PW91/SCPP	$^6\Delta$	1.831		$^5\Gamma$	1.791		^{4}I	1.730		131
B3LYP/SCPP	$^6\Delta$	1.836	836							135
	PuO			PuO^+			PuO^{2+}			
computational method	state	r_e	ω_e ($\omega_e x_e$)	state	r_e	ω_e ($\omega_e x_e$)	state	r_e	ω_e ($\omega_e x_e$)	ref
B3LYP/LCPP				$^6\Sigma^-$	1.875	652	$^5\Sigma^-$	1.96	525	128,129
QCISD/LCPP	$^5\Sigma^-$	1.83	781 (2.77)							125

DOI: 10.1021/cr500426s
Chem. Rev. 2015, 115, 1725−1759

Table A1. continued

	PuO			PuO$^+$			PuO^{2+}			
SO-CASPT2/AE[b]	$^7\Pi_0$	1.820	856	$^6\Pi_{0.5}$	1.789	881	$^5\Gamma_2$	1.731	872	132,182
B3LYP/AE[b]	$^7\Pi$	1.834	820	$^6\Pi$	1.788	899	$^5\Gamma$	1.720	961	182
B3LYP/LCPP	c	1.89	734							183
CASPT2/AE	$^7\Pi$	1.818	858.2 (2.8)	$^6\Pi$	1.777	918.5 (2.2)	$^5\Gamma$	1.720	1012.5 (−1.0)	150
M06/SCPP	$^7\Pi$	1.804		$^6\Pi$	1.767		$^5\Gamma$	1.698		131
PW91/SCPP	$^7\Pi$	1.828		$^6\Pi$	1.788		$^5\Gamma$	1.743		131
B3LYP/SCPP	$^7\Pi$	1.830	821							135
B3LYP/SCPP	c	1.837								272
PBE0/SCPP	c	1.820								272

	AmO			AmO$^+$			AmO^{2+}			
computational method	state	r_e	ω_e ($\omega_e x_e$)	state	r_e	ω_e ($\omega_e x_e$)	state	r_e	ω_e ($\omega_e x_e$)	ref
CASPT2/AE	$^8\Sigma^+$	1.803	917	$^7\Sigma^+$	1.758	924				134
SO-CASPT2/AE	$^8\Sigma_{0.5}{}^+$	1.801		$^7\Sigma_0{}^+$	1.782		$^6\Pi_{0.5}$	1.808		132
CASPT2/AE	$^8\Sigma^+$	1.800	872.2 (3.4)	$^7\Sigma^+$	1.776	964.9 (3.6)	$^6\Pi$	1.774	810.6 (6.0)	150
M06/SCPP	$^8\Sigma^+$	1.820		$^7\Sigma^+$	1.765		$^6\Pi$	1.742		131
PW91/SCPP	$^8\Sigma^+$	1.845		$^7\Sigma^+$	1.787		$^6\Pi$	1.778		131
B3LYP/SCPP	$^8\Sigma^+$	1.836	781							135
PBE0/SCPP	c	1.818								286
B3LYP/SCPP	c	1.835								286

	CmO			CmO$^+$			CmO^{2+}			
computational method	state	r_e	ω_e ($\omega_e x_e$)	state	r_e	ω_e ($\omega_e x_e$)	state	r_e	ω_e ($\omega_e x_e$)	ref
CASPT2/AE	$^9\Sigma$	1.824	858							134
SO-CASPT2/AE	$^9\Sigma_4$	1.836		$^8\Sigma_{0.5}$	1.792		$^7\Sigma_0{}^+$	1.791		132
CASPT2/AE	$^9\Sigma$	1.835	834.9 (2.9)	$^8\Sigma$	1.795	951.3 (2.2)	$^7\Sigma^+$	1.788	819.5 (12.3)	150
M06/SCPP	$^9\Sigma$	1.827		$^8\Sigma$	1.783		$^7\Sigma^+$	1.854		131
PW91/SCPP	$^9\Sigma$	1.840		$^8\Sigma$	1.802		$^7\Sigma^+$	1.780		131
B3LYP/SCPP	$^9\Sigma$	1.842	825							135

BkO				
computational method	state	r_e	ω_e	ref
B3LYP/SCPP	$^8\Phi$	1.835	833	48

CfO				
computational method	state	r_e	ω_e	ref
B3LYP/SCPP	$^7\Pi$	1.822	833	48

EsO				
computational method	state	r_e	ω_e	ref
B3LYP/SCPP	$^6\Delta$	1.822	825	48

FmO				
computational method	state	r_e	ω_e	ref
B3LYP/SCPP	^{3}H	1.850	735	48

MdO				
computational method	state	r_e	ω_e	ref
B3LYP/SCPP	$^2\Pi$	1.898	673	48

NoO				
computational method	state	r_e	ω_e	ref
B3LYP/SCPP	$^1\Sigma$	1.923	650	48

LrO				
computational method	state	r_e	ω_e	ref
ZORA-BP/AE	$^2\Sigma^+$	1.883	756	160
CCSD(T)/SCPP[b]	$^2\Sigma^+$	1.871	764	161
B3LYP/SCPP	$^2\Sigma^+$	1.871	756	135

[a]The bond distances are given in Å, the harmonic vibrational frequencies (ω_e) and anharmonicities ($\omega_e x_e$) in cm^{-1}. The computational levels are characterized by the theory and type of basis set. The theories include scalar relativistic effects, without the inclusion of spin−orbit coupling, except where noted. The basis sets are either all-electron basis set (AE) or ones including relativistic pseudopotentials. The large-, medium-, and small-core pseudopotentials are abbreviated as LCPP, MCPP, and SCPP, respectively. [b]The reference reports calculations performed at several theoretical levels from which only selected significant results are shown in this table. For the full set of calculations, see the original paper. [c]Electronic state not given in the reference. [d]The CCSDT(T) calculations were performed using counterpoise correction for basis set superposition error.

DOI: 10.1021/cr500426s
Chem. Rev. 2015, 115, 1725−1759

Table A2. Compilation of Relevant Quantum Chemical Studies on the Ground-State Properties of Neutral and Ionic Actinide Dioxides[a]

	ThO_2			ThO_2^+			ThO_2^{2+}			
computational method	state	r_e	ω_{as}, ω_s, ω_β	state	r_e	ω_{as}, ω_s, ω_β	state	r_e	ω_{as}, ω_s, ω_β	ref
ZORA-PW91/AE	$^1A_1$	1.911	759, 812, 157							144
DHF/AE	$^1A_1$	1.898	761, 896, 139							191
B3LYP/SCPP	$^1A_1$	1.906	760, 802, 159							170
CCSD(T)/SCPP[b]	$^1A_1$	1.915 (122°)	748, 802, 166							192
B3LYP/SCPP	$^1A_1$	1.899 (119.1°)	772, 824, 157							193
CCSD(T)/SCPP[b]	$^1A_1$	1.9054 (116.47°)	756.0, 807.7, 165.3[c]							224
B3LYP/SCPP	$^1A_1$	1.8992 (119.23)	770.4, 822.5, 156.1							224
SO-CASPT2/AE	$^1A_1$	1.923 (111.9°)		$^2\Sigma_{0.5u}$	1.832		$^1\Sigma_{0g}$	1.903		132
CCSD(T)/SCPP[b]	$^1A_1$	1.905 (116.5°)	755.5, 809.7, 163.8	$^2\Sigma_u$	1.874	607.2, 739.2, 16.0				121
M06/SCPP[b]	$^1A_1$	1.872 (120.8°)		$^2\Sigma_u$	1.827		$^1\Sigma_g$	1.867		131
PW91/SCPP[b]	$^1A_1$	1.898 (118.5°)		$^2\Sigma_u$	1.870		$^1\Sigma_g$	1.856		131
B3LYP/SCPP	$^1A_1$	1.898 (119.0°)	766, 820, 155	$^2\Sigma_u$	1.868	752, 631, 38	$^1\Sigma_g$	1.851	772, 755, 126	150

	PaO_2			PaO_2^+			PaO_2^{2+}			
computational method	state	r_e	ω_{as}, ω_s, ω_β	state	r_e	ω_{as}, ω_s, ω_β	state	r_e	ω_{as}, ω_s, ω_β	ref
DHF/AE				$^1\Sigma_g^+$	1.742	1158, 1029, 130				191
CCSD(T)/SCPP[b]				$^1\Sigma_g^+$	1.812	945, 882, 141				192
SO-CASPT2/AE	$^2\Sigma_{0.5g}$	1.816		$^1\Sigma_{0g}$	1.767		$^2\Sigma_{0.5g}$	1.726		132
M06/SCPP[b]	$^2\Sigma_g$	1.786		$^1\Sigma_g$	1.745		$^2\Sigma_g$	1.738		131
PW91/SCPP[b]	$^2\Sigma_g$	1.813		$^1\Sigma_g$	1.777		$^2\Sigma_g$	1.785		131
B3LYP/SCPP	$^2\Sigma_g$	1.806	871, 828, 59	$^1\Sigma_g$	1.768	995, 938, 108	$^2\Sigma_g$	1.772	891, 626, 94	150

	UO_2			UO_2^+			UO_2^{2+}			
computational method	state	r_e	ω_{as}, ω_s, ω_β	state	r_e	ω_{as}, ω_s, ω_β	state	r_e	ω_{as}, ω_s, ω_β	ref
MP2/LCPP	$^3\Sigma^+_u$	1.779	1022, 947, 294							126
DHF/AE							$^1\Sigma_g^+$	1.650	1294, 1234, 246	191
4c-CCSD/AE							$^1\Sigma_{0g}^+$	1.696	1168, 1040, 180	214
4c-CCSD(T)/AE							$^1\Sigma_{0g}^+$	1.715	ω_s = 974	214
CCSD/SCPP[b]							$^1\Sigma_g^+$	1.702	1148, 1063, 180	215
B3LYP/SCPP[b]							$^1\Sigma_g^+$	1.706	1143, 1041, 150	215
B3LYP/SCPP	$^3\Phi_u$	1.800	931, 874, 138	$^2\Phi_u$	1.764	1010, 936, 148	$^1\Sigma_g^+$	1.705	1140, 1041, 161	157
CASPT2/SCPP				$^2\Phi_u$	1.773	942, 858	$^1\Sigma_g^+$	1.705	1066, 959	206
CASPT2/AE[b]	$^3\Phi_u$	1.806	932, 809							197
SO-CASPT2/AE[b]	$^3\Phi_{2u}$	1.766	923, 948							197
SO-CASPT2/AE[b]	$^3\Phi_{2u}$	1.827	855, 781							132,197
B3LYP/SCPP[b]	$^3\Phi_u$	1.794	937, 875							197
CCSD(T)/SCPP[b]							$^1\Sigma_g^+$	1.702	1111, 1021, 201	192
CCD/LCPP[b]	$^3\Phi_u$	1.766	958, 927, 168	$^2\Phi_u$	1.744	1031, 971, 146	$^1\Sigma_g^+$	1.678	1179, 1100, 194	207
MP2/LCPP[b]	$^3\Phi_u$	1.795	913, 896, 149	$^2\Phi_u$	1.80	955, 901, 101	$^1\Sigma_g^+$	1.728	1024, 923, 126	207
B3LYP/LCPP[b]	$^3\Phi_u$	1.764	933, 880, 222	$^2\Phi_u$	1.746	1001, 916, 191	$^1\Sigma_g^+$	1.678	1126, 1027, 144	207
ZORA-PW91/AE	$^3\Phi_u$	1.807	919, 856							203
QR-BP86/AE	$^3\Phi_u$	1.813	948, 853				$^1\Sigma_g^+$	1.720	1095, 997	130
SO-QR-BP86/AE	$^3\Phi_u$	1.803	934, 863							130
ZORA-PW91/AE				$^2\Phi_u$	1.773	987, 911				208
B3LYP/SCPP[b]				$^2\Phi_u$	1.760		$^1\Sigma_g^+$	1.700		164
DC-IHFSCCSD/AE	$^3\Phi_{2u}$	1.770								57
CCSD(T)/SCPP[b]							$^1\Sigma_g^+$	1.6898	1113.0, 1031.6, 174.5[c]	224
B3LYP/SCPP[b]							$^1\Sigma_g^+$	1.6950	1138.9, 1049.7, 162.7	224
MRCI/AE				$^2\Phi_u$	1.742					209
SO-CASPT2/AE				$^2\Phi_{2.5u}$	1.745		$^1\Sigma_{0g}^+$	1.710		132
M06/SCPP[b]	^3H_g	1.816		$^2\Phi_u$	1.730		$^1\Sigma_g^+$	1.672		131
PW91/SCPP[b]	$^3\Phi_u$	1.808		$^2\Phi_u$	1.764		$^1\Sigma_g^+$	1.710		131
B3LYP/SCPP	$^3\Phi_u$	1.789	926, 874, 141	$^2\Phi_u$	1.753	1005, 937, 151	$^1\Sigma_g^+$	1.693	1135, 1044, 166	150
PBE0/SCPP	*d*	1.777								282
B3LYP/SCPP	*d*	1.795								282

DOI: 10.1021/cr500426s
Chem. Rev. 2015, 115, 1725−1759

Table A2. continued

	NpO_2			NpO_2^+			NpO_2^{2+}			
computational method	state	r_e	ω_{as}, ω_s, ω_β	state	r_e	ω_{as}, ω_s, ω_β	state	r_e	ω_{as}, ω_s, ω_β	ref
SO-CI/LCPP	$^4\Sigma_g$			4_g ($^3H_{4g}$)	1.73	ω_s = 913	2.5_u ($^2\Phi_{2.5u}$)	1.66	ω_s = 1059	255
QR-BP86/AE	$^4\Sigma_g$	1.773	869, 868				$^2\Phi_u$	1.717	1075, 969	130
SO-QR-BP86/AE	$^4\Sigma_g$	1.778	892, 870							130
IHFSCC/AE				4_g ($^3H_{4g}$)	1.701					58
SO-CASPT2/AE	$^4H_{3.5\ g}$	1.761		$^3H_{4g}$	1.723		$^2\Phi_{2.5u}$	1.700		132
M06/SCPP[b]	$^4\Phi_u$	1.795		^3H_g	1.708		$^2\Phi_u$	1.665		131
PW91/SCPP[b]	^4H_g	1.803		^3H_g	1.745		$^2\Phi_u$	1.708		131
B3LYP/SCPP	^4H_g	1.767	933, 874, 194	^3H_g	1.733	1015, 937, 210	$^2\Phi_u$	1.688	1126, 1019, 184	150

	PuO_2			PuO_2^+			PuO_2^{2+}			
computational method	state	r_e	ω_{as}, ω_s, ω_β	state	r_e	ω_{as}, ω_s, ω_β	state	r_e	ω_{as}, ω_s, ω_β	ref
MP2/LCPP	$^5\Sigma_g^+$	1.800	744, 656, 306							219
B3LYP/SCPP[b]							^3H_g	1.688	1144, 1014, 229	215
CISD+Q/SCPP[b]							^3H_g	1.677		220
CCSD(T)/LCPP[b]	$^5\Sigma_g^+$	1.870	828, 792, 109							21
SO-CASPT2/SCPP							$^3H_{4g}$	1.699	1106, 1065	221
QR-BP86/AE	$^5\Sigma_g^+$	1.833	781, 772				^3H_g	1.703	1100, 953	130
SO-BP86/AE	$^5\Sigma_g^+$	1.812	866, 791							130
IHFSCC/AE							4_g ($^3H_{4g}$)	1.645		58
B3LYP/LCPP	*d*	1.88	758, 614, 181							183
B3LYP/AE[b]	$^5\Sigma_g^+$	1.818	ω_s = 773				^3H_g	1.678	ω_s = 1004	182
SO-CASPT2/AE[b]	$^5\Phi_{1u}$	1.744	ω_s = 837	$^4\Phi_{1.5u}$	1.704	ω_s = 962	$^3H_{4g}$	1.675	ω_s = 1019	132,182
M06/SCPP[b]	$^5\Sigma_g$	1.786		$^4\Phi_u$	1.692		^3H_g	1.650		131
PW91/SCPP[b]	$^5\Phi_u$	1.802		$^4\Phi_u$	1.728		^3H_g	1.696		131
B3LYP/SCPP	$^5\Phi_u$	1.748	933, 863, 183	$^4\Phi_u$	1.714	1019, 927, 255	^3H_g	1.673	1117, 997, 251	150
B3LYP/SCPP	*d*	1.822								272
PBE0/SCPP	*d*	1.800								272

	AmO_2			AmO_2^+			AmO_2^{2+}			
computational method	state	r_e	ω_{as}, ω_s, ω_β	state	r_e	ω_{as}, ω_s, ω_β	state	r_e	ω_{as}, ω_s, ω_β	ref
CASPT2/AE	$^6\Pi_u$	1.832								134
CASPT2/AE[b]				$^5\Sigma_g^+$	1.754		$^4\Phi_u$	1.712		223
ZORA-PW91/AE[b]				$^5\Sigma_g^+$	1.744		$^4\Phi_u$	1.697		223
SO-CASPT2/AE	$^6\Pi_{2.5u}$	1.807		$^5\Sigma_{0g}$	1.721		$^4\Phi_{1.5u}$	1.679		132
M06/SCPP[b]	$^6\Pi_u$	1.800		$^5\Sigma_g$	1.690		$^4\Phi_u$	1.642		131
PW91/SCPP[b]	^6X	1.827 (175.1°)		$^5\Sigma_g$	1.733		$^4\Phi_u$	1.688		131
B3LYP/SCPP	$^6\Pi_u$	1.826	795, 740, 90	$^5\Sigma_g$	1.716	997, 876, 267	$^4\Phi_u$	1.666	1089, 948, 306	150
PBE0/SCPP	*d*	1.807								286
B3LYP/SCPP	*d*	1.828								286

	AmO_2^{3+}		
computational method	state	r_e	ref
CASPT2/AE[b]	^3H_g	1.725	223
ZORA-PW91/AE[b]	^3H_g	1.710	223

	CmO_2			CmO_2^+			CmO_2^{2+}			
computational method	state	r_e	ω_{as}, ω_s, ω_β	state	r_e	ω_{as}, ω_s, ω_β	state	r_e	ω_{as}, ω_s, ω_β	ref
SO-CASPT2/AE	$^7\Sigma_{0g}$	1.832		$^6\Pi_{0.5\ g}$	1.746		$^5\Sigma_{0g}$	1.674		132
M06/SCPP[b]	$^7\Sigma_g$	1.815		$^6\Pi_g$	1.716		$^5\Sigma_g$	1.653		131
PW91/SCPP[b]	$^7\Sigma_g$	1.840		$^6\Pi_g$	1.759		$^5\Sigma_g$	1.707		131
B3LYP/SCPP	$^7\Sigma_g$	1.839	779, 720, 96	$^6\Pi_g$	1.748	884, 755, 193	$^5\Sigma_g$	1.688	957, 768, 304	150

	BkO_2			
computational method	state	r_e	ω_{as}, ω_s, ω_β	ref
B3LYP/SCPP	^6X	1.820	791, 725, 152	135

	CfO_2			
computational method	state	r_e	ω_{as}, ω_s, ω_β	ref
B3LYP/SCPP	^5X	1.817	795, 716, 183	135

	EsO_2			
computational method	state	r_e	ω_{as}, ω_s, ω_β	ref
B3LYP/SCPP	^4X	1.795	816, 738, 213	135

DOI: 10.1021/cr500426s
Chem. Rev. 2015, 115, 1725−1759

Table A2. continued

		FmO_2		
computational method	state	r_e	ω_{as}, ω_s, ω_β	ref
B3LYP/SCPP	^3X	1.791	816, 730, 221	135
		MdO_2		
computational method	state	r_e	ω_{as}, ω_s, ω_β	ref
B3LYP/SCPP	^2X	1.812	789, 703, 182	135
		NoO_2		
computational method	state	r_e	ω_{as}, ω_s, ω_β	ref
B3LYP/SCPP	$^1\Sigma$	1.843	753, 668, 170	135
		LrO_2		
computational method	state	r_e	ω_{as}, ω_s, ω_β	ref
B3LYP/SCPP	$^2\Pi$	1.940 (101.5°)	686, 271, 114	135

[a]The bond distances are given in Å, the harmonic vibrational frequencies in cm^{-1}. For the bent structures the bond angles are given in parentheses. The computational methods are characterized by the theory and type of basis set. The theories include scalar relativistic effects, without the inclusion of spin−orbit coupling, except where noted. The basis sets are either all-electron basis set (AE) or ones including relativistic pseudopotentials. The large-, medium-, and small-core pseudopotentials are abbreviated as LCPP, MCPP, and SCPP, respectively. [b]The reference reports calculations performed at several theoretical levels from which only selected significant results are shown in this table. For the full set of calculations, see the original paper. [c]Anharmonic frequencies including also SO corrections from DFT calculations. Order of the symmetric and asymmetric stretch of ThO_2 is given interchanged in ref 224. [d]Electronic state is not given in the reference.

ASSOCIATED CONTENT

Special Issue Paper

This paper is an additional review for *Chem. Rev.* **2013**, *113* (2) "Nuclear Chemistry".

AUTHOR INFORMATION

Corresponding Authors

*E-mail: attila.kovacs@ec.europa.eu.
*E-mail: rudy.konings@ec.europa.eu.

Notes

The authors declare no competing financial interest.

Biographies

Attila Kovács was born in Pápa, Hungary, in 1964. He received his M.Sc. degree at the Faculty of Chemical Engineering of the Technical University of Budapest in 1988. His Univ. Dr. thesis on NMR investigation of heterocyclic compounds was completed in 1992. He then changed his field of research to vibrational spectroscopy and quantum chemical calculations, where he earned Ph.D. and D.Sc. degrees in 1997 and 2005, respectively. He authored or coauthored over 150 research papers. His recent research is focused on the chemical properties of small molecules containing f-elements. He joined the Institute for Transuranium Elements (European Commission, Joint Research Centre) in 2010, while he is also a private university professor of the Budapest University of Technology and Economics.

Rudy Konings graduated from the Utrecht University with a M.Sc. in Earth Sciences in 1985. He then joined The Netherlands Energy Research Foundation ECN as a researcher in the field of thermodynamics of nuclear materials and defended his Ph.D. at the University of Amsterdam in 1990. He stayed at ECN and subsequently at NRG (Nuclear Research and Consultancy Group) working on nuclear fuel-related issues. In 1999 he joined the Institute for Transuranium Elements in Karlsruhe (Germany), which is part of the Joint Research Centre of the European Commission. There he currently is the head of the Materials Research Unit. His research interests are nuclear fuels and actinide materials, with particular emphasis on high temperature chemistry and thermodynamics. He is part-time professor at the Delft University of Technology (Netherlands), where he holds the chair of "Chemistry of the nuclear fuel cycle". He has authored or coauthored more than 250 scientific articles.

DOI: 10.1021/cr500426s
Chem. Rev. 2015, 115, 1725−1759

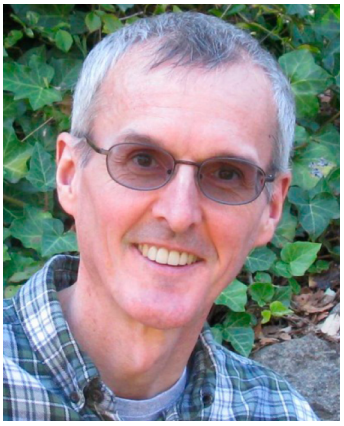

John Gibson is a Senior Scientist in the Chemical Sciences Division of Lawrence Berkeley National Laboratory. Raised in Longmeadow, Massachusetts, he received his B.A. degree (summa cum laude) from Boston University in 1979, and Ph.D. degree in Physical Chemistry from the University of California, Berkeley in 1983 under the supervision of Prof. Leo Brewer. He spent 24 years as a research scientist at Oak Ridge National Laboratory before returning to Berkeley in 2007. His research interests focus on the chemistry of the actinide elements, including those beyond uranium, having performed experiments on the actinides from thorium through fermium. His current research emphasis is on physical and chemical properties of gas-phase actinide molecules and complexes. He has more than 130 refereed journal articles.

Ivan Infante studied chemistry at the Universita della Basilicata (Italy). He then moved to the Vrije Universiteit in Amsterdam where he started his doctorate studies under the supervision of Lucas Visscher and Evert Jan Baerends. Here, he earned his Ph.D. in October 2006 with a thesis aimed at the spectroscopic characterization of actinide molecules using highly precise ab initio computational methodologies. Afterward, he moved to the University of Geneva (Switzerland) as a postdoctoral fellow under the supervision of Laura Gagliardi, where he elucidated the ground- and excited-state nature of transition and heavy metal complexes. In 2008, he was bestowed a Juan de la Cierva grant and moved to the University of the Basque Country (Spain) where he could pursue his independent research career. In May 2014, he was awarded a prestigious Vidi grant from The Netherlands organization for scientific research. This grant will enable him to establish his own research group at the Vrije Universiteit in Amsterdam. His current research is in the field of Computational Materials Chemistry, with an emphasis in solar energy conversion. He currently has published 45 articles in international peer-reviewed journals.

Laura Gagliardi obtained her Ph.D. from the University of Bologna, Italy, in theoretical chemistry working under the guidance of Professor Gian Luigi Bendazzoli. After a postdoctoral appointment at Cambridge, UK with Nicholas Handy, she joined the Department of Chemistry at the University of Palermo in 2002. She then moved to the University of Geneva, Switzerland in 2005. Her move to the University of Minnesota came in 2009, where she is now Distinguished McKnight University Professor and Professor in the Department of Chemistry. Her research interests are in the area of theoretical and computational chemistry, with special focus on inorganometallic materials and molecular systems. She has coauthored 190 publications. In 2004 she won the annual award of the International Academy of Quantum Molecular Science to scientists under 40, with citation: "for her innovative contributions to prediction and understanding of new inorganic molecules using quantum chemical methods". She is currently the director of the Energy Frontier Research Center named Inorganometallic Catalyst Design Center, based at the University of Minnesota.

ACKNOWLEDGMENTS

The seventh Framework Programme of the European Commission under grant no. 323300 (TALISMAN), the Hungarian Scientific Research Foundation under grant no. 75972 (A.K.), Eusko Jaurlaritza under contract no. GIC07/85 IT-330-07, the Spanish Office for Scientific Research under contract no. CTQ2011-27374 (II), and the U.S. Department of Energy Director, Office of Basic Energy Sciences under award number DE-SC002183 (L.G.) and contract number DE-AC02-05CH11231 (J.K.G.).

REFERENCES

(1) Gray, T. *The Elements: A Visual Exploration of Every Known Atom in the Universe*; Black Dog & Leventhal Publishers: New York, 2009.
(2) Greenwood, N. N.; Earnshaw, A. *Chemistry of the Elements*; Butterworth-Heinemann: Oxford, 1997.
(3) Heaven, M. C. *Phys. Chem. Chem. Phys.* **2006**, *8*, 4497.
(4) Marçalo, J.; Gibson, J. K. *J. Phys. Chem. A* **2009**, *113*, 12599.
(5) Heaven, M. C.; Gibson, J. K.; Marçalo, J. In *The Chemistry of the Actinide and Transactinide Elements*; Edelstein, N. M., Fuger, J., Morss, L. R., Eds.; Springer: Dordrecht, 2011; Vol. 6, p 4079.
(6) Dolg, M.; Stoll, H. In *Handbook on the Physics and Chemistry of Rare Earths*; Geschneider, K. A., Jr., Eyring, L., Eds.; Elsevier: Amsterdam, 1996; Vol. 22, Chapter 152.
(7) Dolg, M. In *Encyclopedia of Computational Chemistry*; Schleyer, P. v. R., Allinger, N. L., Clark, T., Gasteiger, J., Kollman, P. A., Schaefer, H. F., III, Schreiner, P. R., Eds.; Wiley: Chichester, 1998; p 1478.
(8) Dolg, M.; Cao, X. In *Computational Inorganic and Bioinorganic Chemistry*; Solomon, E. I., Scott, R. A., King, R. B., Eds.; Wiley: Chichester, 2009.
(9) Pepper, M.; Bursten, B. E. *Chem. Rev.* **1991**, *91*, 719.

DOI: 10.1021/cr500426s
Chem. Rev. 2015, 115, 1725−1759

(10) Schreckenbach, G.; Hay, P. J.; Martin, R. L. *J. Comput. Chem.* **1999**, *20*, 70.
(11) Kaltsoyannis, N. *Chem. Soc. Rev.* **2003**, *32*, 9.
(12) Kaltsoyannis, N.; Hay, P. J.; Li, J.; Blaudeau, J. P.; Bursten, B. E. In *The Chemistry of the Actinide and Transactinide Elements*; Morss, L. R., Edelstein, N. M., Fuger, J., Katz, J. J., Eds.; Springer: Dordrecht, 2006; p 1893.
(13) Wang, D.; van Gunsteren, W. F.; Chai, Z. *Chem. Soc. Rev.* **2012**, *41*, 5836.
(14) Konings, R. J. M.; Beneš, O.; Kovács, A.; Manara, D.; Sedmidubský, D.; Gorokhov, L.; Iorish, V. S.; Yungman, V.; Shenyavskaya, E.; Osina, E. *J. Phys. Chem. Ref. Data* **2014**, *43*, 013101.
(15) Pople, J. A.; Seeger, R.; Krishnan, R. *Int. J. Quantum Chem.* **1977**, *12*, 149.
(16) Bartlett, R. J. *Annu. Rev. Phys. Chem.* **1981**, *32*, 359.
(17) Helgaker, T.; Jørgensen, P.; Olsen, J. *Molecular Electronic-Structure Theory*; Wiley: Chichester, 2000.
(18) Siegbahn, P. E. M. In *Methods in Computational Molecular Physics*; Diercksen, G. H. F., Wilson, S., Eds.; Reidel: Dordrecht, 1982.
(19) Siegbahn, P. E. M.; Almlöf, J.; Heiberg, A.; Roos, B. O. *J. Chem. Phys.* **1981**, *74*, 2384.
(20) Roos, B. O.; Taylor, P. R.; Siegbahn, P. E. M. *Chem. Phys.* **1980**, *48*, 157.
(21) Archibong, E. F.; Ray, A. K. *J. Mol. Struct. (THEOCHEM)* **2000**, *530*, 165.
(22) Cao, X.; Dolg, M.; Stoll, H. *J. Chem. Phys.* **2003**, *118*, 487.
(23) Andersson, K.; Malmqvist, P.-Å.; Roos, B. O. *J. Chem. Phys.* **1992**, *96*, 1218.
(24) Malmqvist, P.-Å.; Pierloot, K.; Shahi, A. R. M.; Cramer, C. J.; Gagliardi, L. *J. Chem. Phys.* **2008**, *128*, 204109.
(25) Li Manni, G.; Aquilante, F.; Gagliardi, L. *J. Chem. Phys.* **2011**, *134*, 034114.
(26) Li Manni, G.; Ma, D.; Aquilante, F.; Olsen, J.; Gagliardi, L. *J. Chem. Theory Comput.* **2013**, *9*, 3375.
(27) Ma, D.; Li Manni, G.; Gagliardi, L. *J. Chem. Phys.* **2011**, *135*, 044128.
(28) Ivanic, J. *J. Chem. Phys.* **2003**, *119*, 9364.
(29) Bartlett, R. J.; Musial, M. *Rev. Mod. Phys.* **2007**, *79*, 291.
(30) Čížek, J. *J. Chem. Phys.* **1966**, *45*, 4256.
(31) Čížek, J. In *Advances in Chemical Physics: Correlation Effects in Atoms and Molecules*; LeFebvre, R., Moser, C., Eds.; Wiley: New York, 1969; Vol. *14*, p 35.
(32) Čížek, J.; Paldus, J. *Int. J. Quantum Chem.* **1971**, *5*, 359.
(33) Paldus, J.; Čížek, J.; Shavitt, I. *Phys. Rev. A* **1972**, *5*, 50.
(34) Bartlett, R. J.; Purvis, G. D. *Int. J. Quantum Chem.* **1978**, *14*, 561.
(35) Bartlett, R. J.; Purvis, G. D., III. *Phys. Scr.* **1980**, *21*, 255.
(36) Pople, J. A.; Krishnan, R.; Schlegel, H. B.; Binkley, J. S. *Int. J. Quantum Chem.* **1978**, *14*, 545.
(37) Sinanoğlu, O. *J. Chem. Phys.* **1962**, *36*, 706.
(38) Nesbet, R. K. In *Advances in Chemical Physics: Correlation Effects in Atoms and Molecules*; LeFebvre, R., Moser, C., Eds.; Wiley: New York, 1969; Vol. *14*, p 1.
(39) Purvis, G. D., III; Bartlett, R. J. *J. Chem. Phys.* **1982**, *76*, 1910.
(40) Lee, Y. S.; Kucharski, S. A.; Bartlett, R. J. *J. Chem. Phys.* **1984**, *81*, 5906.
(41) Noga, J.; Bartlett, R. J.; Urban, M. *Chem. Phys. Lett.* **1987**, *134*, 126.
(42) Kucharski, S. A.; Bartlett, R. J. *Theor. Chim. Acta* **1991**, *80*, 387.
(43) Urban, M.; Noga, J.; Cole, S. J.; Bartlett, R. J. *J. Chem. Phys.* **1985**, *83*, 4041.
(44) Raghavachari, K.; Trucks, G. W.; Pople, J. A.; Head-Gordon, M. *Chem. Phys. Lett.* **1989**, *157*, 479.
(45) Watts, J. D.; Gauss, J.; Bartlett, R. J. *J. Chem. Phys.* **1993**, *98*, 8718.
(46) Mukherjee, D.; Pal, S. In *Advances in Quantum Chemistry*; Löwdin, P.-O., Ed.; Elsevier: Amsterdam, 1989; Vol. *20*, p 291.
(47) Eliav, E.; Kaldor, U.; Ishikawa, Y. *Phys. Rev. A* **1994**, *50*, 1121.
(48) Kaldor, U. *Theor. Chim. Acta* **1991**, *80*, 427.
(49) Lindgren, I.; Mukherjee, D. *Phys. Rep.* **1987**, *151*, 93.
(50) Chattopadhyay, S.; Mitra, A.; Sinha, D. *J. Chem. Phys.* **2006**, *125*, 244111.
(51) Kaldor, U.; Eliav, E. In *Advances in Quantum Chemistry*; Sabin, J. R., Zerner, M. C., Brändas, E., Wilson, S., Maruani, J., Smeyers, Y. G., Grout, P. J., McWeeny, R., Eds.; Elsevier: Amsterdam, 1998; Vol. *31*, p 313.
(52) Sinha, D.; Mukhopadhyay, S. K.; Chaudhuri, R. K.; Mukherjee, D. *Chem. Phys. Lett.* **1989**, *154*, 544.
(53) Borschevsky, A.; Eliav, E.; Vilkas, M. J.; Ishikawa, Y.; Kaldor, U. *Phys. Rev. A* **2007**, *75*, 042514.
(54) Eliav, E.; Kaldor, U.; Ishikawa, Y. *Phys. Rev. A* **1995**, *51*, 225.
(55) Eliav, E.; Kaldor, U.; Ishikawa, Y. *Phys. Rev. A* **1995**, *52*, 291.
(56) Eliav, E.; Kaldor, U.; Ishikawa, Y. *Phys. Rev. A* **1995**, *52*, 2765.
(57) Infante, I.; Eliav, E.; Vilkas, M. J.; Ishikawa, Y.; Kaldor, U.; Visscher, L. *J. Chem. Phys.* **2007**, *127*, 124308.
(58) Infante, I.; Gomes, A. S. P.; Visscher, L. *J. Chem. Phys.* **2006**, *125*, 074301.
(59) Nayak, M. K.; Chaudhuri, R. K. *Eur. Phys. J. D* **2006**, *37*, 171.
(60) Sur, C.; Chaudhuri, R. K. *Phys. Rev. A* **2007**, *76*, 012509.
(61) Visscher, L.; Eliav, E.; Kaldor, U. *J. Chem. Phys.* **2001**, *115*, 9720.
(62) Visscher, L.; Lee, T. J.; Dyall, K. G. *J. Chem. Phys.* **1996**, *105*, 8769.
(63) Yakobi, H.; Eliav, E.; Kaldor, U. *J. Chem. Phys.* **2007**, *126*, 184305.
(64) Hohenberg, P.; Kohn, W. *Phys. Rev.* **1964**, *136*, B864.
(65) Cramer, C. J.; Truhlar, D. G. *Phys. Chem. Chem. Phys.* **2009**, *11*, 10757.
(66) Engel, E.; Dreizler, R. M. *Density Functional Theory: An Advanced Course*; Springer: Berlin, 2011.
(67) Sholl, D.; Steckel, J. A. *Density Functional Theory: A Practical Introduction*; Wiley-Interscience: Weinheim, 2009.
(68) Kohn, W.; Sham, L. J. *Phys. Rev.* **1965**, *140*, A1133.
(69) Jacob, C. R.; Reiher, M. *Int. J. Quantum Chem.* **2012**, *112*, 3661.
(70) Löwdin, P.-O. *Phys. Rev.* **1955**, *97*, 1474.
(71) Kohn, W. *Rev. Mod. Phys.* **1999**, *71*, 1253.
(72) Schuch, N.; Verstraete, F. *Nat. Phys.* **2009**, *5*, 732.
(73) Perdew, J. P.; Schmidt, K. In *Density Functional Theory and Its Applications to Materials*; Doren, V. E. V., Alsenoy, K. V., Geerlings, P., Eds.; American Institute of Physics: Melville, NY, 2001; p 1.
(74) Tao, J.; Perdew, J. P.; Staroverov, V. N.; Scuseria, G. E. *Phys. Rev. Lett.* **2003**, *91*, 146401.
(75) Staroverov, V. N.; Scuseria, G. E.; Tao, J.; Perdew, J. P. *Phys. Rev. B* **2004**, *69*, 075102.
(76) Staroverov, V. N.; Scuseria, G. E.; Tao, J.; Perdew, J. P. *Phys. Rev. B* **2008**, *78*, 239907.
(77) Perdew, J. P. *MRS Bull.* **2013**, *38*, 743.
(78) Reiher, M.; Wolf, A. *Relativistic Quantum Chemistry: The Fundamental Theory of Molecular Science*; Wiley-VCH: Weinheim, 2009.
(79) Dyall, K. G.; Faegri, K. J. *Introduction to Relativistic Quantum Chemistry*; Oxford Univ. Press: New York, 2007.
(80) *Relativistic Electronic Structure Theory - Part 1: Fundamentals*; Schwerdtfeger, P., Ed.; Elsevier Science B. V.: Amsterdam, 2002; Vol. *11*.
(81) *Relativistic Methods for Chemists*; Barysz, M., Ishikawa, Y., Eds.; Springer: London, 2010; Vol. *10*.
(82) Dirac, P. A. M. *Proc. R. Soc. A* **1930**, *126*, 360.
(83) Desclaux, J. P. *Comput. Phys. Commun.* **1975**, *9*, 31.
(84) Desclaux, J. P.; Mayers, D. F.; O'Brien, F. *J. Phys. B: At., Mol. Opt. Phys.* **1971**, *4*, 631.
(85) Dyall, K. G.; Grant, I. P.; Johnson, C. T.; Parpia, F. A.; Plummer, E. P. *Comput. Phys. Commun.* **1989**, *55*, 425.
(86) Grant, I. P. *Adv. Phys.* **1970**, *19*, 747.
(87) Grant, I. P.; McKenzie, B. J.; Norrington, P. H.; Mayers, D. F.; Pyper, N. C. *Comput. Phys. Commun.* **1980**, *21*, 207.
(88) Grant, I. P.; Quiney, H. M. *Adv. At., Mol., Opt. Phys.* **1988**, *23*, 37.
(89) Barthelat, J.-C.; Pélissier, M.; Durand, P. *Phys. Rev. A* **1980**, *21*, 1773.
(90) Cowan, R. D.; Griffin, D. C. *J. Opt. Soc. Am.* **1976**, *66*, 1010.
(91) Hess, B. A. *Phys. Rev. A* **1986**, *33*, 3742.
(92) Jansen, G.; Hess, B. A. *Phys. Rev. A* **1989**, *39*, 6016.
(93) Nakajima, T.; Hirao, K. *Chem. Phys. Lett.* **1999**, *302*, 383.
(94) Nakajima, T.; Hirao, K. *Chem. Rev.* **2012**, *112*, 385.

DOI: 10.1021/cr500426s
Chem. Rev. 2015, 115, 1725−1759

(95) Samzow, R.; Hess, B. A.; Jansen, G. *J. Chem. Phys.* **1992**, *96*, 1227.
(96) Wolf, A.; Reiher, M.; Hess, B. A. *J. Chem. Phys.* **2002**, *117*, 9215.
(97) Wood, J. H.; Boring, A. M. *Phys. Rev. B* **1978**, *18*, 2701.
(98) Dolg, M. In *Relativistic Electronic Structure Theory − Part 1: Fundamentals*; Schwerdtfeger, P., Ed.; Elsevier: Amsterdam, 2002; p 793.
(99) Dolg, M.; Cao, X. *Chem. Rev.* **2012**, *112*, 403.
(100) Hess, B. A.; Marian, C. M.; Peyerimhoff, S. D. In *Advanced Series in Physical Chemistry*; Yarkony, R., Ed.; World Scientific Publishing Co.: Singapore, 1995; Vol. *2*, part I, p 152.
(101) Douglas, N.; Kroll, N. M. *Ann. Phys.* **1974**, *82*, 89.
(102) Hess, B. A.; Marian, C. M.; Wahlgren, U.; Gropen, O. *Chem. Phys. Lett.* **1996**, *251*, 365.
(103) Malmqvist, P.-Å.; Roos, B. O.; Schimmelpfennig, B. *Chem. Phys. Lett.* **2002**, *357*, 230.
(104) Roos, B. O.; Malmqvist, P.-Å. *Phys. Chem. Chem. Phys.* **2004**, *6*, 2919.
(105) van Lenthe, E.; Baerends, E. J.; Snijders, J. G. *J. Chem. Phys.* **1993**, *99*, 4597.
(106) Chang, C.; Pelissier, M.; Durand, P. *Phys. Scr.* **1986**, *34*, 394.
(107) van Lenthe, E.; Baerends, E. J.; Snijders, J. G. *J. Chem. Phys.* **1994**, *101*, 9783.
(108) Iliaš, M.; Saue, T. *J. Chem. Phys.* **2007**, *126*, 064102.
(109) van Wüllen, C. *Z. Phys. Chem.* **2010**, *224*, 413.
(110) Aquilante, F.; De Vico, L.; Ferré, N.; Ghigo, G.; Malmqvist, P.-Å.; Neogrády, P.; Pedersen, T. B.; Pitoňák, M.; Reiher, M.; Roos, B. O.; Serrano-Andrés, L.; Urban, M.; Veryazov, V.; Lindh, R. *J. Comput. Chem.* **2010**, *31*, 224.
(111) te Velde, G.; Bickelhaupt, F. M.; Baerends, E. J.; Fonseca Guerra, C.; van Gisbergen, S. J. A.; Snijders, J. G.; Ziegler, T. *J. Comput. Chem.* **2001**, *22*, 931.
(112) Frisch, M. J.; Trucks, G. W.; Schlegel, H. B.; Scuseria, G. E.; Robb, M. A.; Cheeseman, J. R.; Scalmani, G.; Barone, V.; Mennucci, B.; Petersson, G. A.; Nakatsuji, H.; Caricato, M.; Li, X.; Hratchian, H. P.; Izmaylov, A. F.; Bloino, J.; Zheng, G.; Sonnenberg, J. L.; Hada, M.; Ehara, M.; Toyota, K.; Fukuda, R.; Hasegawa, J.; Ishida, M.; Nakajima, T.; Honda, Y.; Kitao, O.; Nakai, H.; Vreven, T.; Montgomery, J. A., Jr.; Peralta, J. E.; Ogliaro, F.; Bearpark, M.; Heyd, J. J.; Brothers, E.; Kudin, K. N.; Staroverov, V. N.; Keith, T.; Kobayashi, R.; Normand, J.; Raghavachari, K.; Rendell, A.; Burant, J. C.; Iyengar, S. S.; Tomasi, J.; Cossi, M.; Rega, N.; Millam, J. M.; Klene, M.; Knox, J. E.; Cross, J. B.; Bakken, V.; Adamo, C.; Jaramillo, J.; Gomperts, R.; Stratmann, R. E.; Yazyev, O.; Austin, A. J.; Cammi, R.; Pomelli, C.; Ochterski, J. W.; Martin, R. L.; Morokuma, K.; Zakrzewski, V. G.; Voth, G. A.; Salvador, P.; Dannenberg, J. J.; Dapprich, S.; Daniels, A. D.; Farkas, O.; Foresman, J. B.; Ortiz, J. V.; Cioslowski, J.; Fox, D. J. *Gaussian 09*; Gaussian, Inc.: Wallingford, CT, 2010; http://www.gaussian.com.
(113) Werner, H.-J.; Knowles, P. J.; Manby, F. R.; Schütz, M.; P. Celani, G. K., Korona, T.; Lindh, R.; Mitrushenkov, A.; Rauhut, G.; Adler, T. B.; Amos, R. D.; Bernhardsson, A.; Berning, A.; Cooper, D. L.; Deegan, M. J. O.; Dobbyn, A. J.; Eckert, F.; Goll, E.; Hampel, C.; Hesselmann, A.; Hetzer, G.; Hrenar, T.; Jansen, G.; C. Köppl, Liu, Y.; Lloyd, A. W.; Mata, R. A.; May, A. J.; McNicholas, S. J.; Meyer, W.; Mura, M. E.; Nicklaß, A.; Palmieri, P.; Pflüger, K.; Pitzer, R.; Reiher, M.; Shiozaki, T.; Stoll, H.; Stone, A. J.; Tarroni, R.; Thorsteinsson, T.; Wang, M.; Wolf, A. MOLPRO, a package of ab initio programs designed by H.-J. Werner and P. J. Knowles, University College Cardiff Consultants Ltd., 2010; http://www.molpro.net/.
(114) Visscher, L.; Jensen, H. J. A.; Bast, R.; Saue, T.; Bakken, V.; Dyall, K. G.; Dubillard, S.; Ekström, U.; Eliav, E.; Enevoldsen, T.; Faßhauer, E.; Fleig, T.; Fossgaard, O.; Gomes, A. S. P.; Helgaker, T.; Lærdahl, J. K.; Lee, Y. S.; Henriksson, J.; Iliaš, M.; Jacob, C. R.; Knecht, S.; Komorovský, S.; Kullie, O.; Larsen, C. V.; Nataraj, H. S.; Norman, P.; Olejniczak, G.; Olsen, J.; Park, Y. C.; Pedersen, J. K.; Pernpointner, M.; Ruud, K.; Sałek, P.; Schimmelpfennig, B.; Sikkema, J.; Thorvaldsen, A. J.; Thyssen, J.; Stralen, J. v.; Villaume, S.; Visser, O.; Winther, T.; Yamamoto, S. DIRAC13, 2013; http://www.diracprogram.org.
(115) Gibson, J. K.; Haire, R. G.; Marçalo, J.; Santos, M.; Leal, J. P.; Pires de Matos, A.; Tyagi, R.; Mrozik, M. K.; Pitzer, R. M.; Bursten, B. E. *Eur. Phys. J. D* **2007**, *45*, 133.
(116) Gibson, J. K.; Marçalo, J. *Coord. Chem. Rev.* **2006**, *250*, 776.
(117) Dewberry, C. T.; Etchison, K. C.; Cooke, S. A. *Phys. Chem. Chem. Phys.* **2007**, *9*, 4895.
(118) Edvinsson, G.; Lagerqvist, A. *J. Mol. Spectrosc.* **1985**, *113*, 93.
(119) Kaledin, L. A.; McCord, J. E.; Heaven, M. C. *J. Mol. Spectrosc.* **1994**, *164*, 27.
(120) Gong, Y.; Zhou, M.; Andrews, L. *Chem. Rev.* **2009**, *109*, 6765.
(121) Andrews, L.; Gong, Y.; Liang, B.; Jackson, V. E.; Flamerich, R.; Li, S.; Dixon, D. A. *J. Phys. Chem. A* **2011**, *115*, 14407.
(122) Santos, M.; Pires de Matos, A.; Marçalo, J.; Gibson, J. K.; Haire, R. G.; Tyagi, R.; Pitzer, R. M. *J. Phys. Chem. A* **2006**, *110*, 5751.
(123) Santos, M.; Marçalo, J.; Pires de Matos, A.; Gibson, J. K.; Haire, R. G. *J. Phys. Chem. A* **2002**, *106*, 7190.
(124) Hinton, C. S.; Citir, M.; Manard, M.; Armentrout, P. B. *Int. J. Mass Spectrom.* **2011**, *308*, 265.
(125) Gao, T.; Wang, H. Y.; Yi, Y. G.; Tan, M. L.; Zhu, Z. H.; Sun, Y.; Wang, X. L.; Fu, Y. B. *Acta Phys. Sin.* **1999**, *48*, 2222.
(126) Wang, H. Y.; Gao, T.; Yi, Y. G.; Tan, M. L.; Zhu, Z. H.; Fu, Y. B.; Wang, X. L.; Sun, Y. *Acta Phys. Sin.* **1999**, *48*, 2215.
(127) Wang, H. Y.; Zhou, Z. H.; Gao, T.; Fu, Y. B.; Wang, X. L.; Sun, Y. *Mol. Phys.* **2000**, *98*, 875.
(128) Li, Q.; Liu, X. Y.; Gao, T.; Zhu, Z. H.; Fu, Y. B.; Wang, X. L.; Sun, Y. *Acta Phys.-Chim. Sin.* **2000**, *16*, 987.
(129) Li, Q.; Wang, H. Y.; Jiang, G.; Zhu, Z. H. *Acta Phys.-Chim. Sin.* **2001**, *17*, 622.
(130) Liao, M.-S.; Kar, T.; Scheiner, S. *J. Phys. Chem. A* **2004**, *108*, 3056.
(131) Averkiev, B. B.; Mantina, M.; Valero, R.; Infante, I.; Kovács, A.; Truhlar, D. G.; Gagliardi, L. *Theor. Chem. Acc.* **2011**, *129*, 657.
(132) Infante, I.; Kovács, A.; La Macchia, G.; Shahi, A. R. M.; Gibson, J. K.; Gagliardi, L. *J. Phys. Chem. A* **2010**, *114*, 6007.
(133) Kovács, A.; Infante, I.; Gagliardi, L. *Struct. Chem.* **2013**, *24*, 917.
(134) Kovács, A.; Konings, R. J. M.; Raab, J.; Gagliardi, L. *Phys. Chem. Chem. Phys.* **2008**, *10*, 1114.
(135) Kovács, A.; Pogány, P.; Konings, R. J. M. *Inorg. Chem.* **2012**, *51*, 4841.
(136) Edvinsson, G.; Lagerqvist, A. *Phys. Scr.* **1984**, *30*, 309.
(137) Edvinsson, G.; Lagerqvist, A. *Phys. Scr.* **1985**, *32*, 602.
(138) Edvinsson, G.; Lagerqvist, A. *J. Mol. Spectrosc.* **1987**, *122*, 428.
(139) Edvinsson, G.; Lagerqvist, A. *J. Mol. Spectrosc.* **1988**, *128*, 117.
(140) Edvinsson, G.; Lagerqvist, A. *Phys. Scr.* **1990**, *41*, 316.
(141) Marian, C. M.; Wahlgren, U.; Gropen, O.; Pyykkö, P. *J. Mol. Struct. (THEOCHEM)* **1988**, *169*, 339.
(142) Watanabe, Y.; Matsuoka, O. *J. Chem. Phys.* **1998**, *109*, 8182.
(143) Küchle, W.; Dolg, M.; Stoll, H.; Preuss, H. *J. Chem. Phys.* **1994**, *100*, 7535.
(144) Andrews, L.; Zhou, M.; Liang, B.; Li, J.; Bursten, B. E. *J. Am. Chem. Soc.* **2000**, *122*, 11440.
(145) Watanabe, Y.; Matsuoka, O. *J. Chem. Phys.* **2002**, *116*, 9585.
(146) Paulovič, J.; Nakajima, T.; Hirao, K.; Seijo, L. *J. Chem. Phys.* **2002**, *117*, 3597.
(147) Paulovič, J.; Nakajima, T.; Hirao, K.; Lindh, R.; Malmqvist, P.-Å. *J. Chem. Phys.* **2003**, *119*, 798.
(148) Goncharov, V.; Heaven, M. C. *J. Chem. Phys.* **2006**, *124*, 064312.
(149) Buchachenko, A. A. *J. Chem. Phys.* **2010**, *133*, 041102.
(150) Kovács, A.; Konings, R. J. M. *J. Phys. Chem. A* **2011**, *115*, 6646.
(151) Heaven, M. C.; Nicolai, J.-P.; Riley, S. J.; Parks, E. K. *Chem. Phys. Lett.* **1985**, *119*, 229.
(152) Kaledin, L. A.; Shenyavskaya, E. A.; Gurvich, L. V. *Zh. Fiz. Khim.* **1986**, *60*, 1049.
(153) Kaledin, L. A.; Kulikov, A. N.; Gurvich, L. V. *Zh. Fiz. Khim.* **1989**, *63*, 801.
(154) Schläfer, H. L.; Gliemann, G. *Basic Principles of Ligand Field Theory*; Wiley Interscience: New York, 1969.
(155) Figgis, B. N.; Hitchman, M. A. *Ligand Field Theory and Its Applications*; Wiley-VCH: Weinheim, 2000.
(156) Krauss, M.; Stevens, W. J. *Chem. Phys. Lett.* **1983**, *99*, 417.
(157) Zhou, M.; Andrews, L.; Ismail, N.; Marsden, C. *J. Phys. Chem. A* **2000**, *104*, 5495.

DOI: 10.1021/cr500426s
Chem. Rev. 2015, 115, 1725−1759

(158) Paulovič, J.; Gagliardi, L.; Dyke, J. M.; Hirao, K. *J. Chem. Phys.* **2005**, *122*, 144317.
(159) Goncharov, V.; Kaledin, L. A.; Heaven, M. C. *J. Chem. Phys.* **2006**, *125*, 133202.
(160) Hong, G.; Dolg, M.; Li, L. *Chem. Phys. Lett.* **2001**, *334*, 396.
(161) Cao, X.; Dolg, M. *J. Mol. Struct. (THEOCHEM)* **2004**, *673*, 203.
(162) Mazzone, G.; Michelini, M. d. C.; Russo, N.; Sicilia, E. *Inorg. Chem.* **2008**, *47*, 2083.
(163) Tyagi, R. Ph.D. Thesis, Ohio State University, 2005.
(164) Michelini, M. d. C.; Russo, N.; Sicilia, E. *J. Am. Chem. Soc.* **2007**, *129*, 4229.
(165) Edelstein, N. M.; Fuger, J.; Katz, J. J.; Morss, L. R. In *The Chemistry of the Actinide and Transactinide Elements*; Edelstein, N. M., Fuger, J., Morss, L. R., Eds.; Springer: Dordrecht, 2006; Vol. 3, p 1753.
(166) Gibson, J. K.; Haire, R. G.; Marçalo, J.; Santos, M.; Pires de Matos, A.; Mrozik, M. K.; Pitzer, R. M.; Bursten, B. E. *Organometallics* **2007**, *26*, 3947.
(167) Mann, J. B. *Atomic Structure Calculations II. Hartree-Fock Wave Functions and Radial Expectation Values: Hydrogen to Lawrencium*; Internal Report LA-3691; Los Alamos Scientific Laboratory: NM, 1968.
(168) Edvinsson, G.; Selvin, L.-E.; Aslund, N. *Ark. Fys.* **1965**, *30*, 28.
(169) Gabelnick, S. D.; Reedy, G. T.; Chasanov, M. G. *J. Chem. Phys.* **1974**, *60*, 1167.
(170) Zhou, M.; Andrews, L. *J. Chem. Phys.* **1999**, *111*, 11044.
(171) Kushto, G. P.; Andrews, L. *J. Phys. Chem. A* **1999**, *103*, 4836.
(172) Gabelnick, S. D.; Reedy, G. T.; Chasanov, M. G. *J. Chem. Phys.* **1973**, *58*, 4468.
(173) Hunt, R. D.; Andrews, L. *J. Chem. Phys.* **1993**, *98*, 3690.
(174) Infante, I.; Andrews, L.; Wang, X.; Gagliardi, L. *Chem.—Eur. J.* **2010**, *16*, 12804.
(175) Green, D. W.; Reedy, G. T. *J. Chem. Phys.* **1978**, *69*, 544.
(176) Murad, E.; Hildenbrand, D. L. *J. Chem. Phys.* **1980**, *73*, 4005.
(177) Haire, R. G. *J. Alloys Compd.* **1994**, *213/214*, 185.
(178) Santos, M.; Marçalo, J.; Leal, J. P.; Pires de Matos, A.; Gibson, J. K.; Haire, R. G. *Int. J. Mass Spectrom.* **2003**, *228*, 457.
(179) Gibson, J. K. *J. Phys. Chem. A* **2003**, *107*, 7891.
(180) Seijo, L.; Barandiarán, Z.; Harguindey, E. *J. Chem. Phys.* **2001**, *114*, 118.
(181) Krauss, M.; Stevens, W. J. *Mol. Phys.* **2003**, *101*, 125.
(182) La Macchia, G.; Infante, I.; Raab, J.; Gibson, J. K.; Gagliardi, L. *Phys. Chem. Chem. Phys.* **2008**, *10*, 7278.
(183) Chen, J.; Meng, D. Q.; Du, J. G.; Jiang, G.; Gao, T.; Zhu, Z. H. *Acta Phys. Sin.* **2010**, *59*, 1658.
(184) von Bornstedt, A.; Edvinsson, G.; Lagerqvist, A.; Renhorn, I. *Phys. Scr.* **1979**, *20*, 599.
(185) Goncharov, V.; Han, J.; Kaledin, L. A.; Heaven, M. C. *J. Chem. Phys.* **2005**, *122*, 204311.
(186) Malli, G. L. In *The Challenge of d and f Electrons, Theory and Computations*; Salahub, D. R., Zerner, M. C., Eds.; ACS Symposium Series; American Chemical Society: Washington, DC, 1989; Vol. *394*, p 291.
(187) Kaledin, L. A.; Heaven, M. C. *J. Mol. Spectrosc.* **1997**, *185*, 1.
(188) Heaven, M. C.; Goncharov, V.; Steimle, T. C.; Ma, T.; Linton, C. *J. Chem. Phys.* **2006**, *125*, 204314.
(189) Wadt, W. R. *J. Am. Chem. Soc.* **1981**, *103*, 6053.
(190) Pyykkö, P.; Laakkonen, L. J.; Tatsumi, K. *Inorg. Chem.* **1989**, *28*, 1801.
(191) Dyall, K. G. *Mol. Phys.* **1999**, *96*, 511.
(192) Straka, M.; Dyall, K. G.; Pyykkö, P. *Theor. Chem. Acc.* **2001**, *106*, 393.
(193) Hrobárik, P.; Straka, M.; Pyykkö, P. *Chem. Phys. Lett.* **2006**, *431*, 6.
(194) Wood, J. H.; Boring, M.; Woodruff, S. B. *J. Chem. Phys.* **1981**, *74*, 5225.
(195) Michels, H. H.; Hobbs, R. H. *Theoretical Study of the Radiative and Kinetic Properties of Selected Metal Oxides and Air Molecules*; Technical Report, United Technology Research Center, 1985.
(196) Allen, G. C.; Baerends, E. J.; Vernooijs, P.; Dyke, J. M.; Ellis, A. M.; Fehér, M.; Morris, A. *J. Chem. Phys.* **1988**, *89*, 5363.
(197) Gagliardi, L.; Roos, B. O.; Malmqvist, P.-Å.; Dyke, J. M. *J. Phys. Chem. A* **2001**, *105*, 10602.
(198) Chang, Q. Ph.D. Thesis, The Ohio State University, 2002.
(199) Gagliardi, L.; Heaven, M. C.; Krogh, J. W.; Roos, B. O. *J. Am. Chem. Soc.* **2005**, *127*, 86.
(200) Fleig, T.; Jensen, H. J. A.; Olsen, J.; Visscher, L. *J. Chem. Phys.* **2006**, *124*, 104106.
(201) Han, J.; Kaledin, L. A.; Goncharov, V.; Komissarov, A. V.; Heaven, M. C. *J. Am. Chem. Soc.* **2003**, *125*, 7176.
(202) Han, J.; Goncharov, V.; Kaledin, L. A.; Komissarov, A. V.; Heaven, M. C. *J. Chem. Phys.* **2004**, *120*, 5155.
(203) Li, J.; Bursten, B. E.; Andrews, L.; Marsden, C. J. *J. Am. Chem. Soc.* **2004**, *126*, 3424.
(204) Lue, C. J.; Jin, J.; Ortiz, M. J.; Rienstra-Kiracofe, J. C.; Heaven, M. C. *J. Am. Chem. Soc.* **2004**, *126*, 1812.
(205) Merritt, J. M.; Han, J.; Heaven, M. C. *J. Chem. Phys.* **2008**, *128*, 084304.
(206) Gagliardi, L.; Roos, B. O. *Chem. Phys. Lett.* **2000**, *331*, 229.
(207) Majumdar, D.; Balasubramanian, K.; Nitsche, H. *Chem. Phys. Lett.* **2002**, *361*, 143.
(208) Wang, X.; Andrews, L.; Li, J.; Bursten, B. E. *Angew. Chem., Int. Ed.* **2004**, *43*, 2554.
(209) Ruipérez, F.; Danilo, C.; Réal, F.; Flament, J.-P.; Vallet, V.; Wahlgren, U. *J. Phys. Chem. A* **2009**, *113*, 1420.
(210) Denning, R. G.; Snellgrove, T. R.; Woodwark, D. R. *Mol. Phys.* **1979**, *37*, 1109.
(211) Denning, R. G.; Foster, D. N. P.; Snellgrove, T. R.; Woodwark, D. R. *Mol. Phys.* **1979**, *37*, 1089.
(212) Denning, R. G. In *Structure and Bonding*; Clarke, M. J., Goodenough, J. B., Hemmerich, P., Ibers, J. A., Jørgensen, C. K., Neilands, J. B., Reinen, D., Weiss, R., Williams, R. J. P., Eds.; Springer: Berlin, 1992; Vol. *79*, p 215.
(213) Pyykkö, P.; Li, J.; Runeberg, N. *J. Phys. Chem.* **1994**, *98*, 4809.
(214) de Jong, W. A.; Visscher, L.; Nieuwpoort, W. C. *J. Mol. Struct. (THEOCHEM)* **1999**, *458*, 41.
(215) Ismail, N.; Heully, J.-L.; Saue, T.; Daudey, J.-P.; Marsden, C. J. *Chem. Phys. Lett.* **1999**, *300*, 296.
(216) Réal, F.; Vallet, V.; Marian, C.; Wahlgren, U. *J. Chem. Phys.* **2007**, *127*, 214302.
(217) Bleaney, B. *Discuss. Faraday Soc.* **1955**, *19*, 112.
(218) Eisenstein, J. C.; Pryce, M. H. L. *J. Res. Natl. Bur. Stand.* **1966**, *70A*, 165.
(219) Gao, T.; Wang, H. Y.; Huang, Z.; Zhu, Z. H.; Sun, Y.; Wang, X. L.; Fu, Y. B. *Acta Phys.-Chim. Sin.* **1999**, *15*, 1082.
(220) Maron, L.; Leininger, T.; Schimmelpfennig, B.; Vallet, V.; Heully, J.-L.; Teichteil, C.; Gropen, O.; Wahlgren, U. *Chem. Phys.* **1999**, *244*, 195.
(221) Clavaguéra-Sarrio, C.; Vallet, V.; Maynau, D.; Marsden, C. J. *J. Chem. Phys.* **2004**, *121*, 5312.
(222) Jørgensen, C. K.; Reisfeld, R. In *Structure and Bonding*; Clarke, M. J., Goodenough, J. B., Hemmerich, P., Ibers, J. A., Jørgensen, C. K., Neilands, J. B., Reinen, D., Weiss, R., Williams, R. J. P., Eds.; Springer: Berlin, 1982; Vol. *50*, p 122.
(223) Notter, F.-P.; Dubillard, S.; Bolvin, H. *J. Chem. Phys.* **2008**, *128*, 164315.
(224) Jackson, V. E.; Craciun, R.; Dixon, D. A.; Peterson, K. A.; de Jong, W. A. *J. Phys. Chem. A* **2008**, *112*, 4095.
(225) Linevsky, M. J. General Electric Report nos. WADD-TR-60–646 (Pt. IV) and AD-611856, 1963.
(226) Matsika, S.; Pitzer, R. M. *J. Phys. Chem. A* **2001**, *105*, 637.
(227) Pierloot, K.; van Besien, E. *J. Chem. Phys.* **2005**, *123*, 204309.
(228) Pierloot, K.; van Besien, E.; van Lenthe, E.; Baerends, E. J. *J. Chem. Phys.* **2007**, *126*, 194311.
(229) Kovács, A., unpublished data.
(230) Bell, J. T.; Friedman, H. A.; Billings, M. R. *J. Inorg. Nucl. Chem.* **1974**, *36*, 2563.
(231) Mizuoka, K.; Tsushima, S.; Hasegawa, M.; Hoshi, T.; Ikeda, Y. *Inorg. Chem.* **2005**, *44*, 6211.
(232) Bell, J. T.; Biggers, R. E. *J. Mol. Spectrosc.* **1968**, *25*, 312.

DOI: 10.1021/cr500426s
Chem. Rev. 2015, 115, 1725–1759

(233) Görller-Walrand, C.; Vanquickenborne, L. G. *J. Chem. Phys.* **1971**, *54*, 4178.
(234) Görller-Walrand, C.; De Jaegere, S. *Spectrochim. Acta* **1972**, *28A*, 257.
(235) Denning, R. G.; Snellgrove, T. R.; Woodwark, D. R. *Mol. Phys.* **1975**, *30*, 1819.
(236) Denning, R. G.; Snellgrove, T. R.; Woodwark, D. R. *Mol. Phys.* **1976**, *32*, 419.
(237) Flint, C. D.; Tanner, P. A. *J. Chem. Soc., Faraday Trans. 2* **1978**, *74*, 2210.
(238) Barker, T. J.; Denning, R. G.; Thorne, J. R. G. *Inorg. Chem.* **1987**, *26*, 1721.
(239) De Houwer, S.; Görller-Walrand, C. *J. Alloys Compd.* **2001**, *323*−*324*, 683.
(240) Tecmer, P.; Gomes, A. S. P.; Ekström, U.; Visscher, L. *Phys. Chem. Chem. Phys.* **2011**, *13*, 6249.
(241) Dieke, G. H.; Duncan, A. B. F. *National Nuclear Energy Series, Division III*; McGraw-Hill: New York, 1949; Vol. 2.
(242) Rabinowitch, E.; Belford, R. L. *Spectroscopy and Photochemistry of Uranyl Compounds*; Pergamon: New York, 1964.
(243) Denning, R. G. *J. Phys. Chem. A* **2007**, *111*, 4125.
(244) Zhang, Z.; Pitzer, R. M. *J. Phys. Chem. A* **1999**, *103*, 6880.
(245) Wang, F.; Ziegler, T.; van Lenthe, E.; Van Gisbergen, S. J. A.; Baerends, E. J. *J. Chem. Phys.* **2005**, *122*, 204103.
(246) Schipper, P. R. T.; Gritsenko, O. V.; van Gisbergen, S. J. A.; Baerends, E. J. *J. Chem. Phys.* **2000**, *112*, 1344.
(247) Gomes, A. S. P.; Jacob, C. R.; Réal, F.; Visscher, L.; Vallet, V. *Phys. Chem. Chem. Phys.* **2013**, *15*, 15153.
(248) Sjoblom, R.; Hindman, J. C. *J. Am. Chem. Soc.* **1951**, *73*, 1744.
(249) Waggener, W. C. *J. Phys. Chem.* **1958**, *62*, 382.
(250) Hagan, P. G.; Cleveland, J. M. *J. Inorg. Nucl. Chem.* **1966**, *28*, 2905.
(251) Stafsudd, O. M.; Leung, A. F.; Wong, E. Y. *Phys. Rev.* **1969**, *180*, 339.
(252) Leung, A. F.; Wong, E. Y. *Phys. Rev.* **1969**, *187*, 504.
(253) Denning, R. G.; Norris, J. O. W.; Brown, D. *Mol. Phys.* **1982**, *46*, 287.
(254) Denning, R. G.; Norris, J. O. W.; Brown, D. *Mol. Phys.* **1982**, *46*, 325.
(255) Matsika, S.; Pitzer, R. M. *J. Phys. Chem. A* **2000**, *104*, 4064.
(256) Matsika, S.; Pitzer, R. M.; Reed, D. T. *J. Phys. Chem. A* **2000**, *104*, 11983.
(257) Eisenstein, J. C.; Pryce, M. H. L. *Proc. R. Soc. A* **1955**, *229*, 20.
(258) Newton, T. W.; Baker, F. B. *J. Phys. Chem.* **1957**, *61*, 934.
(259) Cohen, D. *J. Inorg. Nucl. Chem.* **1961**, *18*, 211.
(260) Hay, P. J.; Martin, R. L.; Schreckenbach, G. *J. Phys. Chem. A* **2000**, *104*, 6259.
(261) Hildenbrand, D. L.; Gurvich, L. V.; Yungman, V. S. *The Chemical Thermodynamics of Actinide Elements and Compounds, Part 13 - The Gaseous Actinide Ions*; IAEA: Vienna, 1985.
(262) Lias, S. G.; Bartmess, J. E.; Liebman, J. F.; Holmes, J. L.; Levin, R. D.; Mallard, W. G. *Gas-Phase Ion and Neutral Thermochemistry*; American Chemical Society: Washington, DC, 1988.
(263) Konings, R. J. M.; Morss, L. R.; Fuger, J. In *The Chemistry of the Actinide and Transactinide Elements*; Edelstein, N. M., Fuger, J., Morss, L. R., Eds.; Springer: Dordrecht, 2006; Vol. 4, p 2113.
(264) Rand, M.; Fuger, J.; Grenthe, I.; Neck, V.; Rai, D. *Chemical Thermodynamics of Thorium. OECD Nuclear Energy Agency Data Bank - Chemical Thermodynamics*; OECD Publications: Paris, 2008; Vol. 11.
(265) Gibson, J. K.; Haire, R. G.; Marçalo, J.; Santos, M.; Pires de Matos, A.; Leal, J. P. *J. Nucl. Mater.* **2005**, *344*, 24.
(266) Gibson, J. K.; Haire, R. G.; Santos, M.; Pires de Matos, A.; Marçalo, J. *J. Phys. Chem. A* **2008**, *112*, 11373.
(267) Gibson, J. K.; Haire, R. G.; Santos, M.; Marçalo, J.; Pires de Matos, A. *J. Phys. Chem. A* **2005**, *109*, 2768.
(268) Armentrout, P. B.; Beauchamp, J. L. *Chem. Phys.* **1980**, *50*, 21.
(269) Kleinschmidt, P. D.; Ward, J. W. *J. Less-Common Met.* **1986**, *121*, 61.
(270) Armentrout, P. B. *Int. J. Mass Spectrom.* **2003**, *227*, 289.
(271) Boudreaux, E. A.; Baxter, E. *Int. J. Quantum Chem.* **2002**, *90*, 629.
(272) Zaitsevskii, A. V.; Titov, A. V.; Mal'kov, S. S.; Tananaev, I. G.; Kiselev, Y. M. *Dokl. Chem.* **2013**, *448*, 1.
(273) Zaitsevskii, A.; Mosyagin, N. S.; Titov, A. V.; Kiselev, Y. M. *J. Chem. Phys.* **2013**, *139*, 034307.
(274) Haire, R. G. *J. Alloys Compd.* **1995**, *223*, 185.
(275) Haire, R. G. *J. Alloys Compd.* **1995**, *225*, 142.
(276) Pyykkö, P.; Riedel, S.; Patzschke, M. *Chem.—Eur. J.* **2005**, *11*, 3511.
(277) Gibson, J. K.; Haire, R. G. *Radiochim. Acta* **2001**, *89*, 709.
(278) Gabelnick, S. D.; Reedy, G. T.; Chasanov, M. G. *Chem. Phys. Lett.* **1973**, *19*, 90.
(279) Gabelnick, S. D.; Reedy, G. T.; Chasanov, M. G. *J. Chem. Phys.* **1973**, *59*, 6397.
(280) Green, D. W. *Int. J. Thermophys.* **1980**, *1*, 61.
(281) Privalov, T.; Schimmelpfennig, B.; Wahlgren, U.; Grenthe, I. *J. Phys. Chem. A* **2002**, *106*, 11277.
(282) Zaitsevskii, A. V. *Radiochemistry* **2013**, *55*, 353.
(283) Green, D. W.; Reedy, G. T.; Gabelnick, S. D. *J. Chem. Phys.* **1980**, *73*, 4207.
(284) Ronchi, C.; Capone, F.; Colle, J. Y.; Hiernaut, J. P. *J. Nucl. Mater.* **2000**, *280*, 111.
(285) Gao, T.; Zhu, Z. H.; Wang, X. L.; Sun, Y.; Meng, D. Q. *Acta Chim. Sin.* **2004**, *62*, 454.
(286) Zaitsevskii, A., private communication.
(287) Li, Q.; Liu, X. Y.; Wang, R.; Zhu, Z. H.; Fu, Y. B.; Wang, X. L. *Chin. Phys.* **2001**, *10*, 501.
(288) Kiselev, Y. M.; Nikonov, M. V.; Tananaev, I. G.; Myasoedov, B. F. *Dokl. Akad. Nauk* **2009**, *425*, 634.
(289) Huang, W.; Xu, W.-H.; Su, J.; Schwarz, W. H. E.; Li, J. *Inorg. Chem.* **2013**, *52*, 14237.
(290) Domanov, V. P.; Lobanov, Y. V. *Radiochemistry* **2011**, *53*, 453.
(291) Zaitsevskii, A.; Mosyagin, N. S.; Titov, A. V.; Kiselev, Y. M. *Russian-Nordic Symposium on Radiochemistry*; Idea Print: Moscow, 2013.
(292) Pyykkö, P.; Runeberg, N.; Straka, M.; Dyall, K. G. *Chem. Phys. Lett.* **2000**, *328*, 415.
(293) Xiao, H.; Hu, H.-S.; Schwarz, W. H. E.; Li, J. *J. Phys. Chem. A* **2010**, *114*, 8837.
(294) Burns, P. C.; Hughes, K.-A. *Am. Mineral.* **2003**, *88*, 1165.
(295) Ermler, W. C.; Ross, R. B.; Christiansen, P. A. *Int. J. Quantum Chem.* **1991**, *40*, 829.
(296) Christiansen, P. A.; Ermler, W. C.; Pitzer, K. S. *Annu. Rev. Phys. Chem.* **1988**, *36*, 407.
(297) Alecu, I. M.; Zheng, J.; Zhao, Y.; Truhlar, D. G. *J. Chem. Theory Comput.* **2010**, *6*, 2872.
(298) Zheng, J.; Alecu, I. M.; Lynch, B. J.; Zhao, Y.; Truhlar, D. G. *Database of Frequency Scale Factors for Electronic Structure Methods*; University of Minnesota: Minneapolis, MN, 2010; http://comp.chem.umn.edu/freqscale/index.html.

DOI: 10.1021/cr500426s
Chem. Rev. 2015, 115, 1725−1759